Optimisation of casting process of sand cast austenitic stainless-steel pump impeller using numerical modelling and additive manufacturing.

Hudivhamudzimu Mugeri (208063765)

MAGISTER TECHNOLOGIAE: METALLURGICAL ENGINEERING

in the

Department of Metallurgical Engineering

FACULTY OF ENGINEERING AND TECHNOLOGY

VAAL UNIVERSITY OF TECHNOLOGY

Supervisor: Dr. Wallace R. Matizamhuka

Co-Supervisor: Dr. Isaac Damilola Adebiyi

DECEMBER 2018

DECLARATION

I hereby declare that this MTech entitled “Optimisation of casting process of sand cast austenitic stainless-steel pump impeller using numerical modelling and additive manufacturing” dissertation is a presentation of my own un-aided work which has not been submitted to any university or tertiary institution. It is submitted for the Degree Magister Technologiae to the Department of Metallurgical Engineering at Vaal University of Technology in Vanderbijlpark. In text referencing and bibliography has been properly done to acknowledge whoever contributed. This work has been done under guidance of Dr. Wallace Matizamhuka and Dr. Isaac Damilola Adebiyi.

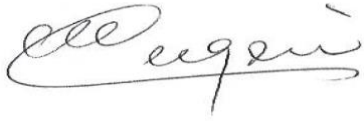

Signature_____

DEDICATION

To all the youth; “Education is not the key to get rich but a key to think better and make better decisions”. Work hard and become a leader; be lazy and become a slave.

ACKNOWLEDGEMENT

Firstly, I would like to acknowledge my family for all the moral support throughout this project. I want to express my sincerest appreciation to my Supervisor Dr Wallace Matizamhuka who never gave up on me all the way till the end of this dissertation. Many gratitude again to Dr Isaac Damilola Adebiyi (Co-Supervisor) and Mr Jacobus Dippenaar (Mentor). The Author wishes to also acknowledge practical support provided by the following organisations and institutions; Vaal University of Technology (VUT) Metallurgical Engineering Department, VUT Science Park, University of Johannesburg, Columbus Stainless, Duvha Foundry, Vereeniging Foundries, Hulamin, National Simulation Network (NSN), Technology Localisation Implementation Unit (TLIU), FOSECO, Metso South Africa and Amatex.

PUBLISHED ARTICLES RELATED TO DISSERTATION

International Conference on Sustainable Materials Processing and Manufacturing, SMPM 2017, 23-25 January 2017, Kruger National Park

Procedia Manufacturing 00 (2016) 000–000

1st Paper: Effect of Wall Thickness on the Quality of 1060 Aluminum Produced By Sand Casting

Hudivhamudzimu Mugeri[a,1], Wallace Matizamhuka[b], Damilola Isaac Adebiyi[c], and Jacobus Hendrik Deppinnar[d]

Vaal University of Technology, Vanderbijlpark, Andries Potgieter Blvd, South Africa

The demand for thin-walled sections in the industry is continuously increasing due to their light-weight. However, the production of thin-wall sections (<2 mm) using sand casting process present a huge challenge in the foundry industry. This paper will investigate the filling defects which are associated with thin-walled sections, thus affecting the quality of 1060 aluminium casting using sand casting process as a manufacturing process. The results showed quick solidification of thin-walled section (1 mm-2.5 mm) before the metal completely filled the mould cavity. Some of the important factors which contributed to this quick solidification were wall thickness, backpressure and presence of junctions. The higher the number of junctions the higher the backpressure and the lower the fillability. A small increase in wall thickness reduced the backpressure which increased the metal flow. The temperature of the molten metal remained constant at different places for all different test samples. A slight increase in wall thickness yielded a minimum of 12.5 % and a maximum of 32 % increase in fillability. It was observed that as the wall thickness increases, so does the fillability.

Peer-review under responsibility of the organizing committee of SMPM 2017.

Keywords: fillability; sand casting process; mould cavity; backpressure; junctions and solidification

---

[1] Corresponding author. Tel.: 076 99 906.
E-mail address: hmugeri@gmail.com

EFFECT OF CASTING TEMPERATURE ON THE FILLABILITY OF 1060 ALUMINUM PRODUCED BY SAND CASTING

H. Mugeri[1]*, W.R. Matizamhuka[2], D.I. Adebiyi[3], & J.H. Dippenaar[4]

[1]Deparment of Metallurgical Engineering

Vaal University of Technology, South Africa

[1]Email: hmugeri@gmail.com

[2]Email: wallace@vut.ac.za

[3]Email:damilolaa@vut.ac.za

[4]Email: kobusd@vut.ac.za

Thin-walled sections are more susceptible to filling defects due to inadequate metal filling. The present study is focused on investigating the effect of casting temperature on the quality of 1060 aluminum casting using sand casting as a manufacturing process. A 2 mm test sample was optimized at six different casting temperatures of 700 °C, 730 °C, 760 °C, 790 °C, 800 °C and 860 °C using MAGMAsoft casting software. An increase in casting temperature by 30 °C yielded minimum a of 4 % increase in fillability and maximum of 8.5 % fillability increase. The results obtained shows a good correlation between the casting temperature and fillability of thin walled sections.

Abstract

The production of austenitic stainless-steel pump impellers in foundries present a huge challenge mainly due to its thin-walled blades, pouring temperature, presence of junctions and chemical composition. Two different alloys were used namely nodular cast iron and austenitic stainless-steel. Nodular cast iron was used as a comparison alloy due to its excellent flowability whereas austenitic stainless-steel was chosen due to its attractive corrosion and wear resistant properties. Austenitic stainless-steel alloy showed difficulties during casting because of its chemical composition and freezing range. Thin-walled sections are more susceptible to filling defects like misrun and cold-shut. This results in high scrap rate and high processing costs during high production of thin-walled components. High pouring temperature is considered one of the most effective methods to improve filling ability of thin-walled castings. However, there is a major drawback in using this method owing to the high occurrence of shrinkage defects and hot tearing especially at junctions. 1060 aluminium was used as a benchmark to evaluate the effect of wall thickness on the filling and feeding of thin-walled Al components with complex geometry during sand casting.

The aim of this dissertation is therefore to optimize casting process of sand cast austenitic stainless-steel pump impeller. Numerical modelling and additive manufacturing were used to optimize the production of this product. The use of casting simulation software combined with three-dimensional (3D) mould printing technology has enabled optimisation of casting parameters to minimise the occurrence of casting defects. Casting parameters of five test samples of complex geometry and varying thicknesses (1.0 mm;1.5 mm;2 mm;2.5 mm and 3.0 mm) were optimised using MAGMAsoft® at a constant pouring temperature of 700 °C and 1060 Aluminium as an alloy. Simulation and casting results showed that complete filling was only possible at a wall thickness of 3 mm. The simulation results showed that as the wall thickness increased from 1 mm to 3 mm the filling ability increased by 67.5 % whereas experimental casting results showed that filling ability increase by 75 %. The combination of MAGMAsoft® simulation and 3D printed moulds proved to be effective tools in predicting filling and feeding of thin-walled aluminium components during sand casting.

MAGMAsoft® casting software was used to simulate metal flow and predict the degree of filling at different pouring temperatures. Test samples were cast using 1060 Aluminium alloy at temperatures of 702 °C, 729 °C, 761 °C, 794 °C, 800 °C and 862 °C. Complete mould filling was predicted at 800 °C using the simulation model and 761°C during actual casting. At temperatures above 761°C tearing at the junction was quite pronounced. An optimal of 761°C

pouring temperature was found to be appropriate pouring temperature when casting thin-walled aluminum components using sand casting. MAGMAsoft® casting software proved to be an effective tool in optimizing filling and feeding of thin-walled aluminium components during sand casting.

Nodular cast iron pump impeller was optimized at 1500 °C using MAGMAsoft® and 3D mould printing technology. Design variables used were feeder radius (17 mm, 18 mm, 19 mm and 20 mm), feeder height (32 mm, 33 mm, 34 mm, 35 mm) and number of feeders of (3, 4 and 5). Simulation and casting results showed a completely-filled casting. The high fluidity of nodular cast iron promotes mould filling ability and prevent any form of misrun defect. Minimum shrinkage was noted at the junctions and top surface of the casting. A new design was proposed to eliminate shrinkage defects at the junctions of the nodular cast iron pump impeller. The design used a tapered circular runner bar with straight ingates. Optimization of nodular cast iron was now done at 1390 °C with the use of MAGMAsoft® and real casting was done 1385 °C. Simulation and casting were in correlation to each other since both showed completely-filled mould cavity with no misrun, cold-shut and shrinkage porosity defect. Simulation proved to be an effective tool in optimizing filling and solidification of nodular cast iron during sand casting.

Austenitic stainless-steel pump impeller was optimized at 1500 °C using MAGMAsoft® and 3D mould printing technology. A high quality mould and core print were printed with the use of Voxeljet VX1000 at a minimum period of time. Design variables used were feeder radius (17 mm, 18 mm, 19 mm and 20 mm), feeder height (32 mm, 33 mm, 34 mm, 35 mm) and number of feeders of (3, 4 and 5). An increase in feeder size and the number of feeders greatly reduced hot spot and porosity of the casting but it also reduced the casting yield. The quality of the casting was found to be inversely proportional to the casting yield. Simulation showed a completely-filled casting with actual casting showing only 50 % filling ability. High viscosity of the molten metal and thin walled blades promote quick solidification which caused misrun defects. A new design was proposed to eliminate misrun defects of the first design. MAGMAsoft® was used to optimize this design at 1550 °C. The design used a tapered circular runner bar with tapered ingates. The actual casting showed improved filling ability from 50 % to 80 % while simulation showed completely-filled mould cavity (100 %). Major factors which contributed to low filling ability of austenitic stainless-steel pump impeller were chemistry, runner system and men. Numerical modelling and additive manufacturing did optimize filling and feeding of sand cast austenitic stainless-steel pump impeller.

Table Contents

List of Figures

List of Tables

DISSERTATION

CHAPTER 1

INTRODUCTION

1.1 Background

The sand casting technology is an ancient manufacturing process utilised in the production of metallic components in large quantities at a relatively low-cost in comparison to other manufacturing processes (Mugeri et al. 2017). The technology is used widely to produce lightweight thin-walled components which find use in the automotive and aircraft industries. This has been driven by the increased demand for light-weight automotive and aircraft components which offer benefits such as low fuel consumption hence, lower damaging emissions to the environment (Raza 2015). However, there are great challenges in the production of thin-walled sections, thin-walled castings tend to solidify prematurely before filling the mould cavity (Voigt 2002). This premature solidification has a negative impact on the microstructure and mechanical properties of the casting. In accordance to Voigt (2002), misrun and cod-shut can also be a result of premature solidification during filling. As the wall thickness reduces, the cooling rates increases, and castings become more prone to misrun and cold-shut defects (Gorny and Tyrala 2012).

An impeller is a rotating component which is situated inside the centrifugal pump to transport fluid by rotation (Iratkar and Gandigude 2017). It consists of an inlet where the fluid enters and an outlet where the fluid discharges. It contains thin-walled blades with different wall thicknesses and junctions which adds to the complexity of a sand casting design as seen in pump impellers (Figure 1.1). The greatest challenge is a result of premature solidification in the thin-walled blades causing a misrun or cold-shut. Figure 1.2. shows example of cold-shut and misrun defect (Prajapati and Sutaria 2013). To overcome this problem, foundries have adopted the use of expensive high pressure die casting (HPDC) and investment casting (Fang et al. 2014). In HPDC molten metal is forced into confined spaces through a hydraulically operated high-pressure system. This normally requires massive and costly equipment to obtain good quality castings at high production rate. Thus, for the small-to-medium scale foundry establishments, sand casting remains a more attractive method due to its low-cost and versatility (Nadiah et al. 2015). The production of high quality stainless steel pump impeller with the use of cheap normal gravity sand casting still present huge challenges in the casting manufacturing industry.

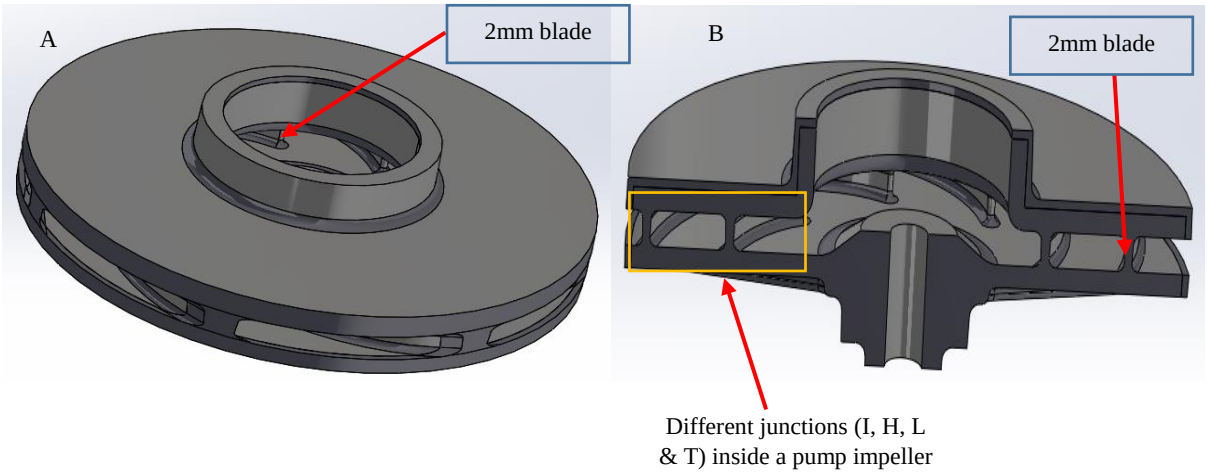

Figure 1. 1: Thin-walled (2mm) blades inside pump impeller, isometric view (A) section view (B)

Source: This figure was taken from one of the foundries where there have been austenitic stainless-steel production challenges.

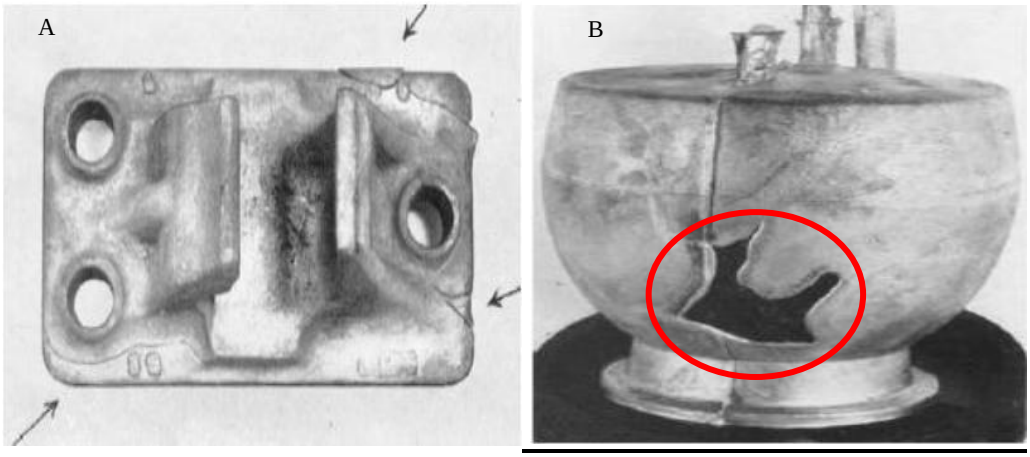

Figure 1. 2: Flow related defects cold-shut (arrowed regions) (A) and misrun (red circle) (B)

Source: (Prajapati and Sutaria 2013)

Casting operations can be classified according to the type of mould material used with the most common being sand, metal or composite materials (Mugeri et al. 2017). Sand casting is one of the most versatile and cheap methods utilised over the years to produce components of varying shapes and sizes in large quantities (Nadiah et al. 2015). Some of the major attractions in using sand casting operations include the low-cost, its ability to cast a wide range of alloys (both ferrous and non-ferrous) and sizes (Sulaiman and Pio 2004). However, the main drawbacks that have been cited include poor surface finish and poor filling of thin sections (<5mm thickness), which normally results in misrun and cold-shut (Voigt 2002).

Voigt (2002) state that that thin walled sections solidify according to Chvorinov's Equation 1 which shows that the solidification time of the casting is in relation to the casting volume and surface area. In principle, thin-walled sections tend to solidify faster than thicker sections due to their lower volume/surface area ratio referred to as the modulus (Voigt 2002).

$$t = C\left[\frac{V}{A}\right]^n \quad (1.1)$$

where *t* is solidification time in sec, *V* is casting volume in m^3, *A* is surface area of casting that contact mould in m^2, *C* is constant in $^{s}/_{m^2}$, and n is also a non-dimensional constant usually varying between 1.5 and 2, typically used as 2.

Premature solidification affects the way the molten metal will fill up the mould cavity. The ease with which molten metal can fill the mould cavity to produce well-defined surfaces of the cast product is called mould filling ability (Bouska 2008). Poor mould filling ability promote misrun and cold-shut defects. It must be noted however that the rheology of molten metal also plays a crucial role in the filling ability of thin sections (Raza 2015).

The presence of junctions in castings further complicates the situation by introducing some mass concentration posing an ever much greater risk for the formation of shrinkage cavities or porosity defects (Saxena et al. 2013). Kumar and Ravi (2006) suggested the use of fillets (act as flow and feed paths for molten metal), which are to be configured in such a way that the biggest area must lie close to the riser and the smallest away from it so that solidification proceeds towards the riser and be the last part to solidify. This effectively assists in eliminating sharp inside corners and the resulting problems of stress concentration. Thus, an I-junction would require a larger fillet than a T-junction to prevent hot tearing at the fillet area. This is a result of restrained contraction stresses present in I-junction as illustrated in Figure 1.3.

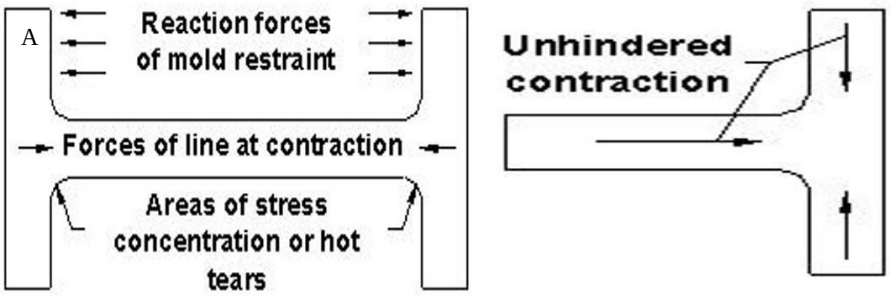

Figure 1. 3: Schematic representation of contraction stresses distribution in an I section (A) and T section (B)

Source: (Kumar and Ravi 2006)

Although there are a number of factors affecting the filling ability of thin-walled sections, the most prominent factors, however, include (i) the mould-metal heat transfer coefficient, (ii) mould thermal conductivity, (iii) mould wall friction factor, (iv) pouring temperature and pouring basin head pressure, (v) wall thickness and (vi) feeding distance.

The feeding distance, is affected by metal viscosity and can be varied. It also has a direct impact on the feeding efficiency of metal fed into the various sections of a casting. According to Shouzhu et al. (2002), the feeding distance as exemplified in Figure 1.4 is the maximum distance a riser can feed a casting without any discontinuities such as porosity, shrinkage, misrun or cold-shuts. Metals with high viscosity tend to have a short feeding distance, which promotes the formation of a misrun defect. This distance is measured from the edge of the riser to the furthest point in the casting section fed by that riser (Steel founders' society of America 2001). Feeding distance can also be affected by the relationship between the size of the feeder and the distance from the feeder to the feeding point. If the feeder size is small, insufficient metal will be available to feed and shrinkage voids will form. If the feeder is sufficiently big, enough metal will be available but the distance from the feeder to the feeding spot must be in relation to the feeder size so that metal can reach the spot without forming misrun defect. If a feeder is very big, enough metal will still be available, but this will now affect the casting yield (Rundman 2005).

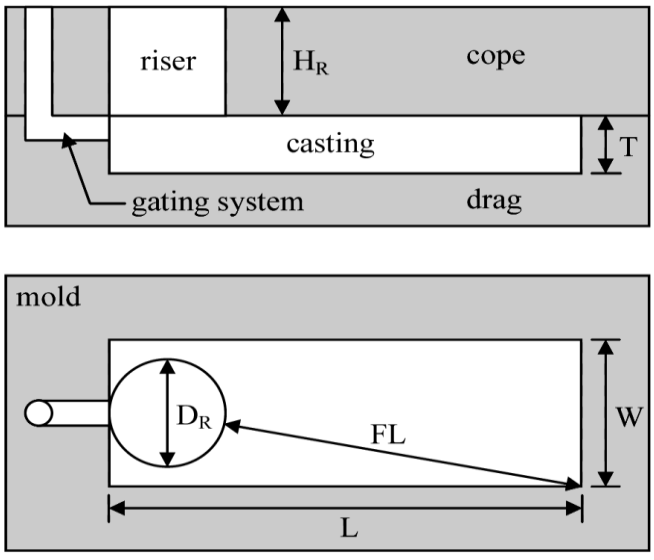

Figure 1. 4: A schematic representation of the feeding distance (FD)

Source: (Carlson et al. 2002)

where H_R is the riser height, T is the casting thickness, D_R is the riser diameter, FL is the feeding length, W is the casting width and L is the casting length.

It is noteworthy to mention here that the use of the sand casting process to produce good quality thin-walled components requires an optimised mould system design to minimise the formation of defects already mentioned. Traditionally, this has been achieved by trial and error practice which is common with most of the small-to-medium scale foundry establishments. Therefore, the use of numerical methods, which make use of the physical and thermal properties of the metal/alloy being cast to predict the quality of the casting (with minimum of defect formation) has proven much faster and more accurate approach (Pedersen et al. 2006). Numerical modelling assist in visualising the real casting process with the use of computer software. This will assist in reducing possible defects which might appear during casting process before real casting is done. This may also include an analysis on other useful properties, which affect the integrity of the final component such as thermal stress distribution and distortions. One such approach involves MAGMAsoft® simulation, and this was adopted in the present study. Furthermore, the use of additive manufacturing methods in the production of high quality moulds can minimise the formation of defects during casting. The moulds used in this project were produced through a 3-D printing technology using the Voxeljet VX1000 machine. The use of Voxeljet VX1000 in the production of sand moulds and complex core print has gained popularity owing to its low lead time and high-quality moulds produced (Nyembwe et al. 2016). Traeger (2016) also claimed that the traditional production of sand mould can take several weeks while the use of Voxeljet VX1000 can only take days. Thus, the aim of this study is to develop an optimised filling and feeding system to produce a sound austenitic stainless-steel pump impeller using a normal and less costly gravity sand casting process using 3D printed moulds.

1.2 Motivation

Sand casting has been identified as one of the cheaper routes in the small to medium-sized foundry establishments when producing pump impellers. However, sand casting of austenitic stainless-steel pump impeller with thin sections of 2 mm blades and junctions presents a challenge owing to the poor filling ability of molten metal into confined spaces. Poor filling ability manifests itself in the form of discontinuities in the casting (i.e. misrun, cold-shuts, mould erosion, gas entrapment etc.) which have a negative impact on the component functionality (Prajapati and Sutaria 2013). Feeding pattern which is highly affected by feeder size and feeding distance also play a big role in the quality of the impellers produced. Poor feeding result in shrinkage defects which negatively affect the quality of the impeller produced.

It is by this cause that the present study investigates the effectiveness of numerical and additive manufacturing methods in sand casting process in the production of austenitic stainless-steel pump impellers. Furthermore, the investigative tools sought are accessible within the Vaal University of Technology Southern Gauteng Station, Sebokeng.

1.3 Problem statement

1.3.1 General problem statement

Casting of high quality stainless-steel pump impellers using the normal sand casting process presents a challenge in most foundry establishments owing to the number of associated filling and solidification defects. To mitigate this problem, high pressure die casting (HPDC) and investment casting are normally used (Fang et al. 2014). However, HPDC method makes use of high pressure to force molten metal into the mould to improve the filling ability of thin sections. HPDC involves the use of a die which is preheated before pouring to improve the feeding distance by lowering solidification time. Austenitic stainless steel is an alloy which solidifies with more complexity than a pure metal (Fang et al. 2015). This coupled with the complex geometry of pump impellers can result in shrinkage defects. Therefore, there is need to find a solution to these filling and solidification defects which are found when casting austenitic stainless-steel pump impellers from less costly sand casting process.

1.3.2 Specific problem statement

This study will evaluate the filling and solidification defects encountered while casting stainless-steel pump impeller via sand casting. The pump impeller design is intricate and consists of thin blades (2 mm) and junctions. Thin-walled sections have low volume/area ratio (modulus), which presents a relatively larger surface area per unit volume and increases the cooling rate in accordance with Chvorinov's relation (Rundman 2005). This means that solidification in the thinner section is relatively faster, and thereby likely to solidify before completely filling the entire mould, thus resulting in misrun and cold-shut defects. According to Saxena et al. (2013), junctions are known to have the tendency of mass concentration development, which can be locations for shrinkage porosity during solidification. Bad junctions also result in additional resistance in metal flow due to surface area and heat transfer inefficiencies.

1.4 Objectives

1.4.1 Main objective

To optimise sand casting process (filling and solidification) of austenitic stainless-steel pump impeller using a combination of numerical modelling (MAGMAsoft® simulation) and additive manufacturing (Voxeljet VX1000 series).

1.4.2 Specific objectives

a) To use 1060 aluminium as a benchmark in evaluating effect of pouring temperature and wall thickness on the quality of sand cast products.
b) To evaluate the effect of wall thickness and junctions on the filling and feeding of sand cast austenitic-stainless steel pump impeller using a 3D printed mould.
c) To evaluate effect of pouring temperature on the filling and feeding of sand cast austenitic stainless-steel pump impeller using a 3D printed mould.
d) To compare filling and feeding of sand cast austenitic stainless steel with nodular cast iron pump impellers using 3D printed moulds.

1.5 Research questions

a) What is the effect of pouring temperature and wall thickness on the quality of 1060 aluminium?
b) How does wall thickness and junctions affect filling and feeding of sand cast austenitic-stainless steel pump impeller?
c) What is the effect of pouring temperature on the filling and feeding of austenitic stainless -steel pump impeller?
d) How does filling and feeding of sand cast austenitic stainless steel and nodular cast iron pump impellers differ?

CHAPTER 2

LITERATURE REVIEW

2.1 Sand Casting Process

The sand casting process is widely used for the manufacture of complex shaped components which are normally difficult and expensive to produce by other manufacturing processes (Figure 2.1). It involves heating material to its melting point followed by pouring in a mould cavity of a desired shape and allowed to solidify (Kamble and Kadam 2016) and (Zhang et al. 2009). When solidification is complete, the mould made of sand, is broken and the casting ejected for further processing. Both filling and solidification affect the quality of the casting produced. In accordance to Kamble and Kadam (2016), filling can be defined as a process which involves pouring of the molten into pouring basin/sprue and channelled through the gating system towards the mould cavity. After filling, the molten metal will solidify inside the mould before shaking out and knocking off. Solidification can be defined as phase transformation from liquid state to solid state with the decrease in viscosity as the temperature drops (Kurz and Fisher 1986). During the solidification process, heat is transmitted in three different forms namely conduction, convection and radiation. As the casting solidifies, it shrinks/contracts and the characteristic mode of contraction depends on the alloy composition. Alloys solidify through solute rejection and result in a dendritic structure which promotes compositional variations, segregation and micro-porosity throughout the casting (Askeland & Phule 2006). These micro-pores are referred to as shrinkage voids and they affect the quality of the product. Feeders are normally used to avoid shrinkage defects by providing excess material as the casting shrinks (Askeland & Phule 2006). Figure 2.1 shows an example of an overview of a gating system of the sand casting process.

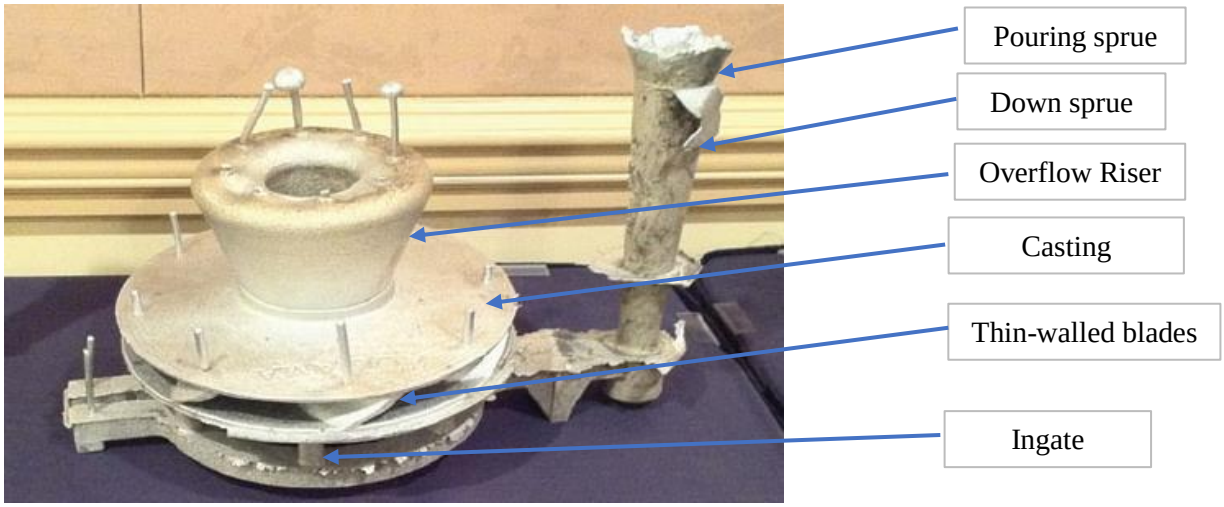

Figure 2. 1: A 3D view of a sand cast with runner system after shake-out.

Source: (Whitley 2013)

One of the major disadvantages of sand casting is in the production of thin-walled sections of good quality (free from defects) (Voigt 2002). One such example is the pump impeller which consist of thin-walled sections and junctions. Thin-walled blades inside the impeller promote filling defects (cold-shut and misrun) while junctions promote solidification defects (shrinkage porosity).

Cold-shuts appear as a crack with round edges and are normally associated with operating at low pouring temperatures and poor gating system design (Figure 2.2A). When two metal streams do not fuse together because of low operating temperatures they end up just touching each other and leave a crack like appearance in between them which is called a cold-shut defect (Jadeja et al. 2016). On the other hand, misrun defects appear as unfilled voids with a section or whole member of the casting remaining unfilled. This can be because of insufficient casting metal, low melting temperature, small wall thickness and poor gating system (Figure 2.2B).

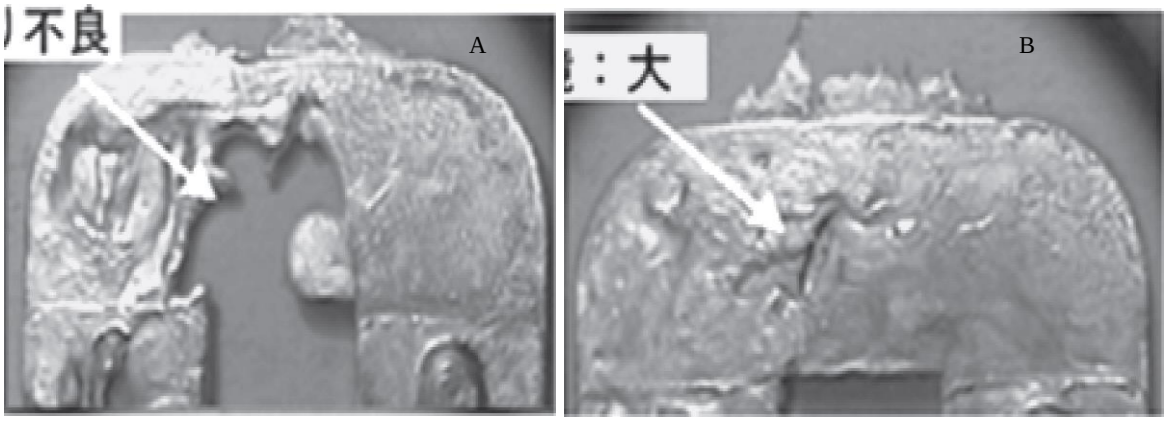

Figure 2. 2: Misrun (A) and cold-shut (B) defect

Source: (Iwata et al. 2014)

There are two different types of shrinkage namely open and close shrinkage. Shrinkage defects of short freezing range metals/alloys tends to be internal such as porosity while in long freezing range metals/alloys they mostly appear on the surface as surface depression (Choudhari et al. 2014). Open shrinkage is open to atmosphere and it can be categorised as pipe and carved surface. Closed shrinkage forms inside the casting and are also referred to as shrinkage porosity. The most common shrinkage defect is the closed shrinkage which is caused by hot spots inside the casting in regions where solidification is slow (Jadeja et al. 2016).

By improving the gating system and using feeders, casting defects like shrinkage cavities, cold-shut and misrun can be eliminated (Hebsur and Mangshetty 2014). A study by Jadeja et al.

(2016) found shrinkage defects to be the major cause of casting rejection and thus important the use of a simulation software to detect and eliminate them before the actual casting process is carried out.

Impellers are used in a variety of industries like automotive, mines, petrochemical, water industries, electrical plants, agriculture and aerospace (Iratkar and Gandigude 2017). They are designed to work in the corrosive environments and the selection of good corrosion resistant alloys is of utmost importance. To promote the filling process in thin-walled blades of pump impellers, aluminium, cast iron and gun metal are widely used as the casting alloys (Casting quality 2009). These alloys have shown accelerated deterioration in service thus justifying the importance of using more corrosion resistant alloys such as austenitic stainless-steel (Sharma 2014). Austenitic stainless-steel is an excellent corrosion resistant material consisting of alloying elements (Ni, Mo and Cr) which reduce the feeding distance and cause filling defects owing to solute diffusion during the solidification process (Fang et al. 2014). It shrinks more and loses heat faster during the solidification process. This promotes solidification defects and it is therefore important to understand filling and feeding processes of austenitic stainless-steel pump impeller.

Working environment of pump impeller and blade orientation can affect its life span during service. In some cases, pump impellers fail due to erosion corrosion which is caused by the synergistic effect of erosion of the solid particles present and the corrosive nature of the liquid. This was also noted by Sharma (2014) who did a failure investigation on a failed pump impeller which was produced from ductile iron and only lasted for 8 months. Sharma (2014) concluded that a severe metal loss was observed close to impeller blade. The impeller blades worn out quickly as compared to other parts of the impeller because of wall thickness and the fact that it is the working part of an impeller. According to Lei et al. (2014), the angle at which the blades are situated can also play a big role in the product functionality. The bigger the angle, the higher would be the pressure and lesser would be the chances for erosion corrosion and vice versa. Because of the impeller orientation which consist both of thin-walled sections and junctions, pump impellers are susceptible to both filling and solidification defects.

2.2 Filling Process

The filling process initiates when molten metal from the ladle is poured into the runner system to fill the mould cavity. The molten metal travels through different channels of the gating system before it reaches the mould cavity (Kamble and Kadam 2016). Possible defects which are associated with the filling when casting thin wall sections are misrun and cold-shut (Ziolkowski and Apelian, 2002). When molten metal is poured into a mould cavity the heat is lost to the mould wall and the surroundings.

Some of the factors which affect filling ability of a mould cavity are metal fluidity, metal viscosity, pouring temperature, superheat, oxides and inclusions, backpressure, surface tension and gating system (Voigt 2002). Below are brief discussions on how these factors plays a role in the way the mould cavity is filled.

2.2.1 Metal fluidity

Fluidity shows how well the molten metal can flow into the entire mould cavity before freezing (Rundma 2005). The higher the fluidity value, the higher the filling ability or the lower the fluidity value, the lower the filling ability (Ding et al. 2013). Fluidity is measured with the use of spiral test in millimetres (Campbell 1995). Possible defects which are associated with inadequate flow are misrun and cold-shut (Ding et al. 2013).

2.2.2 Metal viscosity

Viscosity is a measure of how thick the metal is due to internal friction mostly caused by applied force. It measures the fluid's resistance to flow when force is applied (Sleigh and Noakes 2008). Sleigh and Noakes (2008) states that viscosity is dependent on the temperature. As temperature increases cohesive forces which hold the molecules together decreases and movement of molecules increases, reducing viscosity. Pressure also affect viscosity of the liquid because under high pressure, molecules need a lot of energy for interaction and this makes viscosity to increase. Viscosity is inversely proportional to fluidity, the higher the viscosity the difficult it would be for the molten metal to flow (Sleigh and Noakes 2008). Viscosity can also be expressed as shear stress divide by shear strain as shown in equation 2.1;

$$\mu = \frac{shear\ stress}{Shear\ strain} = \frac{F/A}{v/l} \tag{2.1}$$

where μ is the coefficient of dynamic viscosity, F is the force, A is area and $^{v}/_{l}$ is the change in velocity gradient. A ratio of dynamic viscosity to mass density is called kinematic viscosity and can be mathematically represented by equation as:

$$v = \frac{\mu}{\rho} \tag{2.2}$$

where v is kinematic viscosity, μ is coefficient of dynamic viscosity and ρ is mass density.

2.2.3 Pouring temperature

The pouring temperature is an important parameter which indicates the energy content of the liquid metal during the casting operation. It is normally taken as the sum of the liquidus temperature and the superheat allowance which depends on the type of material being cast (Rundman 2005). At low pouring temperature, molecules of the molten material are more closely packed and rigid making it hard to flow the melt when force is applied. However, when the pouring temperature is increased, the cohesion force which keep the molecules together weakens up and molecules start to move more freely thus improving the fluidity of the molten metal. When the pouring temperature increases, viscosity decreases, and the filling ability increases. However, operating at high temperatures has its drawbacks which includes the formation of shrinkage porosity, hot tearing and low mechanical properties (Li et al. 2015). Castings produced at low pouring temperature tend to have globular-shaped fine grains while castings produced at high pouring temperature have dendritic-shaped coarse grains (Ferguson et al. 2014). This is a result of the low cooling rates associated with high pouring temperatures.

For instance, the filling ability of aluminium alloy was investigated at varying pouring temperatures of between 680 °C and 750 °C with a die preheated to 50 °C by Ding et al. (2013). Results showed low filling ability in the temperature range (680-730 °C) was attributed to high viscosity and low pouring temperature. Increasing the pouring temperature to 740 °C, resulted in a reduction in viscosity and an increase in filling ability. However, further increase in the pouring temperature to 750 °C resulted in the formation of shrinkage defects at the thicker sections of the casting (Ding et al. 2013).

When casting thin-walled sections, moulds need to be preheated before pouring to prevent premature solidification (Anglada et al. 2013). However, this practice cannot be used in sand moulds since their quality deteriorate with heat application (Anglada et al. 2013). For steels

with pouring temperature of about 1480 °C, moulds can be preheated to a temperature of about 1050 °C. This will reduce the heat transfer coefficient between the metal and the mould giving enough time for metal to fill the mould cavity without premature solidification. This was also noted by Zhang et al. (2009) who used a Low Pressure Die Casting (LPDC) process to cast a thin-walled aluminium (A356 aluminium) of about 1.5 mm wall thickness. The results showed an increase in filling ability of thin-walled section as pouring temperature and die temperature increase. This is because an increase in pouring temperature reduces the solidification rate and the metal will be hot for a long period of time to fill the entire mould cavity.

2.2.4 Degree of Superheat

Rundman (2015) defined degree of superheat as the temperature difference between the pouring temperature and melting temperature. It is mostly denoted as ΔT. It can be mathematically expressed as;

$$T_{superheat} = \Delta T = T_{pouring} - T_{melting} \quad (2.3)$$

where $T_{superheat}$ is the superheat temperature, $T_{pouring}$ is the pouring temperature and $T_{melting}$ is the melting temperature.

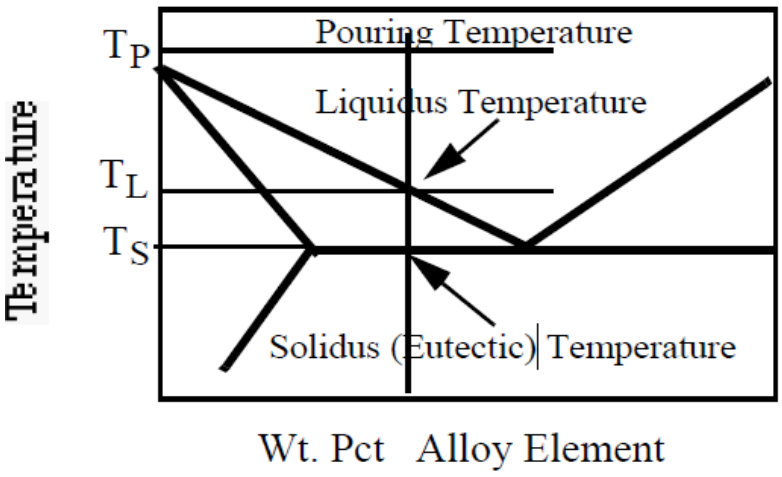

Figure 2. 3: A schematic representation of pouring temperature

Source: (Rundman 2005)

Rundman (2005) also state that when superheat is increased the viscosity decreases and filling increases. The decrease in viscosity is due to the decrease in cohesive forces which hold the molecules of liquid metal together. Bouska (2008) demonstrated the effect of superheat on the

flowability of aluminium alloy. Clearly when superheat increases, flowability also increases thus a linear curve was obtained in Figure 2.4.

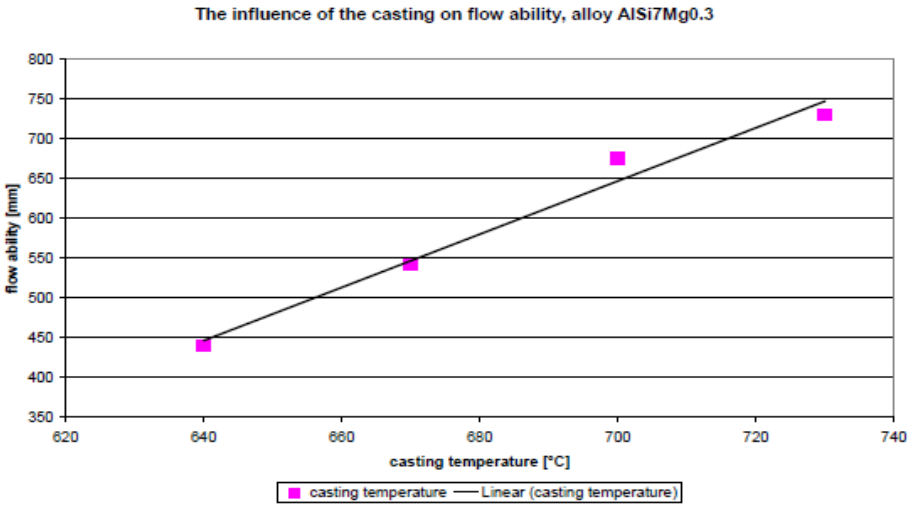

Figure 2. 4: The influence of the pouring temperature on flowability of an aluminium $AlSi_7Mg_{0.3}$ alloy.

Source: (Bouska 2008)

2.2.5 Oxides and inclusions

The presence of oxides and inclusions in the liquid aluminium metal during casting depends on the type of material melted (Di Sabatino et al. 2005). The amount of scrap used during melting determines the amount of oxides and inclusions formed (Di Sabatino et al. 2005). There are different types of oxides which can be found in metals like aluminium oxide and sulphur oxide. There are two types of inclusions namely endogenous and exogenous inclusions. Beňo and Špirutová (2014) defined endogenous inclusions as inclusions occurring within the metal due to chemical reactions of elements. Exogenous inclusions occur outside the metal due to slag, gasses, flux and others (Beňo and Špirutová 2014). Oxides and inclusions can be reduced/avoided by improving the melting process and controlling of scrap melted. According to Di Sabatino et al. (2005), presence of inclusions and oxides in the melt reduces the superheat temperature which in turn reduces metal flow and therefore the mould filling ability. This ultimately affects the quality of the casting produced (Di Sabatino et al. 2005) and (Rundman 2005). Therefore, it is important to make sure that the material used is cleaned prior to the casting process (Rundman 2005). Slag can be removed by skimming process as slag is light and will float at the top of the molten metal.

Based on the results from the investigation done by Di Sabatino et al. (2005), an aluminium alloy with no scrap proved to have high fluidity length. Scrap addition showed an increase of oxide content of aluminium alloy and decreases the fluidity length (See Figure 2.5). It was concluded that scrap addition does not only increase the oxides in the melt but also the inclusions (Di Sabatino et al. 2005). Both tend to block the pathway for metal flow and reduce the fluidity length. This can also cause defects like misrun and shrinkage porosity in the casting (Di Sabatino et al. 2005). Fluidity is also affected by the amount of inclusions and oxides in the metal (cleanliness of metal or scrap). It was clear from Figure 2.5 that pure A356 aluminium with no scrap addition has high fluidity level as compared to the one with 20 % and 50 % scrap addition. There was no change in fluidity level between aluminium with 20 % and 50 % scrap addition. This indicates the negative impact that oxide content has on the fluidity length (Di Sabatino et al. 2005).

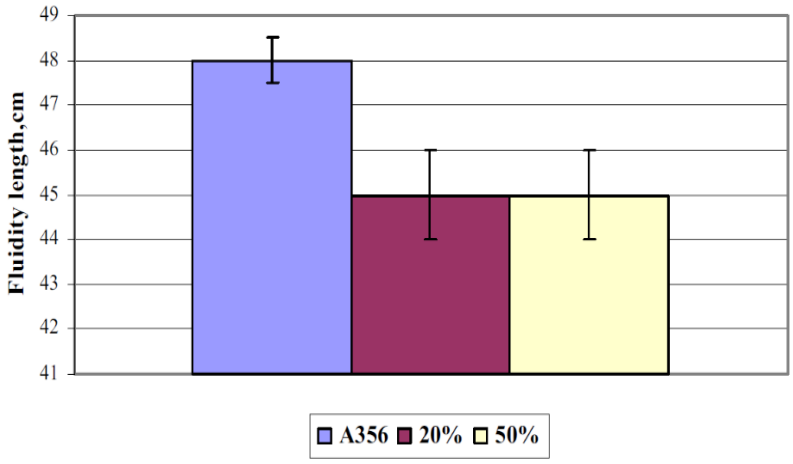

Figure 2. 5: Effect of scrap quantity on the fluidity measurements of three different alloys: Aluminium A356 with no scrap addition, aluminium A356 + 20 % scrap addition, aluminium A356 + 50 % scrap addition.

Source: (Di Sabatino et al. 2005)

2.2.6 Backpressure and surface tension

The backpressure is generated as a mould pressure which opposes the direction of fluid flow (Voigt 2002). Surface tension is an opposing force to the direction of fluid flow and this can be due to high metal viscosity and low superheat (Voigt 2002). Poor mould coating can also promote surface tension. Surface tension has a direct relation to backpressure, thus when it increases so does the backpressure (Voigt 2002). Backpressure can be expressed in terms of surface tension as Equation 2.4 (Campbell 1995);

$$P_{st} = \gamma[\frac{1}{R} + \frac{1}{r}] \quad (2.4)$$

where P_{st} is backpressure due to surface tension, γ is surface tension and *R* and *r* are orthogonal radii which characterise local shape of surface. For circular section channels, two radii will be equal and Equation (2.4) will be re-written as Equation (2.5) below.

$$P_{st} = {}^{2\gamma}/_{r} \quad (2.5)$$

It is therefore clear that as the radius is reduced, the backpressure increases. Equation (2.5) also shows that the surface tension has a direct relation with the backpressure. Thus, if the surface tension increases the backpressure also increases. In accordance to Voigt (2002), the resistance of metal flow inside the mould increases as the surface tension increase. Therefore, a decrease in wall thickness results in high surface tension and backpressure which reduce filling ability of thin-walled sections. Iwata et al. (2014) have shown the effect of backpressure on the filling ability of the mould cavity. An increase in backpressure which can be caused by casting complexity result in resistance of molten metal to flow. It was recommended that the molten metal pressure be increased by increasing plunger pressure and avoid casting defects like misrun and cold-shut.

2.2.7 Gating system design

A gating system as illustrated in Figure 2.6 below, is a sequence which direct liquid metal from the ladle to the mould cavity. It consists of different sections like pouring sprue, down sprue, sprue well, runner bar, ingate and feeders (Kamble and Kadam 2016). It must be designed in such a way that it promotes moderate mould cavity filling. Filling must be fast to fill the entire mould cavity but not too fast to prevent formation of turbulence flow. Slow mould filling can result in misrun and cold-shut defect. If the sprue height is short, velocity is reduced because of head pressure (Voigt 2002). This will reduce the speed of molten metal (Vaghasia and Ravi 2009).

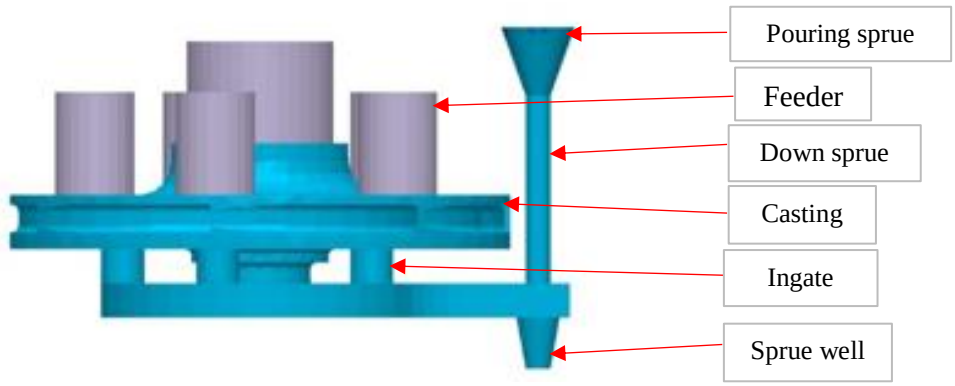

Figure 2. 6: Gating system overview

Source: (Mugeri et al. 2018)

The size and orientation of all these sections plays a vital role in the way the mould cavity is filled and solidifies. Poor gating design can cause various defects like gas porosity, shrinkage porosity, flow lines, cold-shuts and poor surface finish (Hu et al. 2012). When casting, the liquid metal is poured from the ladle into the pouring sprue which has a cone/cup like shape. The metal will then go down through a vertical pipe shaped down sprue before reaching the runner bar. (Vaghasia and Ravi 2009). Vaghasia and Ravi (2009) states that a sprue well can be used to trap the gasses and lower the velocity of the metal. A sprue well is placed at the bottom of the sprue and is conically shaped. The runner bar is normally rectangular bar shaped and it is used to further trap inclusions and gasses and to lower the velocity of the molten metal. The gate is a gateway for metal to enter the mould cavity and it is normally rectangular (Vaghasia and Ravi 2009). Depending on the velocity of the molten metal required, either a pressurized or unpressurized gate can be used. Vaghasia and Ravi (2009) states that a pressurized gating system can be used when high velocity inside the casting is required and an unpressurized gating system can be used when low velocity is needed. Feeders form an integral part of the casting and several solidification defects form because of poor feeder design (Choudhari et al. 2014). Thus, the feeder size, the number of feeders and the position of feeders play an important role on how a casting solidifies (Choudhari et al. 2014).

2.3 Solidification Process

The solidification process is a process where high temperature liquid changes to low temperature solid (Ding et al. 2013). It is a function of the alloy composition or metal. For pure metals, solidification occurs at a constant temperature when the molten metal drops to its freezing temperature. On the other hand, alloys solidify through solute rejection and this occurs

over a temperature range which is defined as the mushy zone (Askeland & Phule 2006). Mushy zone can be expressed mathematically as shown in equation 2.6 (Askeland & Phule 2006).

$$Mushy\ zone = \frac{\Delta T_f}{G} \tag{2.6}$$

where ΔT_f shows temperature interval between solidification start and where solidification finish. G is the free energy which is expressed in equation 2.7 (Askeland & Phule 2006).

$$G = H - TS \tag{2.7}$$

where *H* is the enthalpy, *S* is the entropy and *T* is the absolute temperature.

The width of the mushy zone is an important factor during solidification and defines the resulting structure forming after solidification (Askeland & Phule 2006). The formation of dendrites during alloy solidification results in detrimental factors such as segregation, compositional variation and most importantly micro-porosity because of shrinkage (Askeland & Phule 2006). Normally, feeders (liquid metal reservoir) are used to provide excess material to compensate for that shrinkage (Jadeja et al. 2016).

A feeder is normally lined up with an exothermal sleeve around it to prolong the time to the solidification onset Gajbhiye et al. (2014). The importance of sleeves was also noted by Gajbhiye et al. (2014) where a feeder of the correct size and placed in correct position was used but the hot spot still existed because the temperature of the molten metal inside the feeder solidified fast and reduced the effectivity of the feeder. Such hot spot according to Jadeja et al. (2016), is an analogous to a hot island likely to solidify last and promote formation of shrinkage porosity.

2.3.1 Feeder location

In recent years, the casting modulus can be automatically calculated using computer simulation software. Rundman (2005) defined casting modulus as a volume per surface area of the casting. Feedmod results from simulation showed locations in the casting which are susceptible to hot spots and porosity after solidification. It can be defined as a modulus required to feed a specific location in a casting. The results also showed the modulus of the specific hot spots which is used in sizing the feeder to be used (Whitley 2013). When casting sections with junctions, it has been noted that hot spots and porosity are most likely to happen at the junctions (Choudhari et al. 2014). Choudhari et al. (2014) concluded that depending on the results from simulation,

a feeder of right size can significantly remove the shrinkage porosity from the casting junction to the feeder.

2.3.2 Feeder size

The size of the feeder is dependent on the casting size (i.e. volume per surface area) which is called the modulus. In most cases a feeder is designed in such a way that it must solidify last so that it can draw the shrinkage voids out of casting to the feeder (Rundman 2005). The smaller the feeder size, the smaller is the amount of the metal to feed the casting (Kamble and Kadam 2016). According to Rundman (2005), the size of the feeder directly influences the casting yield. Kamble and Kadam (2016) defined casting yield as the ratio of the total amount of metal of the casting to the total amount of the metal poured during casting.

$$Casting\ yield = W_c/(W_c + W_g) \tag{2.8}$$

where W_c is the weight of the casting and W_g is the weight of the gating system (including feeders).

The importance of using correctly sized feeders was noted by Bhatt et al. (2014) where feeders of small size were used, and shrinkage porosity was observed inside the casting. An increase in feeder size from 50 mm diameter to 140 mm diameter showed positive results since all the hot spots were removed from the casting to the feeders. For optimization purpose, feeder size was increased further but there was insignificant change in the results (Bhatt et al. 2014). Bhatt et al. (2014) concluded that a further increase in feeder size decrease the yield of the casting. Khade and Sawant (2014) used a brake disc to perform an experiment with the help of a computer simulation software. The simulation results showed the upper thick part of the brake disc had a hot spot which after solidification caused porosity and shrinkage defects (Khade and Sawant 2014). This was because of a large modulus of the thick section making it the last part to solidify and causing a hot spot inside the casting.

According to Ciobanu et al. (2014) an equation for calculating modulus can be defined as a geometric solidification equation and a more accurate equation should be the one which will consider factors such as the feeders, the cores and hot corners.

$$M = \frac{V}{\sum_{i=1}^{i=n} k_i S_i} \quad (2.9)$$

where, n is the number of the surfaces through which the cooling occurs, i is the index of the surface, S_i is the surface with the index i, k_i is the cooling coefficient of the S_i surface. Equation (2.9) shows that cooling will only happen through one surface since i=1 and i=n (therefore n=1). It was also confirmed that the amount of the liquid metal in the feeder must be equal or greater than the alloy contraction at solidification (Ciobanu et al. 2014). This means that the amount of the metal to be used in the feeder depends on the alloy type and how that specific alloy contracts as shrinkage occurs. This amount of metal can be calculated as;

$$V_{RM} = \beta(V_T)/100 \quad (2.10)$$

where, V_{RM} is the volume of the metal required for alloy contraction is, β is the percentage of the volume shrinkage of the alloy during solidification and V_T is the total volume (volume of the casting, volume of riser neck and volume of the riser) (Ciobanu et al. 2014). Ciobanu et al. (2014) also claim that for a sound casting, a feeder must have a certain efficiency,ε,

$$\varepsilon . V_f \geq \alpha(V_c + V_f) \quad (2.11)$$

where, V_f the volume of the feeder, V_c is the volume of the casting and α is the volumetric contraction factor.

2.3.3 Feeder neck

A feeder neck as shown in figure 2.7 is placed at the base of the feeder connecting a feeder to the casting. Its main purpose or function is for ease removal of the feeder after casting (Radisa, Gulisija and Manasijevic 2009). Radisa et al. (2009) proclaim that when using MAGMAsoft®, feeder neck must be 'denotated' as a feeder neck for better simulation results.

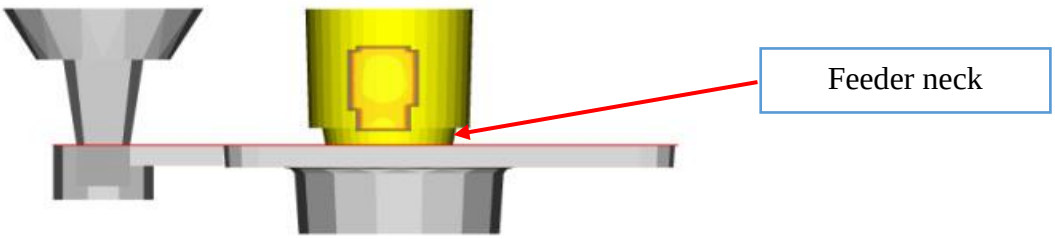

Figure 2. 7: Representation of feeder neck in a casting.

Source: (Choudhari et al. 2014)

For directional solidification, a feeder neck must have smaller modulus than the feeder (Ciobanu et al. 2014). Directional solidification according to Choudhari et al. (2014), states

that solidification must start from thinner to the thicker section of the casting with constant supply of the liquid metal to feed thicker section of the casting. For instance, in the work of Hebsur and Mangshetty (2014), shrinkage porosity was observed due to the use of smaller feeder neck which solidifies rapidly and prevent metal feed to the casting. Increasing the feeder neck by 10 mm and connecting it to the thicker section of the casting improved metal feed to the casting and removed the shrinkage defect from the casting to the feeder (Hebsur and Mangshetty 2014). The size of feeder neck is important since it affect how effective a feeder will be more than the size of the feeder (Ciobanu et al. 2014). This was again noted by (Gwidz, Pysz and Dworak 2010) who used MAGMAsoft® simulation to optimize feeder neck of the side feeders used during production of tooth casting. The first design showed massive porosity after actual casting due to feeder ineffective. Though there was metal in the feeder, feeding path was closed due to solidified feeder neck. Gwidz et al. (2010) increased the size of the feeder neck in the second design and the metal from the feeder was able to feed the casting and reduced the porosity which was caused by poor feeding of the casting.

Solidification of casting can be affected by a couple of parameters like wall thickness, junctions, composition, mould material and thermal properties. All these factors are discussed in section 2.3.4, section 2.3.5, section 2.3.6, section 2.3.7 and section 2.3.8.

2.3.4 Wall thickness

With high demand of thin-walled sections, it is important to understand the way they solidify because it determines the microstructure produced and the quality of the casting. In some cases, thin-walled sections solidify during pouring process before the mould cavity is entirely filled due to high rates of heat transfer between molten metal and mould wall (Li et al. 2015).

Fang et al. (2014) used ProCAST software package for simulations to optimise filling and solidification of manifold exhaust using investment casting. Shrinkage defects were observed at the exhaust body due to insufficient metal to feed the casting. It was reported that the shrinkage was also caused by rapid solidification at the pipes of the exhaust. This blocked the flow of the metal feed to the exhaust body. Fang et al. (2014) confirmed that increasing feeder size provided enough metal to feed exhaust body and eliminate shrinkage porosity from the casting to the feeder.

2.3.5 Junctions

A junction can be defined as a point of intersection where two or more sections coexist (Kumar and Ravi 2006). When two or more sections connect, the area of the point at which they connect to one another increases resulting in a high modulus. This results in higher solidification time thus making the casting prone to shrinkage defect at that point.

The size of the junction depends more on the number of the sections which are meeting. The higher the amount of sections meeting, the bigger will be the junction and the higher will be the shrinkage possibility at that junction (Saxena et al. 2013). There are different types of junctions such as L, T, V, +, Y, X and K. Junctions are more susceptible to hot spot and shrinkage porosity defects after solidification because they take time to solidify (Joshi and Ravi 2010). Sharp corners in junctions must be avoided because they promote stress raisers and shrinkage porosity (Singh et al. 2008). Such sharp corners also result in the unidirectional solidification of the casting and must be avoided by filleting. When casting an L-junction (illustrated in Figure 2.8 below), an inside fillet radius must be equal to the wall thickness and outside fillet radius double the wall thickness.

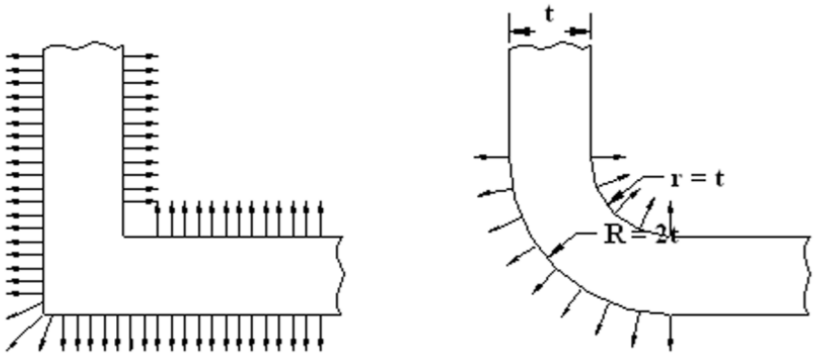

Figure 2. 8: Direction of heat transfer from solidifying metal to mould.

Source: (Kumar and Ravi 2006)

2.3.6 Composition

Different materials solidify in different ways depending on their composition. Some alloying elements when added either increase or decrease the filling ability of mould cavity (Hu et al. 2012). An example is strontium, which when added to aluminium decreases its filling ability (Bouska 2008). However, with copper addition the opposite was the case. Hu et al. (2012) used MAGMAsoft® simulation to determine effect of die casting on surface characteristics of thin-

walled AZ91D magnesium component. It was noticed that an addition of zinc alloy in AZ91D Magnesium can improve filling ability up to a certain composition as illustrated in figure 2.9. If too much zinc is added (>2%), the magnesium component will become susceptible to hot cracking which will affect its service because of premature failure during service (Hu et al. 2012).

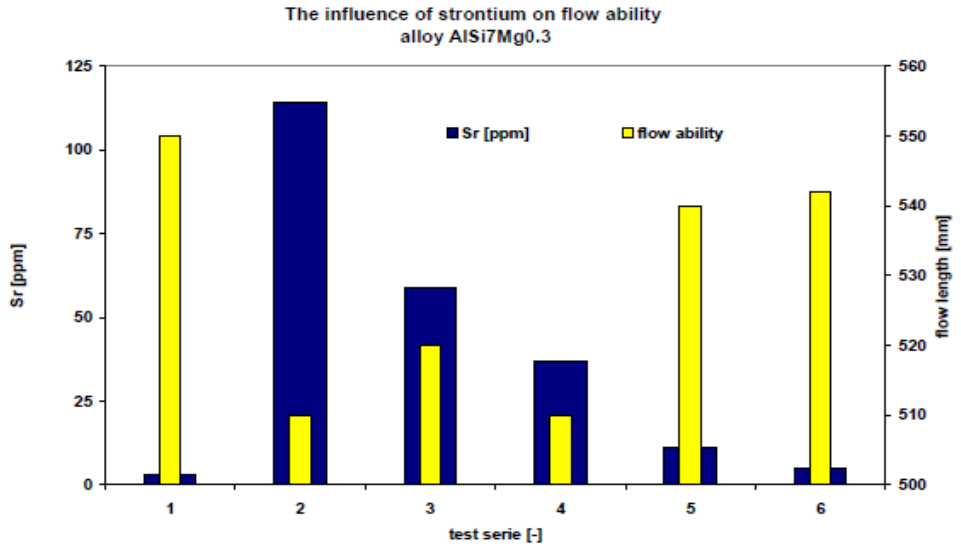

Figure 2. 9: Effect of strontium during solidification process.

Source: (Bouska 2008)

2.3.6.1 Pure metals

A pure metal has a defined melting point and will solidify at constant and defined temperature (Askeland & Phule 2006). In figure 2.10A, (A-B) shows a constant solidification temperature. Its solidification front will start at the mould walls towards the centre of the mould. At the mould walls, the metal solidifies much faster forming fine chill grains (Askeland & Phule 2006) as illustrated in figure 2.10B. Chill grains are normally distributed randomly, and they offer bad mechanical properties to the casting. This is due to cooling variation between the casting surface and the centre of the casting which solidifies last. This will be followed by long columnar grains which will grow in the direction opposite to that of heat transfer (Askeland & Phule 2006).

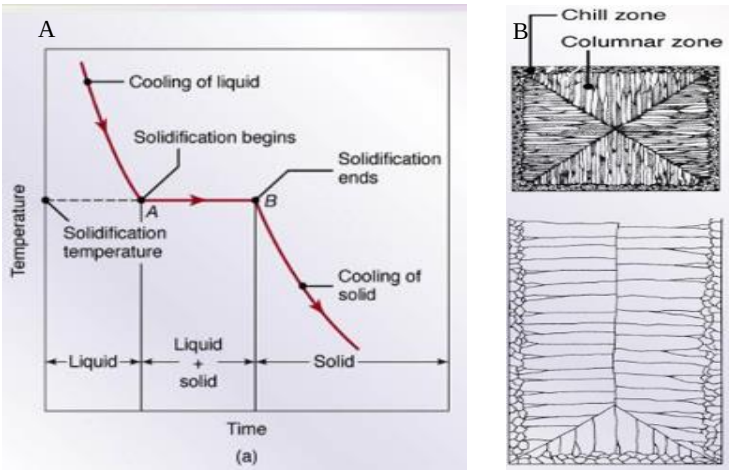

Figure 2. 10: Temperature as a function of time for pure metal (A) and microstructure of metal (B).

Source: (Askeland & Phule 2006)

2.3.6.2 Alloy

Figure 2.11A shows solidification of an alloy which starts when the temperature drops below the liquidus and finish when solidus temperature is reached (Askeland & Phule 2006). In between the liquidus and solidus temperature the metal will be in mushy/pasty state consisting of columnar dendrites which can hinder the easy at which the metal flows inside the mould cavity as shown in Figure 2.11B (Askeland & Phule 2006). High fluidity is commonly associated with pure metals because they do not form solid solution which in turn block the way for metal to flow.

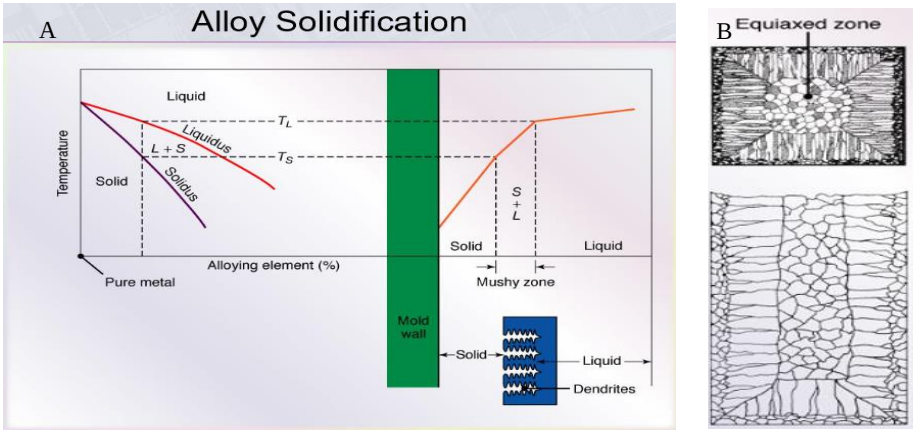

Figure 2. 11: Schematic illustration of alloy solidification (A) and alloy microstructure (B)

Source: (Askeland & Phule 2006)

2.3.7 Mould material

The type of the mould has an influence in the solidification pattern because it affects the rate of cooling of metal in the mould **(**Gorny and Tyrala 2013). Sand is the most preferred moulding material owing to its high refractoriness, high permeability, low-cost and availability (Mugeri et al. 2017). Two moulds which were made from two different types of sand i.e. low-density alumina silicate ceramic (LDASC) and silica sand were investigated by Gorny and Tyrala (2013). Varying wall thicknesses of 2 mm (1), 3mm (2), 5 mm (3) and 13 mm (4) were used. Results from that work showed that as the wall thickness decreases the cooling rate increase thus increasing the risk of filling defects as illustrated in Figure 2.12a and 2.12b below.

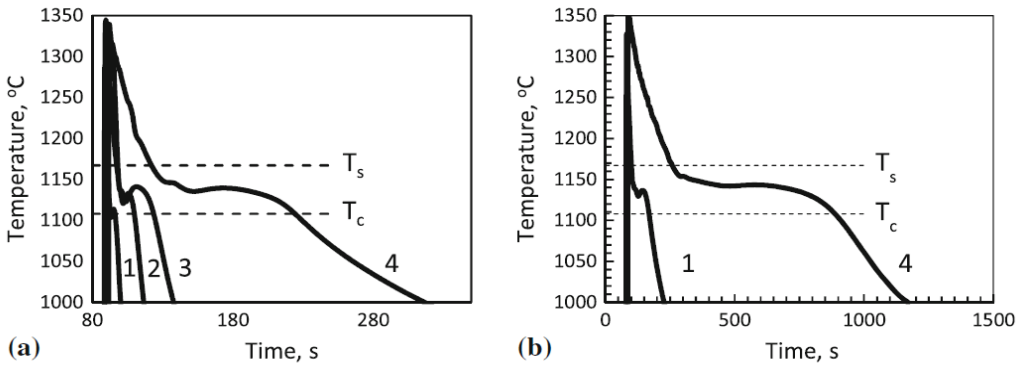

Figure 2. 12: Cooling curves of ductile iron in samples with different wall thicknesses: (a) foundry mould with the silica sand (SMS), (b) foundry mould with the LDADC sand.

Source: **(**Gorny and Tyrala 2013)

However, the decrease in cooling rate was different for two different mould materials due to low heat transfer of LDASC mould (See Table 2.1). Its cooling rate was lower than that of silica sand (See Figure 2.11a and 2.11b). Hence the filling ability of LDASC sand was higher than that of silica sand. Based on the results obtained, it was concluded that the cooling rate of 2 mm nodular cast iron casting made from LDASC mould can be compared to a 13 mm nodular cast iron casting which is made from silica sand (See Figure 2.13)

Table 2. 1: Relationship between mould material and heat transfer coefficient

Mould material type	Mould ability to absorb heat in $cm^2\ ^oC\ s^{1/2}$
Chromite	0.15
Zircon	0.13-0.15
Quartz sand	0.08-0.12
Olivine	0.10
Chemically bonded urethane moulding sand	0.10-0.12
Chemically bonded furan moulding sand	0.08-0.10
Chemically bonded shell moulding sand	0.10-0.11
LDASC, (Ashland Company)	0.018-0.03

Source: (Górny 2007)

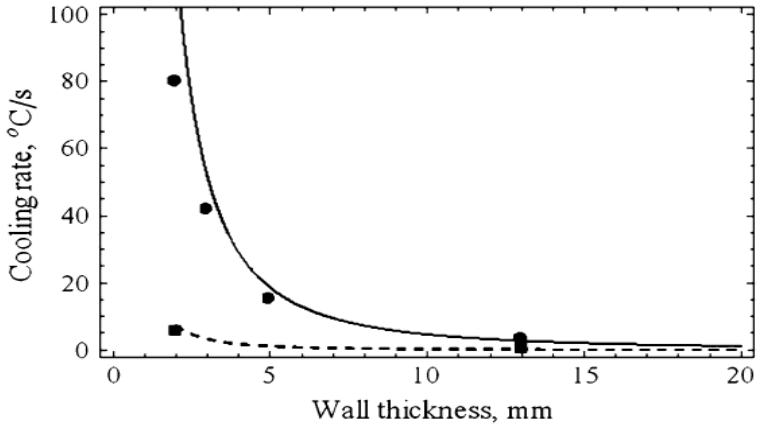

Figure 2. 13: Effect of wall thickness on the cooling rate of the casting: solid curve represents experimental points for SMS mould, dotted curve represents experimental points for LDASC mould.

Source: **(**Gorny & Tyrala 2013)

Thermal properties of the sand play a big role in the solidification of the casting. The mould with high heat transfer will have low filling ability compared to the one with high heat transfer. High heat transfer coefficient causes solidification to be fast because of high transfer of heat from the molten metal to the mould walls (Gorny 2012)

2.3.8 Thermal properties

There are different types of thermal properties like heat capacity, thermal conductivity, heat transfer coefficient and the rest. Heat capacity shows amount of heat energy needed to raise the

temperature of a given material (Askeland & Phule 2006). It is expressed mathematically in equation 2.12.

$$C = \frac{dQ}{dT} \tag{2.12}$$

where dQ is the energy required to produce a temperature change equal to dT and C is the heat capacity.

Thermal conductivity on the other hand shows the ability of a given material to allow heat energy to pass through it from high temperature to low temperature (Askeland & Phule 2006). Heat transfer coefficient shows how fast or slow the heat will be transferred from one surface to another (Pedersen et al. 2006) and it is expressed in equation 2.13.

$$h = \frac{q}{\Delta T} \tag{2.13}$$

where h is the heat transfer coefficient, q is the amount of heat required (Heat Flux) and ΔT is the difference in temperature between the solid surface and surrounding fluid area.

Generally, a higher temperature signifies a higher heat transfer coefficient. Sun and Chao (2009) showed that as the temperature drops, so does the heat transfer coefficient. As the distance between the mould and the molten metal increases, the latent heat decreases. The increase in the gap between mould wall and molten metal due to contraction during solidification also result in decrease in heat transfer coefficient. Heat transfer coefficient is highest when the metal is in contact with the mould wall and as the distance between the mould wall and the metal increases, heat transfer coefficient starts to decrease (Pedersen et al. 2006) (See Figure 2.14). The higher the heat transfer coefficient the faster will be the cooling rate (Cellini and Tomesani 2008). Heat transfer coefficient is more dependent on the temperature of molten metal, the type of the sand used to make mould and the distance from the mould wall to the molten metal. Figure 2.14 shows that as the fraction solid increases the heat transfer coefficient decreases but up to a specific point and then remain constant (Pedersen et al. 2006).

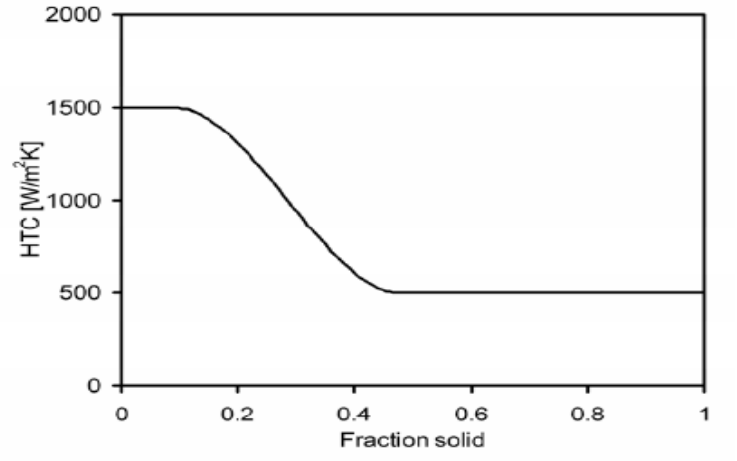

Figure 2. 14: Heat Transfer Coefficient (HTC) as a function of the solid fraction in the surface of the casting next to the mould.

Source: (Pedersen et al. 2006)

2.4 Conventional vs Digital mould making process

Mould cavity resembles an inverse of the casting to be produced (Rundman 2005). The production of this cavity involves pattern manufacturing, core box manufacturing, production of core, production of drag and cope and assembly. This can take weeks if not months depending on the complexity and size of the mould cavity produced (Traeger 2016). With the availability of additive manufacturing technology (AM) in the foundry industry, the production of mould cavity and core prints have been improved through reduction of lead time and ease of complex moulds and cores production (Nyembwe et al. 2016). Approximately 50% of the lead time can be reduced with the use of 3-Dimensional (3D) printing technology (Traeger 2016).

AM is a layered based technology process used to produce 3D components from a digital CAD file (Chougala and Bansode 2016). This process can be used in the production of the end products of automotive, medical implants and aircraft. Lately, it has been highly recommended in the production of sand moulds and cores (Nyembwe et al. 2016). There are different types of AM depending on the process and material used. Selective Laser Sintering (SLS) is one of the AM processes where the material is first melted to make a layer. Whereas in steriolithography (SLA) a photo-reactive resin is cured using ultraviolent (UV) laser one layer at a time. Voxeljet VX 1000 as illustrated in Figure 2.15 was designed to use both sand and plastic as a printing material.

Figure 2. 15: Overview of Voxeljet VX1000 3D printer

Source: (Mauchline, Van Tonder and De Beer 2017)

Foundry industry has adopted the use of Voxeljet VX1000 (Voxeljet, Germany) in the production of sand moulds and cores due to its advantages which involve reduction of design lead time, and capability to produce complex moulds (Nyembwe et al. 2016). This is due to the elimination of traditional production steps by using the digital AM process as demonstrated in Figure 2.16 below (Whitley 2013).

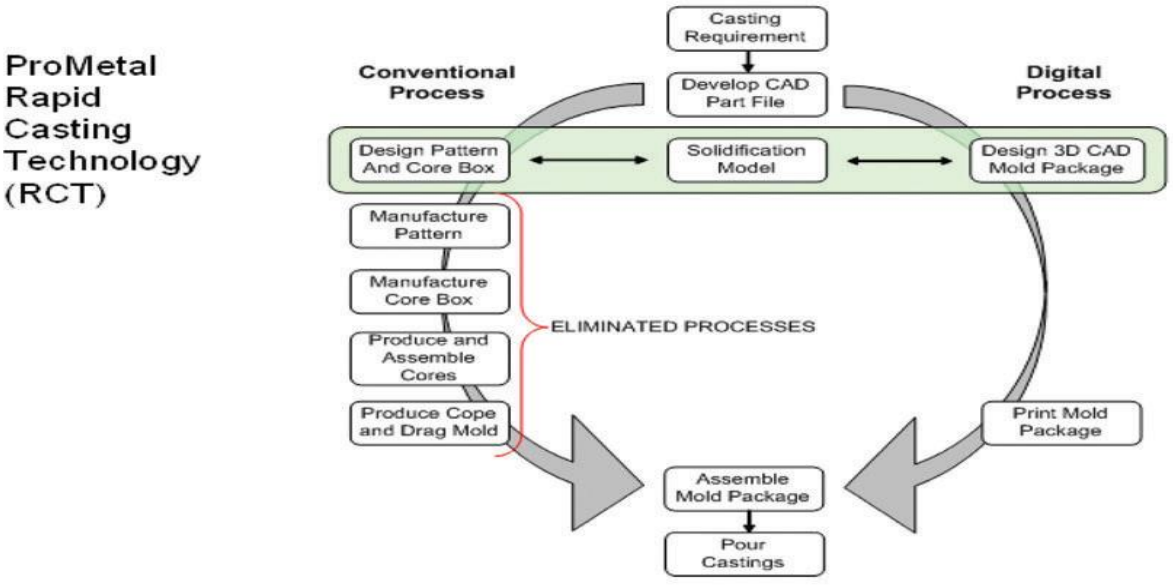

Figure 2. 16: Conventional vs digital mould making process.

Source: (Whitley 2013)

The process of mould printing using Voxeljet VX1000 as illustrated in Figure 2.17 involves design of a 3D component with the use of computer software and save it as an STL File format. An STL CAD file is imported to the Voxeljet VX1000 machine and a 3D component printed. This machine uses silica sand which is pre-coated with sulphonic acid. The binder used is furan binder (Nyembwe et al. 2016). The printing process involves depositing a thin layer (typically 300 µm) of coated silica sand on the building platform. The printing will only follow selected part per CAD file. The application of furan binder will promote bonding of sand particles by closing the spaces between them. The infrared radiation speeds up hardening process by preheating the building platform. This process continues until a 3D component is finished printing followed by sand recycling (Traeger 2016). Chougala and Bansode (2016) state that the unfused sand provides support to a 3D component being printed. Depending on the alloy to be cast, the mould can be oven dried for approximately 2 hours at 110°C to increase its strength for handling purpose (Nyembwe et al. 2016).

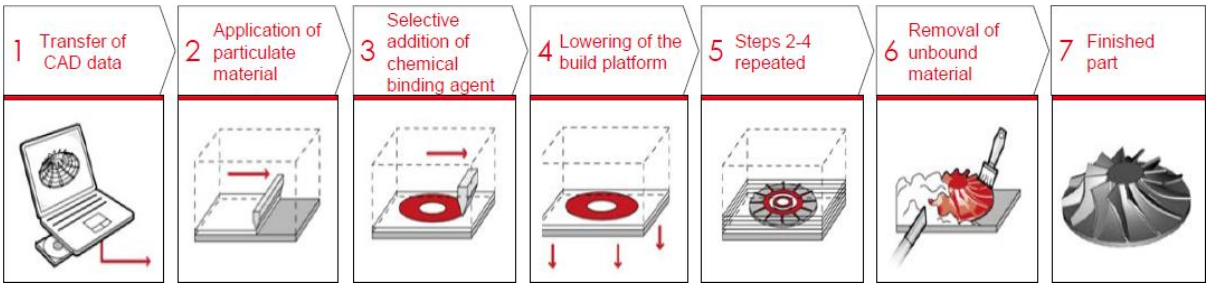

Figure 2. 17: Voxeljet VX1000 step by step printing process

Source: (Traeger 2016)

2.5 Casting Modelling and Simulation

Casting simulation is a method where a computer software is used to imitate the real casting process. The software was developed to improve the casting process through defect elimination, yield improvement and production improvement (Arunkumar et al. 2015). It consists of different thermodynamics and fluid flow mathematical equations. Some of these equations were derived as follows;

2.5.1 Mathematical modelling and simulation

Modelling of casting simulation is derived from the conservation of mass, conservation of momentum and conservation of energy (Ding et al. 2014). All these three conservations form part of Navier-Stokes equations (Guofa, Xiangyu, Kuangfei and Hengzhi 2009). Below are

derivations of conservation of mass, conservation of momentum and conservation of energy. Simulation of mould filling is governed by gravitational force, heat transfer of the molten metal and movement of alloying element.

When the molten metal enters the mould cavity, its velocity can be correlated to the static pressure. The Bernoulli's equation at the gate can be expressed by equation 2.14 (Iqbal et al. 2012).

$$p_1+\frac{1}{2}\rho_1 v_1^2+\rho_1 g h_1=p_2+\frac{1}{2}\rho_2 v_2^2+\rho_2 g h_2+\Delta p_{loss,1-2} \quad (2.14)$$

where p is static pressure, ρ is the density, *v* is the velocity, *g* is the gravitational force, *h* is the height from the reference.

The loss of molten metal pressure can be mathematically represented by equation 2.15.

$$\Delta p_{loss,1-2}=f\frac{L_{1-2}}{d}\frac{\rho v^2}{2} \quad (2.15)$$

where L_{1-2} is the length of the of the gate between cross sectional areas, *d* is the diameter and *f* is the friction force.

Iqbal et al. (2012) proclaims that if volume through which the molten metal flows is considered constant, Eulerian approach can be used to derive conservation of mass as shown in equation 2.16.

$$\frac{\Delta m}{\Delta t}=\sum_i mi \quad (2.16)$$

From equation 2.16, continuity equation can be simplified to equation 2.17 when the molten metal is assumed to be flowing uniformly is x_1, x_2 and x_3 direction (Iqbal et al. 2012), (Ding et al. 2014), (Guofa et al. 2009) and (Zhang, Liu and Wang 1995).

$$\frac{\partial u_1}{\partial x_1}+\frac{\partial u_2}{\partial x_2}+\frac{\partial u_3}{\partial x_3}=0 \quad (2.17)$$

where u_1, u_2 and u_3 are velocity vectors in x_1, x_2 and x_3 coordinate directions.

For Newtonian fluids, normal and shear components of viscous stress tensor acting on the molten metal in x_1, x_2 and x_3 direction can be written as shown equation 2.18 (Iqbal et al. 2012).

$$\tau_{11}=-\mu\left[2\frac{\partial u_1}{\partial x_1}-\frac{2}{3}\left(\frac{\partial u_1}{\partial x_1}+\frac{\partial u_2}{\partial x_2}+\frac{\partial u_3}{\partial x_3}\right)\right]$$

$$=-\mu\left[2\frac{\partial u_1}{\partial x_1}-\frac{2}{3}divu\right] \tag{2.18}$$

where τ_{11} is the stress tensor, μ is the dynamic viscosity and div is divergence operator applied to velocity vector. Therefore, viscous stress tensor, τ, of Newtonian fluid can be written as equation 2.19;

$$\tau=\begin{bmatrix}\tau_{11} & \tau_{12} & \tau_{13}\\ \tau_{21} & \tau_{22} & \tau_{23}\\ \tau_{31} & \tau_{32} & \tau_{33}\end{bmatrix}$$

$$=\begin{bmatrix}-\mu\left(2\frac{\partial u_1}{\partial x_1}-\frac{2}{3}divu\right) & -\mu\left(2\frac{\partial u_1}{\partial x_2}+\frac{\partial u_2}{\partial x_1}\right) & -\mu\left(2\frac{\partial u_1}{\partial x_3}+\frac{\partial u_3}{\partial x_1}\right)\\ -\mu\left(2\frac{\partial u_2}{\partial x_1}+\frac{\partial u_1}{\partial x_2}\right) & -\mu\left(2\frac{\partial u_2}{\partial x_2}+\frac{2}{3}divu\right) & -\mu\left(2\frac{\partial u_2}{\partial x_3}+\frac{\partial u_3}{\partial x_2}\right)\\ -\mu\left(2\frac{\partial u_3}{\partial x_1}+\frac{\partial u_1}{\partial x_3}\right) & -\mu\left(2\frac{\partial u_3}{\partial x_2}+\frac{\partial u_2}{\partial x_3}\right) & -\mu\left(2\frac{\partial u_3}{\partial x_3}+\frac{2}{3}divu\right)\end{bmatrix} \tag{2.19}$$

Conservation of momentum (Navier-Stokes equation) takes into consideration the velocity of the molten metal as it goes down through a down sprue. Gravitational acceleration acting on the metal, viscosity of the metal, density of the molten metal and the pressure as shown in equation 2.20, 2.21 and 2.22 (Ding et al. 2014).

$$\frac{\partial u_1}{\partial t}+u_1\frac{\partial u_1}{\partial x_1}+u_2\frac{\partial u_1}{\partial x_2}+u_3\frac{\partial u_1}{\partial x_3}=-\frac{1}{\rho}\frac{\partial p}{\partial u_1}+g_{u_1}+\gamma\left(\frac{\partial^2 u_1}{\partial u_1^2}+\frac{\partial^2 u_1}{\partial u_2^2}+\frac{\partial^2 u_1}{\partial u_3^2}\right) \tag{2.20}$$

$$\frac{\partial u_2}{\partial t}+u_1\frac{\partial u_2}{\partial x_1}+u_2\frac{\partial u_2}{\partial x_2}+u_3\frac{\partial u_2}{\partial x_3}=-\frac{1}{\rho}\frac{\partial p}{\partial u_2}+g_{u_2}+\gamma\left(\frac{\partial^2 u_2}{\partial u_1^2}+\frac{\partial^2 u_2}{\partial u_2^2}+\frac{\partial^2 u_2}{\partial u_3^2}\right) \tag{2.21}$$

$$\frac{\partial u_3}{\partial t}+u_1\frac{\partial u_3}{\partial x_1}+u_2\frac{\partial u_3}{\partial x_2}+u_3\frac{\partial u_3}{\partial x_3}=-\frac{1}{\rho}\frac{\partial p}{\partial u_3}+g_{u_3}+\gamma\left(\frac{\partial^2 u_3}{\partial u_1^2}+\frac{\partial^2 u_3}{\partial u_2^2}+\frac{\partial^2 u_3}{\partial u_3^2}\right) \tag{2.22}$$

where *t* is time, g_{u_1}, g_{u_2} and g_{u_3} are gravitational accelerations in x_1, x_2 and x_3 direction respectively. γ is the kinematic viscosity.

During filling process, heat is being transferred from the molten metal to the mould walls. This makes the first metal to enter the mould cavity to be colder compared to the metal entering the mould cavity. Thus, the heat transfer energy during filling can be expressed by equation 2.23 (Ding et al. 2014).

$$\rho_L C_L\frac{\partial T}{\partial t}=\rho_L C_L u_1\frac{\partial T}{\partial u_1}+\lambda_L\frac{\partial^2 T}{\partial u_1^2}+S \tag{2.23}$$

where $\rho_L C_L \frac{\partial T}{\partial t}$ is convective heat transfer, $\lambda_L \frac{\partial^2 T}{\partial u_1^2}$ is conduction heat transfer and *S* is the source term. ρ_L is liquid metal density, C_L is the specific heat of liquid metal, λ_L is the thermal conductivity of liquid metal and L is the crystallization latent heat of molten metal.

According to Ding et al. (2014), solidification during casting occurs in three different heat transfer ways namely conduction, convection and radiation. Fourier differential equation was used to describe this heat transfer process during solidification in equation 2.24.

$$\frac{\partial T}{\partial t} = \alpha \left(\frac{\partial^2 T}{\partial u_1^2} + \frac{\partial^2 T}{\partial u_2^2} + \frac{\partial^2 T}{\partial u_3^2} \right)$$

$$= \alpha \nabla^2 T \qquad (2.24)$$

where α is thermal diffusivity, ∇^2 is Laplace operator and *T* is the moving interface.

There are several commercial simulation software that can be used to simulate casting process such as AutoCAST, ProCAST, SolidCAST, MAGMAsoft®, Z-CAST etc. MAGMAsoft® was adopted for simulation in the present study. This software was adopted due to its availability and user friendly.

After simulation, filling and solidification processes are visualised with the associated defects. This gives a chance to eliminate possible defects before real casting process is performed. Many foundries have adopted the use of simulation software in their production since both filling and solidification defects can be identified and eliminated/reduced before real production takes place (Hebsur and Mangshtty 2014). Some of these defects are air entrapment, misrun, cold-shut gas porosity, sand inclusion, burn on, porosity, shrinkage and cracks. The location, size and number of feeders can be identified with the software. With the use of simulation software, trial and error methods which leads to high cost and low yield are eliminated (Hebsur and Mangshtty 2014). However, for better results and understanding foundry experience is required (Hebsur and Mangshtty 2014).

2.5.2 MAGMAsoft®

MAGMAsoft® is a software designed to perform the numerical simulation of molten metal flow and solidification phenomena in different casting processes such as sand casting, die casting and investment casting (Sulaiman and Pio 2004). MAGMAsoft® simulation was used by Sulaiman and Pio (2004) and they noticed that the runner tip with lowest thickness of 7mm solidifies after 60 seconds and the centre of the casting solidifies after 400 seconds (because of

high modulus value). Filling and solidification results were found useful to make decisions on designing the mould, feeder, down sprue, runner and gating system as well as setting the casting process parameters to achieve the desired casting quality (Sulaiman and Pio 2004).

Iqbal et al. (2012) used MAGMAsoft® software to optimise an impeller after the first design showed mould erosion and gas porosity. The first design showed high velocity and pressure with turbulence flow. Hot spots and porosity were noticed at the thicker sections since the location of the feeder was misplaced by connecting it to the thinner section of the casting. Therefore, an optimised design was proposed with an improved orientation of the casting and the location of the feeder. This design consisted of a pressurized gating system to improve metal flow and feeder location was changed. The feeder was placed at the thicker section which was the exact location of shrinkage porosity. Shrinkage porosity was then completely moved out of the casting into the feeder.

The importance of MAGMAsoft® software was again noticed by Glonia et al. (2013) who improved the quality of the yoke casting which is used in the mining industry. Porosity defects were noted inside the casting because of poor directional solidification. MAGMAsoft® software was used to improve gating system and the use of chills promoted directional solidification to obtain a sound casting. A change in gating system from bottom to side improved uniform filling of mould cavity. Directional solidification was improved using chills. Chills improve heat transfer between molten metal and the sand. The casting therefore solidified faster than the feeder, removing all the porosity out of the casting to the feeder.

CHAPTER 3

METHODOLOGY

Summary

To optimize casting process of the sand cast austenitic stainless-steel pump impeller, several experiments were carried out. Literature has shown factors which could contribute to filling and feeding of this complex product. However, industry experiments were done to validate and optimize the current practice. Modelling and simulation were used as the tools to optimize filling and feeding of pump impellers. Modelling was done with the use of Solidworks 2016 while simulation was done with the use of MAGMAsoft® version 5.3. Voxeljet VX1000 was used as an additive manufacturing (AM) tool to optimize the moulding process used to produce moulds.

Experimental study 1 was performed to evaluate the effect of pouring temperature on the filling ability of complex geometry with junctions. Alloy used for this experiment was 1060 aluminium because of its high filling ability and availability. This study showed how backpressure inside the mould could affect filling ability of the mould. Effect of junctions on the quality of the casting was also investigated. The study showed how pouring temperature affect cooling rate which at the end affect the mechanical properties of the casting produced. Microstructural change as the pouring temperature changes was also evaluated.

Experimental study 2 was more focused on the filling and feeding of different wall thicknesses (1 mm, 1.5 mm, 2 mm, 2.5 mm and 3 mm) at a constant pouring temperature of 700 °C. This experiment used 1060 Aluminium due to its availability and high filling ability. The study showed how quality of the casting can be affected by change in wall thickness.

Experimental study 3 and 4 was the first trial to compare filling and feeding of austenitic stainless steel and nodular cast iron. Austenitic stainless-steel was discussed in Experimental study 3 as Design VX01 and Design VX02 while the comparison alloy (nodular cast iron) was discussed in experimental study 4 as Design VX03. Modelling was done with the use of Solidworks 2016 while simulation was done with the use of MAGMAsoft® version 5.3. Voxeljet VX1000 was used as an additive manufacturing (AM) tool to optimize the moulding process used to produce moulds. A 50 kg capacity induction furnace was used to melt both austenitic stainless steel and nodular cast iron scrap. A laser pyrometer was used to check the temperature before casting. After melting, a ladle was used to hold the metal to the casting bay where casting was done. Thermo-fisher spectrometer was used to verify chemical composition

of the scrap melted. Manual polishing machine was used to prepare the samples for metallographic investigations which were done using Nikon optical microscope. Vickers hardness machine was used to check hardness of the samples. The study showed how modelling and simulation can be used to optimize filling and feeding of the casting. The study also showed how wall thickness and junctions can affect different types of materials (austenitic stainless-steel and nodular cast iron). Effect of pouring temperature on the filling ability was also studied. An effect of how a design can affect the casting produced was also investigated.

The first trial produced defective casting and the second trial was done which was discussed in Experimental study 5 and 6. Austenitic stainless-steel used an improved Design VX04 of Design VX02 in Experimental study 5. Nodular cast iron on the other hand used Design VX05 as an improved design of Design VX03 in Experimental study 6. The changes which were done in Experimental study 5 and 6 were; runner system and feeding system and pouring temperature. The changes were done to mitigate the challenges encountered during the first trial (in Design VX02 and Design VX03). The main objective of this dissertation was focused in experimental study 3, 4, 5 and 6.

3.1 Experimental study 1: To optimise filling and feeding of thin-walled aluminium alloy component with complex geometry during sand casting.

3.1.1 Geometry

A sample geometry with a wall thickness fixed at 2mm was prepared using Solidworks 2016 software and fed into the MAGMAsoft® casting software. The test sample was designed to include different types of junctions i.e. ‘L’, ‘+’ and ‘T’ as illustrated in Figure 3.1. This was done to test the maximum fluidity required for the metal to flow through such intricate sections and able to solidify without tearing. Junctions are known to be more prone to tearing owing to mass and thermal concentration at these points (Kumar and Ravi 2006).

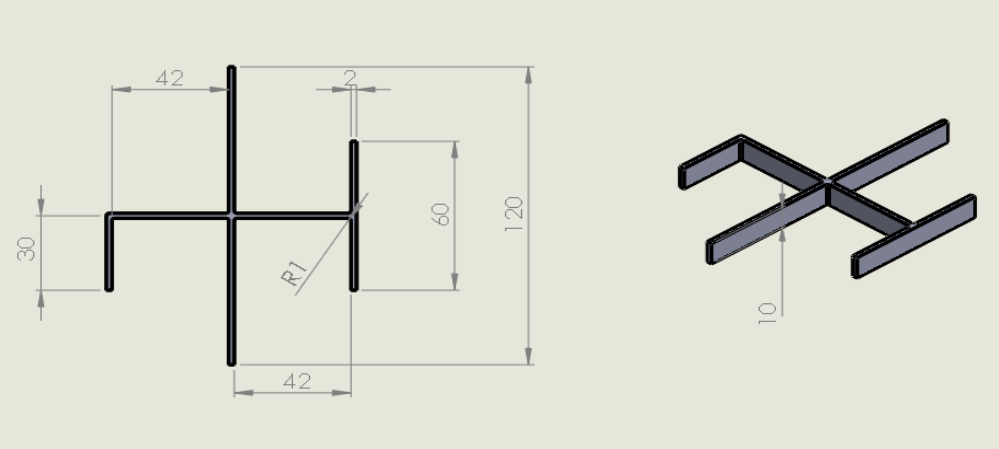

Figure 3. 1: A schematic representation of the 2mm test sample showing different junction geometries.

3.1.2 Simulation

Metal flow through the test samples (Figure 3.1) was simulated using MAGMAsoft® with a feeding effectivity of 20 %. The volume and surface area of the mould used were 22179 mm^3 and 22 mm^2 respectively. Mould used room temperature of 20 °C. The distance from the ladle to the inlet was 50 mm with a pouring time of 1.16 seconds. The casting was simulated at temperatures 700 °C, 730 °C, 760 °C, 790 °C,800 °C and 860 °C. Pressure simulation was carried out at different stages of metal flow to predict the molten metal flow against back-pressure inside the mould cavity. Comparative results were collected at approximately 430 milliseconds; 640 milliseconds and 1.1 seconds after pouring and the extent of mould filling. The pressure results were correlated with the pouring temperature values.

3.1.3 Moulding

The sand mould was prepared by 3D printing technology using the Voxeljet VX1000 series and was made up of silica sand with 1 % of furan binder and sulphonic acid as a catalyst. The strength of the mould was further improved by baking inside an oven at 100 °C for approximately 2 hours (Nyembwe et al. 2016).

3.1.4 Alloy and casting

Material used was 1060 aluminum alloy with the composition summarized in Table 3.1 determined by Thermo-Fisher Spectrometer (Figure 3.2). The selection of this material was

due to its good filling ability and availability. To verify the simulation results, a 1060 aluminum alloy was melted in a muffle furnace (See Figure 3.3) fitted with a temperature controller for accurate temperature measurements. The tapping temperature was read-off the temperature controller of the muffle furnace. Pouring temperature was read-off the laser pyrometer (Figure 3.4) at the pouring onset and was recorded in Table 3.2. The test sample (as in Figure 3.1) was cast and left to solidify for 24 hours.

Figure 3. 2: Thermo-Fisher Spectrometer

Table 3. 1: Chemical composition of 1060 aluminum

Element	Si	Mn	Al	Cu	Fe	Mg	Ti	V	Zn
Comp (%)	0.25	0.03	99.5	0.01	0.15	0.03	0.01	0.01	0.01

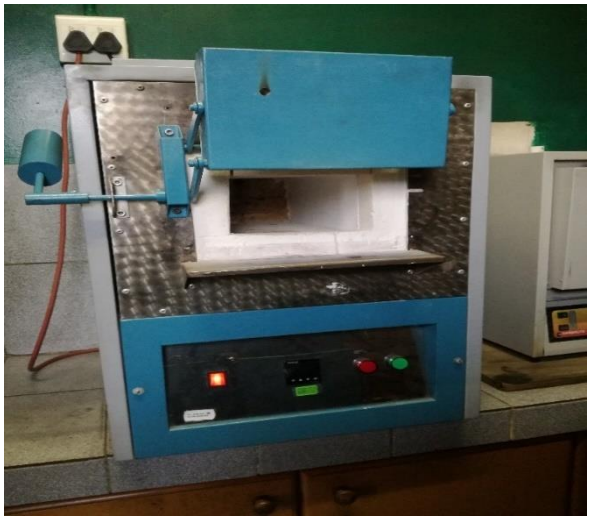

Figure 3. 3: Overview of Muffle furnace

Figure 3. 4: Laser pyrometer

Table 3. 2: Summary of temperature conditions used when casting the test samples.

Sample #	Pouring temperature (°C)
1	702
2	729
3	761
4	794
5	800
6	862

3.1.5 Testing

The cast samples were visually inspected to check for defects like misrun, cold-shut and shrinkage. Metallography samples were cut from each of the samples from approximately the same location for imaging and hardness testing. The samples were prepared using manual grinding and polishing machine (See Figure 3.5 and 3.6) respectively. The grit size of the papers used for grinding were 200 grit, 400 grit, 600 grit, 800 grit and 1200 grit. For polishing, 3µm followed by 1µm were used.

Microstructures were taken using a Nikon optical microscope (Figure 3.7) and the effect of pouring temperature was studied. Furthermore, a comparison on the dendrite/grain sizes for the different samples was made to ascertain the degree of cooling. This was done by firstly etching samples with the use of hydrofluoric acid etchant and micrographs were taken at 40X magnification. Hardness measurements were carried out with Vickers hardness machine (Figure 3.8) on each sample and an average of 71.65 HV_5

measurements was taken as a representative hardness value. For each sample, a load of 5 kg was used for a period of 10 seconds.

Figure 3. 5: Grinding machine

Figure 3. 6: Polishing machine

Figure 3. 7: Nikon eclipse MA200 optical microscope

Figure 3. 8: Vickers hardness machine (FV700)

3.2 Experimental study 2: Evaluating effect of wall thickness on the filling and feeding of thin-walled aluminium alloy components during sand casting

3.2.1 Geometry and alloy

A numerical model presented in Figure 3.1 was used to simulate metal flow during casting at varying thicknesses i.e. 1 mm, 1.5 mm, 2 mm, 2.5 mm and 3 mm. Solidworks 2016 software was used to sketch the model which was subsequently saved in a suitable file format and fed into MAGMAsoft® software for simulation. This was done to evaluate effect of wall thickness on the filling and feeding of casting produced at a preselected pouring temperature which is low enough to avoid the formation of shrinkage defects. A constant pouring temperature of 700 °C was used and a 1060 aluminum alloy was used. This temperature is slightly above the melting temperature of the 1060 aluminium alloy (645 °C) partly to conserve the energy of heating and avoid hot tearing associated with high pouring temperatures.

3.2.2 Simulation and moulding

During simulation, the mould temperature used was 20 °C and a pouring temperature was 700 °C. The distance from the ladle to the inlet was 50 mm (See Figure 3.9A) with an estimated pouring time of 1.16 seconds and feeding effectivity of 20 %. The purpose of simulation was to identify the primary thermal and pressure centers within the casting and to find the extent of filling after complete solidification. After simulation, moulds were prepared the same way as the moulds used in Experimental study 1. Figure 3.9 is a 3D view of cope (A) and drag (B) of test sample.

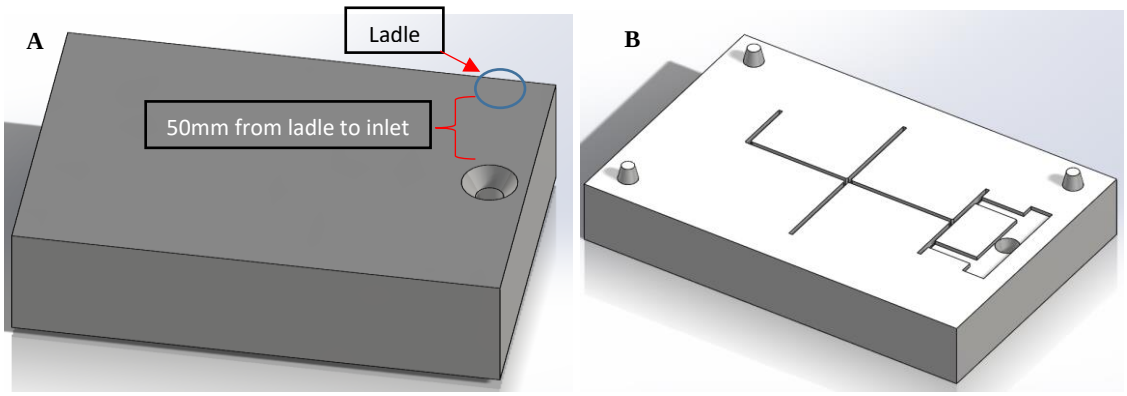

Figure 3. 9: 3D view cope (A) and drag (B) of test sample mould

3.2.3 Casting and Testing

To validate the simulation results and quality of the casting as earlier indicated, casting and testing was done. The charge was melted in muffle furnace. The furnace was heated to approximately 710 °C for 67 minutes for the first sample. When melted, slag was removed before pouring with the use of de-slagging spoon. After removing slag, temperature was measured again using infrared/laser pyrometer. When the temperature was 705 °C, ladle was taken out of the furnace and casting was done. For the second till final sample, the melting time was reduced because the furnace was already hot and availability of returned metal. Metallographic samples were prepared, and microstructural analysis was performed by means of an optical microscope on specimens etched with hydrofluoric acid etchant and micrographs were taken at 40X magnification to observe the grain sizes. The castings were also qualitatively inspected by visual examination for visual defects like misrun, cold-shut and shrinkage. Hardness tests were also carried out using a Vickers hardness tester from to correlate the cooling rate with the casting hardness.

3.3 Experimental study 3 & 4 (1st Trial): Optimization of filling and feeding of austenitic stainless steel and nodular cast iron pump impeller produced by sand casting using 3D printed mould.

3.3.1 Geometry

A pump impeller was designed using Solidworks 2016 software (See Figure 3.10). The product consists of an upper part, bottom part and the middle part. The middle part consists of thin-walled (2mm) blades. The choice of this product was because of the difficulties encountered during its production. Therefore, this will evaluate;

- How wall thickness and junctions affect the filling and feeding of sand cast austenitic stainless-steel and nodular cast iron pump impeller.
- How filling and feeding of austenitic stainless-steel pump impeller can be compared with the one of nodular cast iron.
- How pouring temperature affects filling and feeding of both austenitic stainless-steel and nodular cast iron pump impeller.

Thin-walled sections are known for quick solidification which promote casting defects like
A cold-shut and misrun (Voigt 2002).

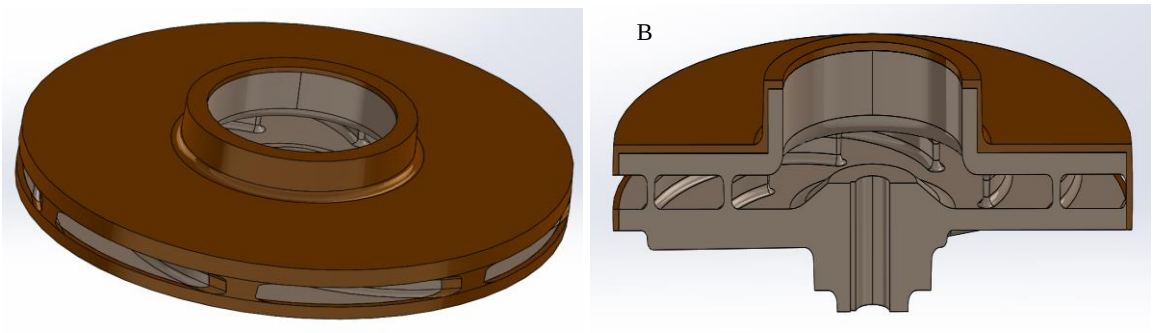

Figure 3. 10: 3D view (A) and section view (B) of a pump impeller

3.3.2 The Alloys

Two different alloys were used during production of pump impeller namely; austenitic stainless-steel and nodular cast iron. Austenitic stainless steel was used as a material of choice owing to its good corrosion and wear resistant properties (See Table 3.3 for chemical composition). Nodular cast iron was used because of its good flowability (See Table 3.4 for chemical composition).

Table 3. 3: Chemical composition of austenitic-stainless steel

Element	C	Mn	Si	P	S	Ni	Cr	Mo	Fe
Comp (%)	0.05	1.5	1	0.04	0.03	10	18	2.5	66.88

Table 3. 4: Chemical composition of nodular cast iron

Element	C	Cu	Mg	Mn	P	S	Si	Fe
Comp (%)	3.40	0.03	0.03	0.25	0.01	0.02	2.2	94.06

3.3.3 Simulation

Simulation set-up for both alloys was as follows: Simulation was done using MAGMAsoft® simulation software. The simulation was performed to identify feeder size, feeder location and number of feeders required during casting. It was also performed to optimise filling of pump impeller which is known to be highly affected by thin-walled blades. Feeding effectivity of 20 % was used. The total volume of the mould was 10782152 mm^3 with a total surface area of 650379 mm^2. Sand mould was at room temperature of 20 °C prior to pouring. The distance from the ladle to the inlet was 50 mm. The pouring temperature used was 1500 °C.

3.3.3.1 Austenitic stainless-steel pump impeller

Two different designs were analysed namely design VX01 (Figure 3.11A) and design VX02 (Figure 3.11B). Design VX01 is an old design which foundries normally used to produce austenitic stainless-steel pump impeller in sand casting and result in defective casting. A new optimised design (Design VX02) was done to improve the quality of the first design (VX01) which at the end will improve the lifespan of the pump impeller produced.

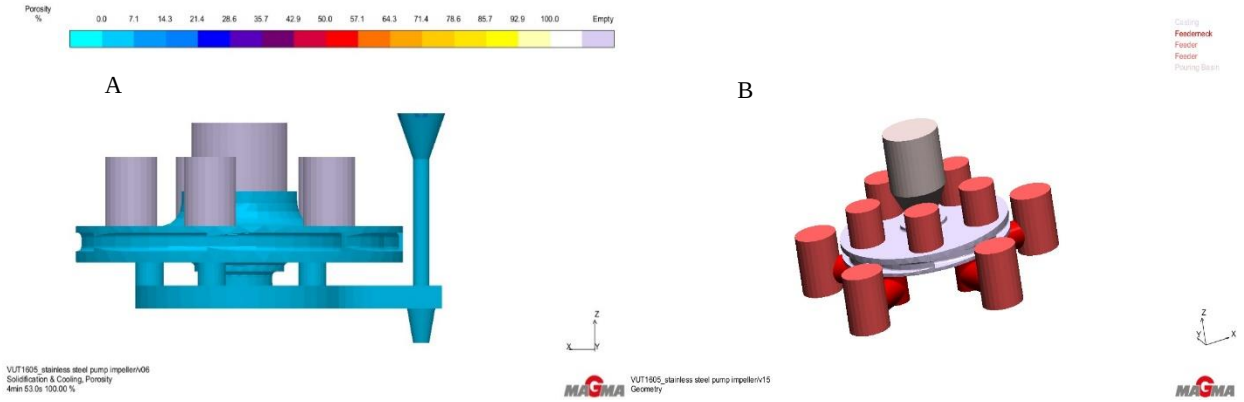

Figure 3. 11: Design VX01 (A) vs design VX02 (B)

Design VX02 was further optimized using optimization simulation package of MAGMAsoft® to improve the casting while maintaining the quality of the casting. In optimization simulation, variables which need to be changed were specified together with the objectives needed. Table 3.5 shows variables used for optimization simulation. Objectives specified were low porosity, low hot spot and high casting yield.

Table 3. 5: Design variables of austenitic stainless-steel pump impeller at 1500 °C pouring temperature

Design	Variables			
Feeder Radius (mm)	17	18	19	20
Feeder Height (mm)	32	33	34	35
No. of Feeders	3	4	5	

3.3.3.2 Nodular cast iron

Nodular cast iron used design VX03 during simulation process. Design VX03 was done to compare filling and feeding of nodular cast iron pump impeller with the austenitic stainless-steel pump

impeller. An optimization simulation of nodular cast iron was done for better quality and casting yield with the following variable; feeder radius, feeder height and number of feeders (as shown in Table 3.6). Objectives specified were as follows; low porosity, low hot spot and high casting yield.

Table 3. 6: Design variables of nodular cast iron pump impeller at 1500 °C pouring temperature

Design Variables				
Feeder Radius (mm)	17	18	19	20
Feeder Height (mm)	32	33	34	35
No. of Feeders	3	4	5	

3.3.4 Moulding

Both Design VX02 (for austenitic stainless-steel pump impeller) and Design VX03 (for nodular cast iron pump impeller) were moulded by 3D printed with the use of Voxeljet VX1000 series. Moulds of Design VX02 are shown in Figure 3.12A and 3.12B (cope), Figure 3.12C and 3.12D (drag) and Figure 3.12E and 3.12F (core) print. Moulds of Design VX03 are shown in Figure 3.13A and 3.13B (cope), Figure 3.13C and 3.13D (drag) and Figure 3.13E and 3.13F (core) print. The strength of the moulds was further improved by baking inside an oven at 100 °C for 4 hours.

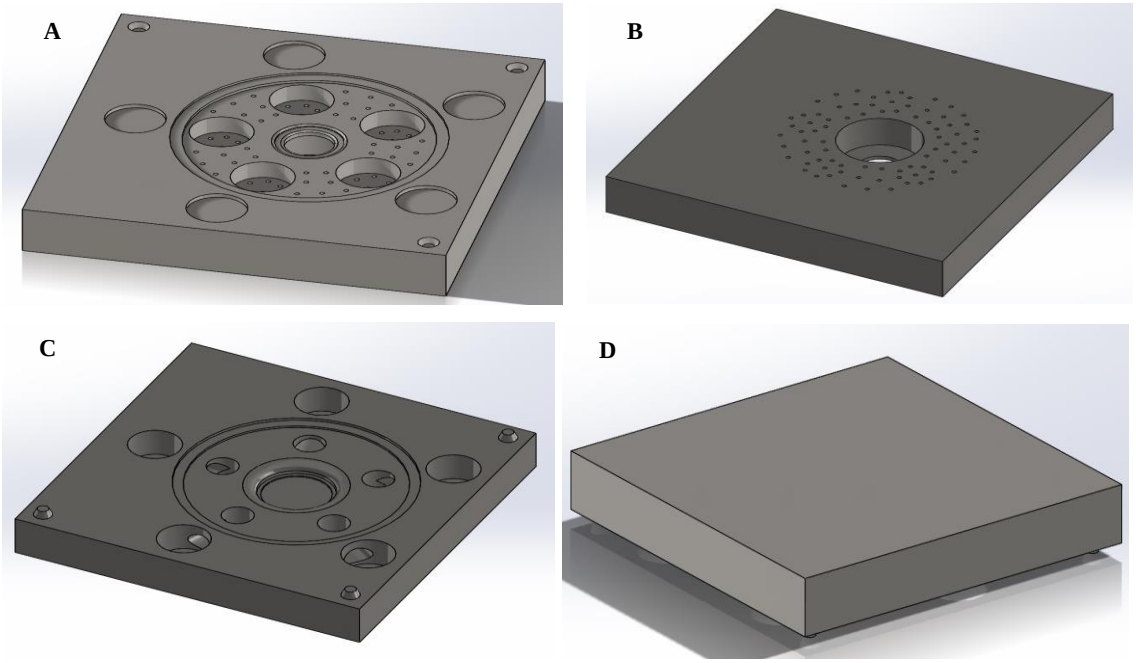

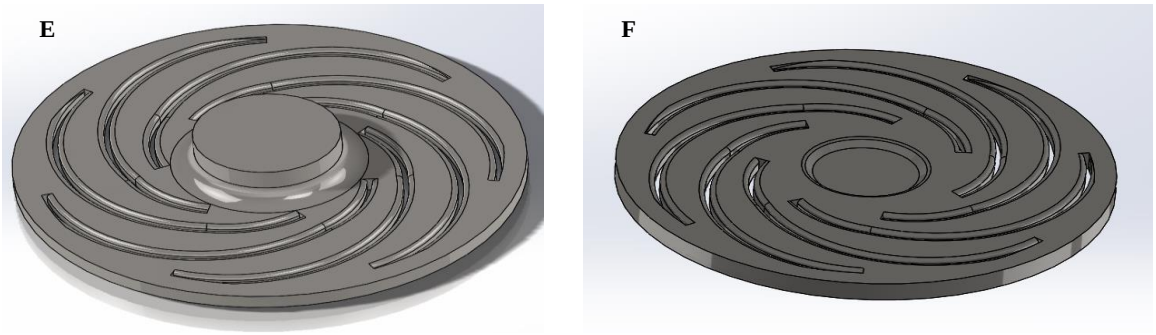

Figure 3. 12: Austenitic stainless-steel moulds cope (A and B), drag (C and D) and core (E and F).

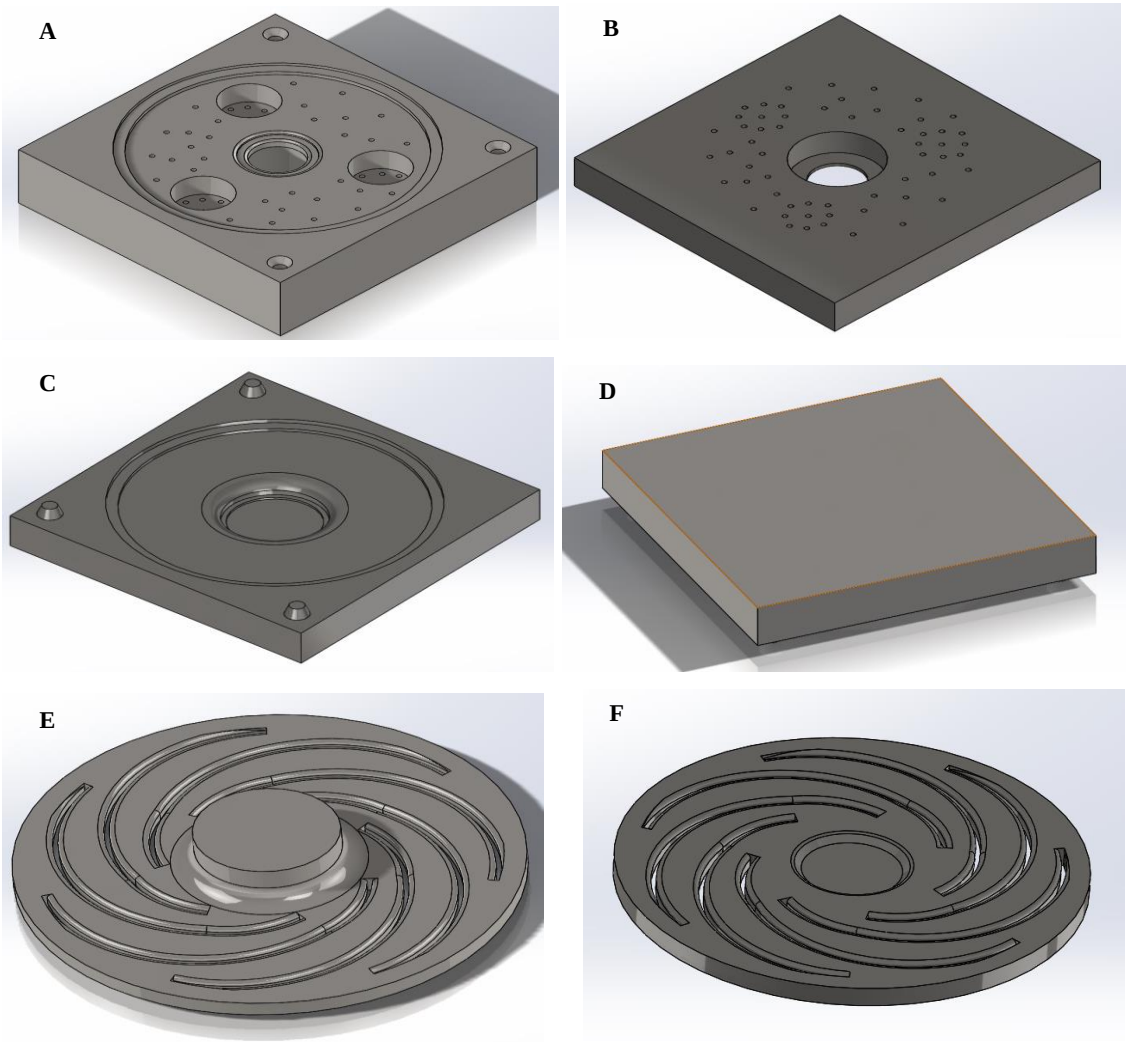

Figure 3. 13: Nodular cast iron moulds cope (A and B), drag (C and D) and core (E and F).

3.3.5 Casting and Testing

The charge was melted inside a 50 kg capacity induction furnace which was heated to approximately 1550 °C for 2 hours. When melted, slag coagulant was added on top of the melt. Slag coagulant of perlite ore traps slag inside the melt and make it float on top of the furnace for ease removal before pouring. After slag removal, a sample was taken to verify chemical composition of an alloy. Then the temperature was measured again using portable pyrometer. The molten metal was then tapped into a ladle and taken to a casting bay. The metal was then poured from the ladle into the mould cavity and allowed to solidify for 24 hours for both austenitic stainless steel and nodular cast iron. A solidified casting was then shaken out of the moulding sand and visually inspected. A polishing machine was used to prepare metallographic samples for microstructural analysis. Microstructural analysis was performed by means of a Nikon optical microscope on specimens etched with 3% Nitral etchant and micrographs were taken at 40X magnification. Hardness tests were also carried out using a Vickers hardness tester to correlate the cooling rate with the casting hardness.

3.4 Experimental study 5 & 6 (2nd Trial): Optimization of filling and feeding of austenitic stainless steel and nodular cast iron pump impeller produced by sand casting using 3D printed mould.

Both Design VX02 (austenitic stainless-steel pump impeller) and Design VX03 (nodular cast iron pump impeller) of the first trial were defective and a second trial was performed with a new and optimized runner system. In this 2nd trial, Design VX02 was optimize as Design VX04 (figure 3.14A) and Design VX03 was optimized as Design VX05 (figure 3.14B). The same pump impeller as the one used in Section 3.3.1 (Figure 3.10) was used.

3.4.1 Simulation

The moulding temperature used for both austenitic stainless steel and nodular cast iron was 20 °C. Pouring temperature of austenitic stainless-steel was increased to 1550 °C from 1500 °C with the feeding efficiency kept constant at 20 %. The increase of pouring temperature was to improve filling ability of Design VX02. The volume and surface area of austenitic stainless-steel pump impeller mould was 869984 mm^3 and 277357 mm^2 respectively. On the other hand, pouring temperature of nodular cast iron was reduced from 1500 °C to 1390 °C with a constant feeding efficiency of 20 %. This temperature was reduced to reduce chances of high temperature defects like shrinkage porosity. The volume and surface of nodular cast iron was 763652 mm^3 and 267100 mm^2 respectively.

Simulation software used was MAGMAsoft® for both austenitic stainless-steel and nodular cast iron.

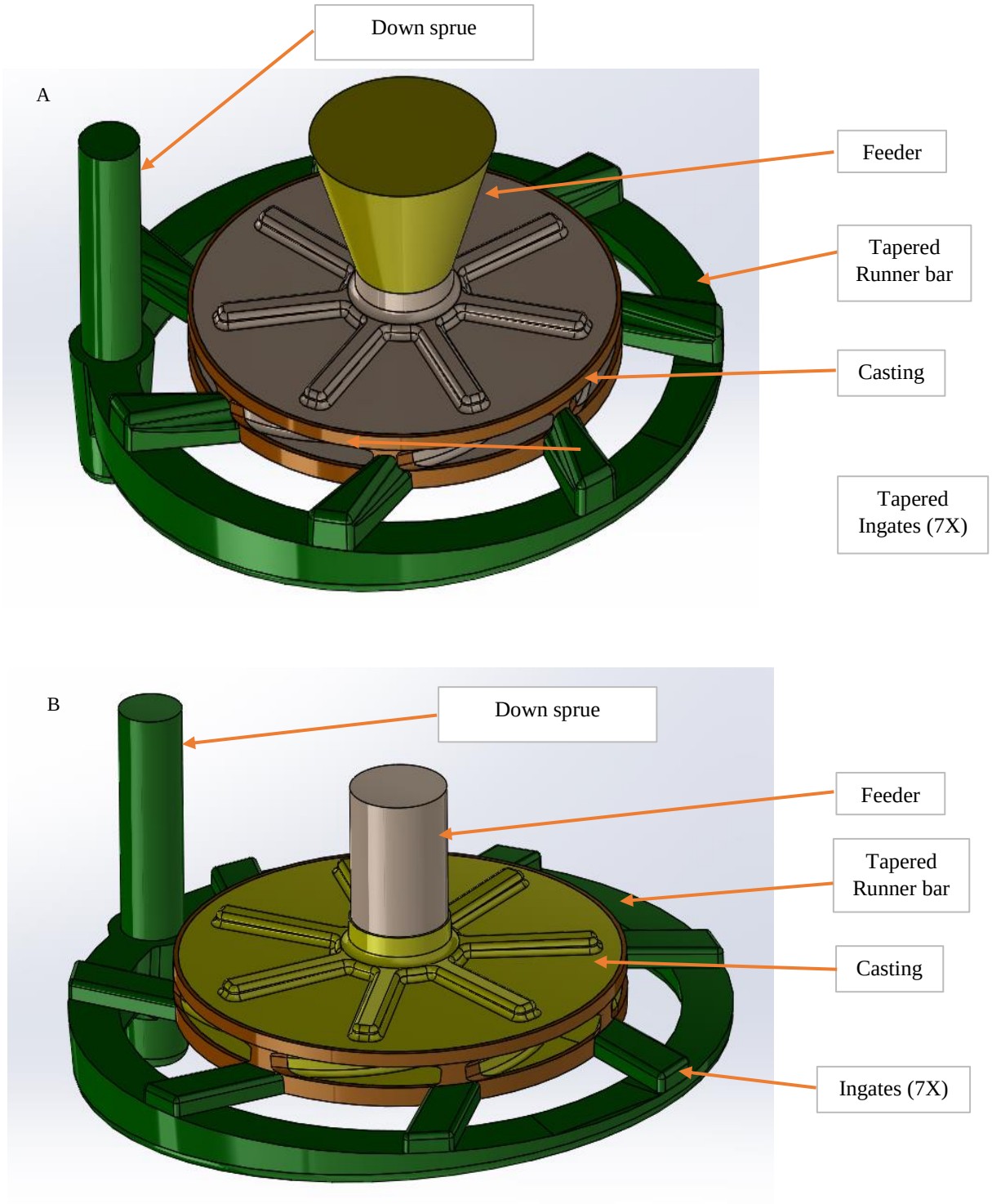

Figure 3. 15: Optimized Design VX04 (A) and Design VX05 (B) runner system.

3.4.2 Moulding

The production of the moulds was done with the use of Voxeljet VX1000. The strength of the mould was improved for handling purpose by baking inside the oven at 100°C for 4 hours. Moulds of Design VX04 are shown in Figure 3.16A and 3.16B (cope), Figure 3.16C and 3.16D (drag) and Figure 3.16E and 3.16F (core) print. Moulds of Design VX05 are shown in Figure 3.17A and 3.17B (cope), Figure 3.17C and 3.127 (drag) and Figure 3.17E and 3.17F (core) print.

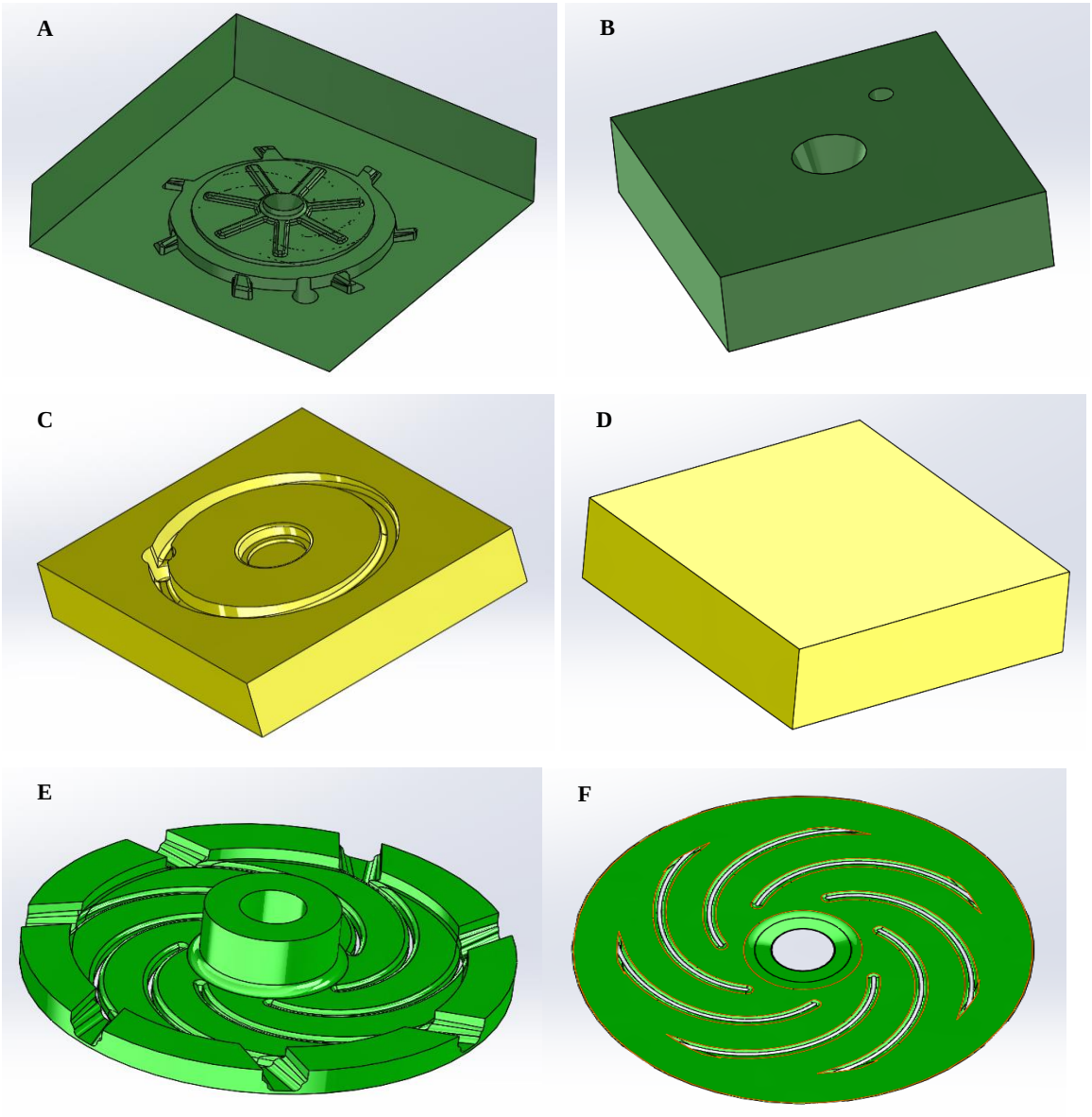

Figure 3. 16: Austenitic stainless-steel moulds cope (A and B), drag (C and D) and core (E and F).

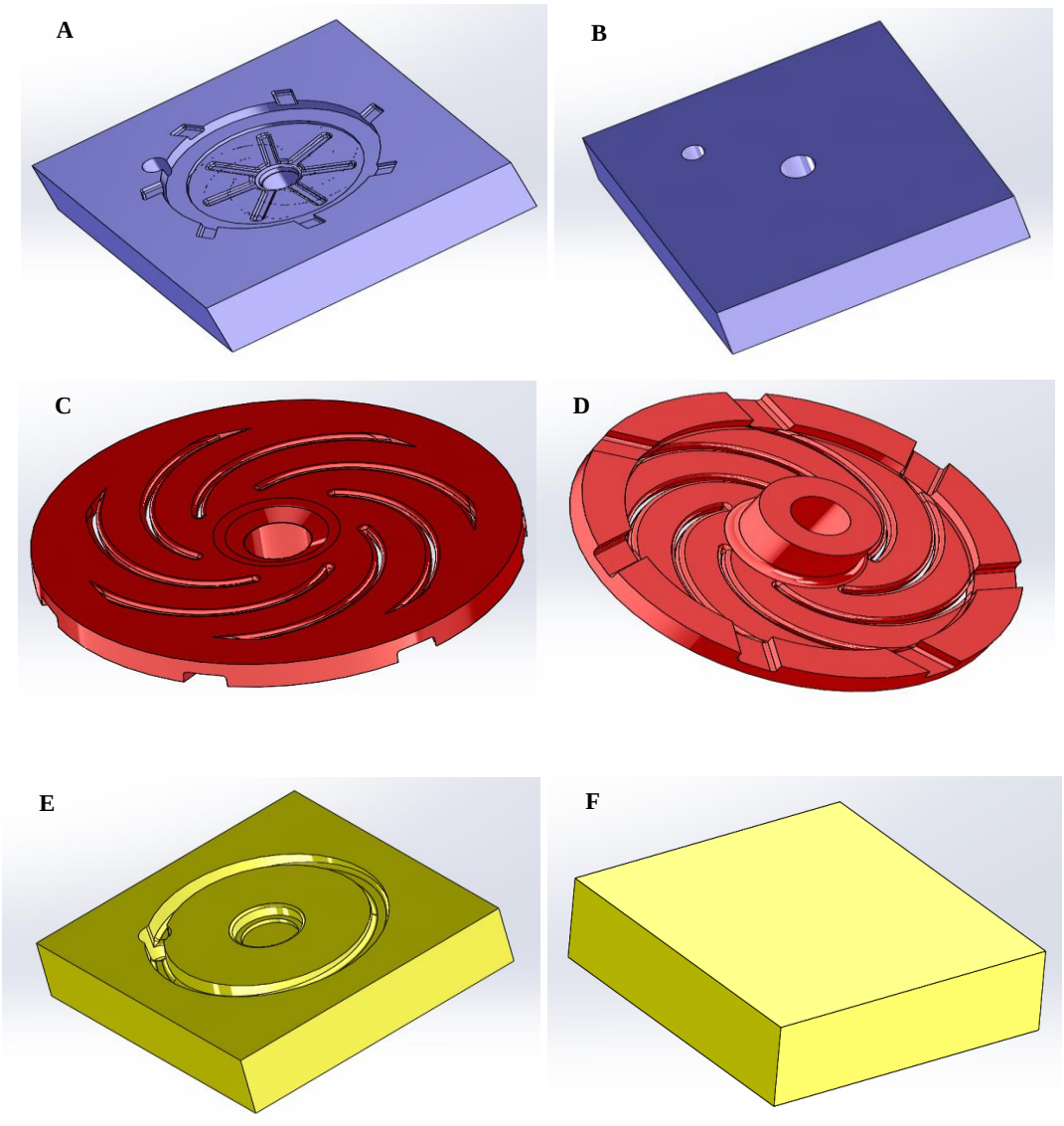

Figure 3. 17: Nodular cast iron moulds cope (A and B), drag (C and D) and core (E and F).

3.4.3 Casting and Testing

A 50-kg capacity induction furnace was used to melt nodular cast iron and stainless-steel scrap. For Design VX04, the furnace was heated to approximately 1600 °C for 150 minutes. Chemical composition of the charged scrap is shown in Table 3.7. For better de-slagging practice, a slag coagulant was added, and slag was nicely removed from the furnace (Cooper 2013). A sample was then taken to verify the chemical composition. Then the temperature was measured after taking the sample for chemical analysis using portable pyrometer. The pouring temperature used was 1497 °C (targeted aim was 1500 °C).

The metal was then poured from the ladle into the mould cavity and allowed to solidify for 24 hours and shake-out, visual inspection, microstructural analysis, chemical analysis and hardness testing were done. Metallographic preparation was carried out on the samples for microstructural analysis. Microstructural analysis was performed by means of a Nikon optical microscope on specimens etched with Adler etchant and micrographs were taken at 20X and 40X magnification. Hardness tests were also carried out using a Vickers hardness tester to correlate the cooling rate with the casting hardness. The average hardness obtained was 156.4 HV_5 with the standard deviation of 11.44 and a standard error of 5.11.

Table 3. 7: Chemical composition of the austenitic stainless-steel scrap charged

Element	C	Mn	Si	P	S	Ni	Cr	Mo
Aim	0.02	1.32	0.48	0.02	0.00	10.07	16.64	2.00

On the other hand, for Design VX05 the furnace was heated to 1450 °C for 115 minutes. The chemical composition of the scrap charged is shown in Table 3.8. Due to less scrap charged, de-slagging was not properly practiced. If de-slagging had been properly practiced, the metal would have been less causing short cast defect. After checking chemical composition of the final sample, casting process was done at 1385 °C and casting was allowed to solidify for 24 hours. Microstructural analysis was performed by means of a Nikon optical microscope on specimens etched with 3% Nital. Micrographs were taken at 20X and 50X magnification. Hardness tests were also carried out using a Vickers hardness tester from to correlate the cooling rate with the casting hardness. The average hardness obtained was 196 HV_5 with the standard deviation of 17.42 and a standard error of 7.79.

Table 3. 8: Chemical composition of the nodular cast iron scrap charged

Element	C	Cu	Si	P	S	Mg	Mn
Aim	3.92	0.01	2.19	0.02	0.01	0.00	0.27

CHAPTER 4

RESULTS

4.1 Results of experimental study 1

To optimise filling and feeding of thin-walled aluminium alloy component with complex geometry during sand casting.

4.1.1 Simulation results

The filling simulation results are shown in Figure 4.1. It is evident that at a temperature of 700 °C approximately 84.5 % of the mould cavity was filled as obtained from the simulation software. An increase in pouring temperature by 30 °C resulted in an increase in filling ability by 8.5 %. Complete filling ability was obtained at pouring temperatures above 800 °C.

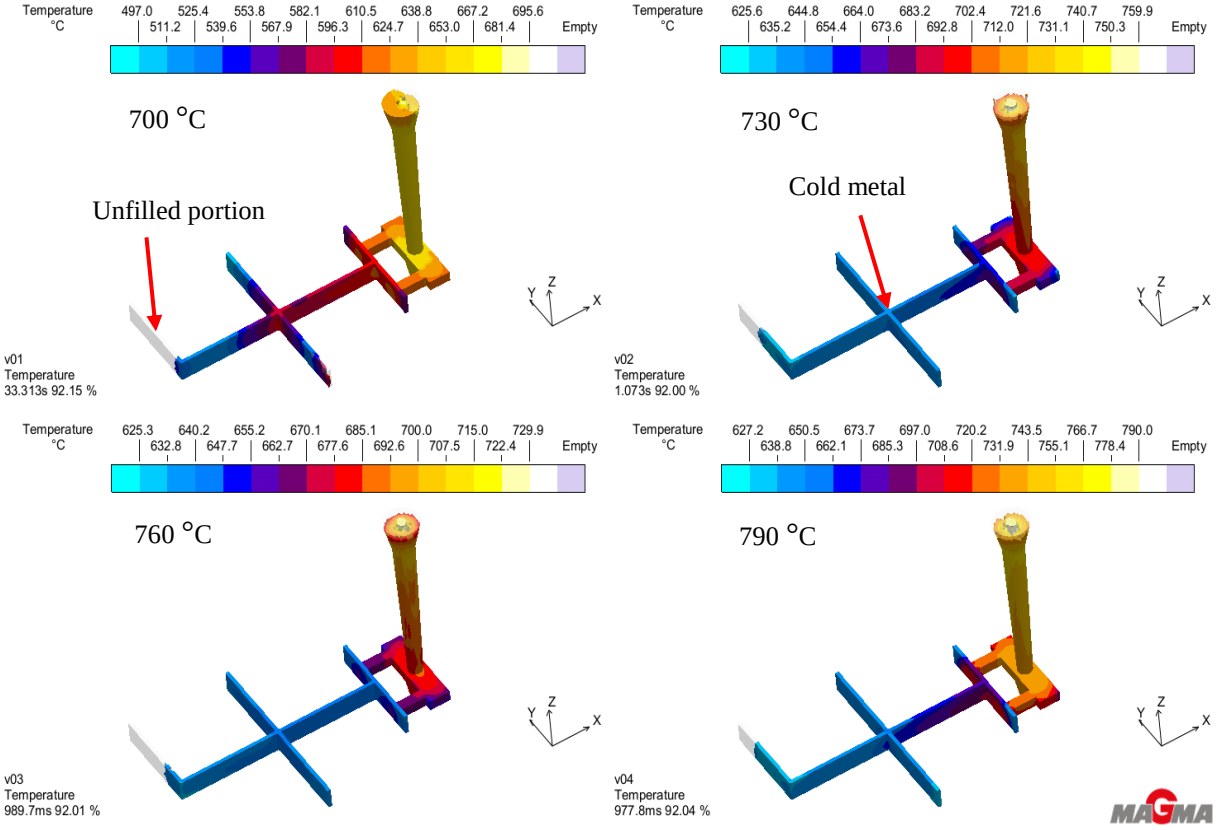

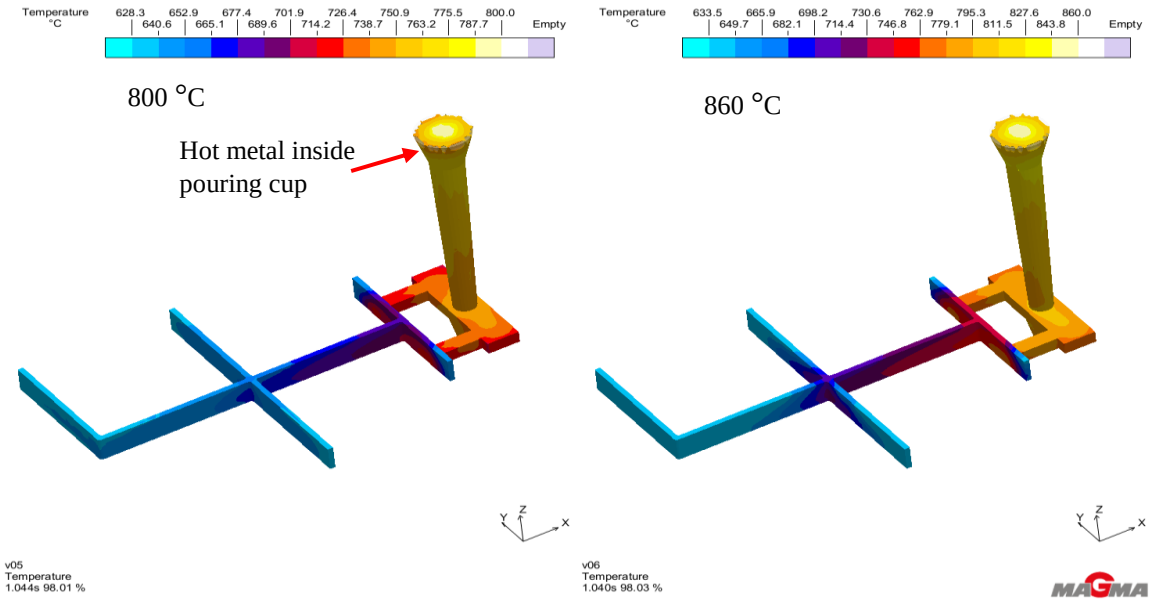

Figure 4. 1: Schematic representation of the simulation results showing the degree of molten metal filling at progressively increasing temperatures. The blue colour represents solidified metal, white represents unfilled portion and pale yellow represents hot metal.

It is apparent that the simulation results show progressive increase in mould filling with increasing pouring temperature as summarized in Figure 4.2.

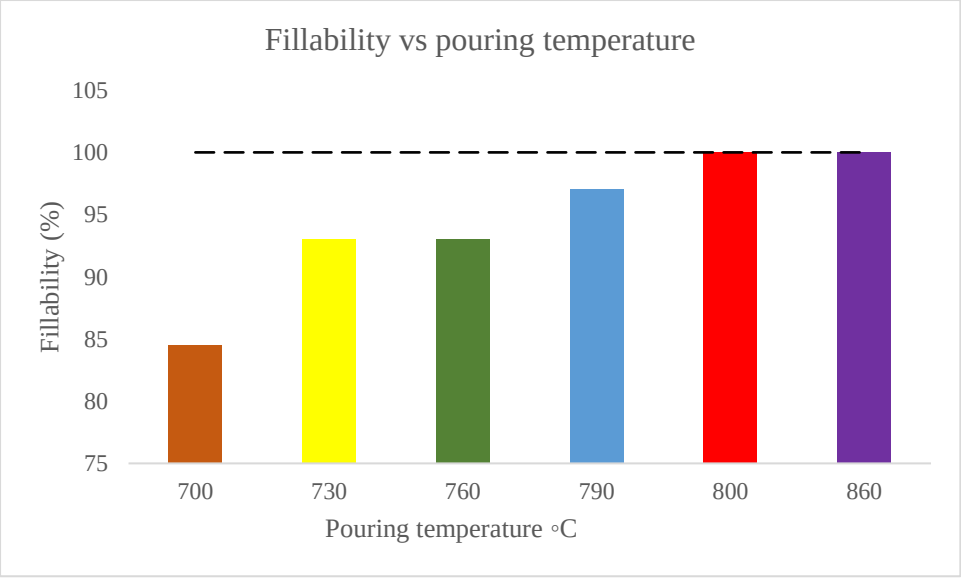

Figure 4. 2: Pouring temperature vs filling ability percentage

Figures 4.3A, 4.3B and 4.3C represent pressure results of molten metal at different pouring stages. The molten metal pressure after 430 milliseconds (figure 4.3A) is high within the runner

system, filling is observed at all pouring temperature values at this stage. After 640 milliseconds, the molten metal pressure builds up in the mould cavity to various magnitudes depended on the pouring temperature as illustrated in Figure 4.3B. The test samples with low pouring temperature (< 760 °C) possess the lowest metal pressure values. At this stage, the moulds are at varying stages of filling. The situation changed after 1.1 seconds which shows near complete filling for tempertures above 800 °C. The test sample in Figure 4.3C at 700 °C pouring temperature shows that approximately the entire volume of the mould cavity is incompletely-filled and is showing the lowest pressure. The situtation was however slightly different for the test samples at temperatures of 730 °C, 760 °C,and 790 °C. The low pressure was only at the tips which may instead prevent any further movement of the molten metal. The sample cast at 860 °C shows complete filling of the mould cavity.

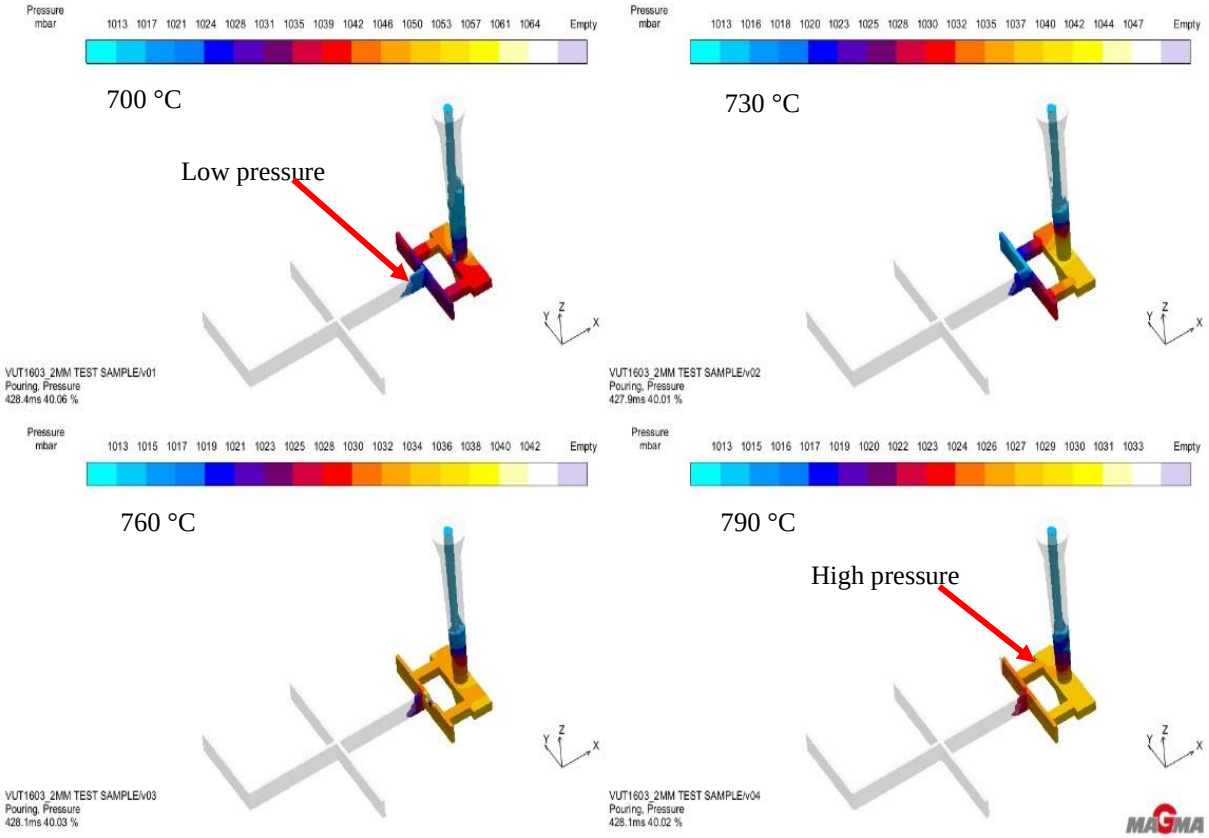

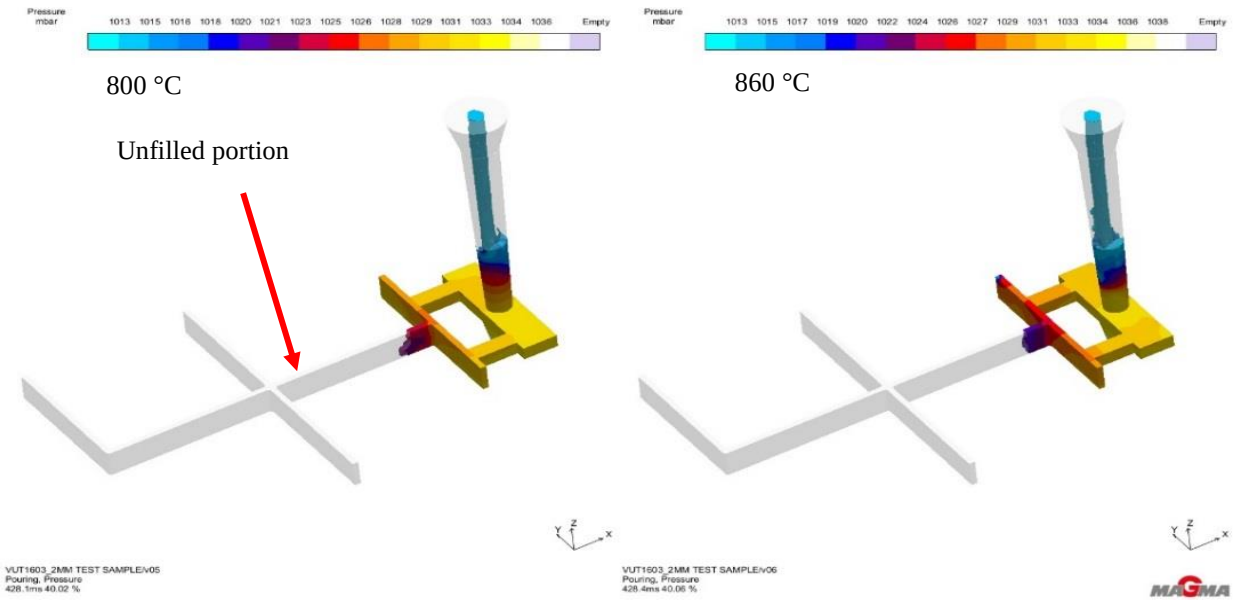

Figure 4. 3A: A representation of the metal pressure after 430 milliseconds of 2 mm test sample at 700 °C to 860 °C pouring temperature. The blue colour represents the lowest pressure of poured metal, red representing the average pressure, pale yellow indicating highest pressure and white shows unfilled portion.

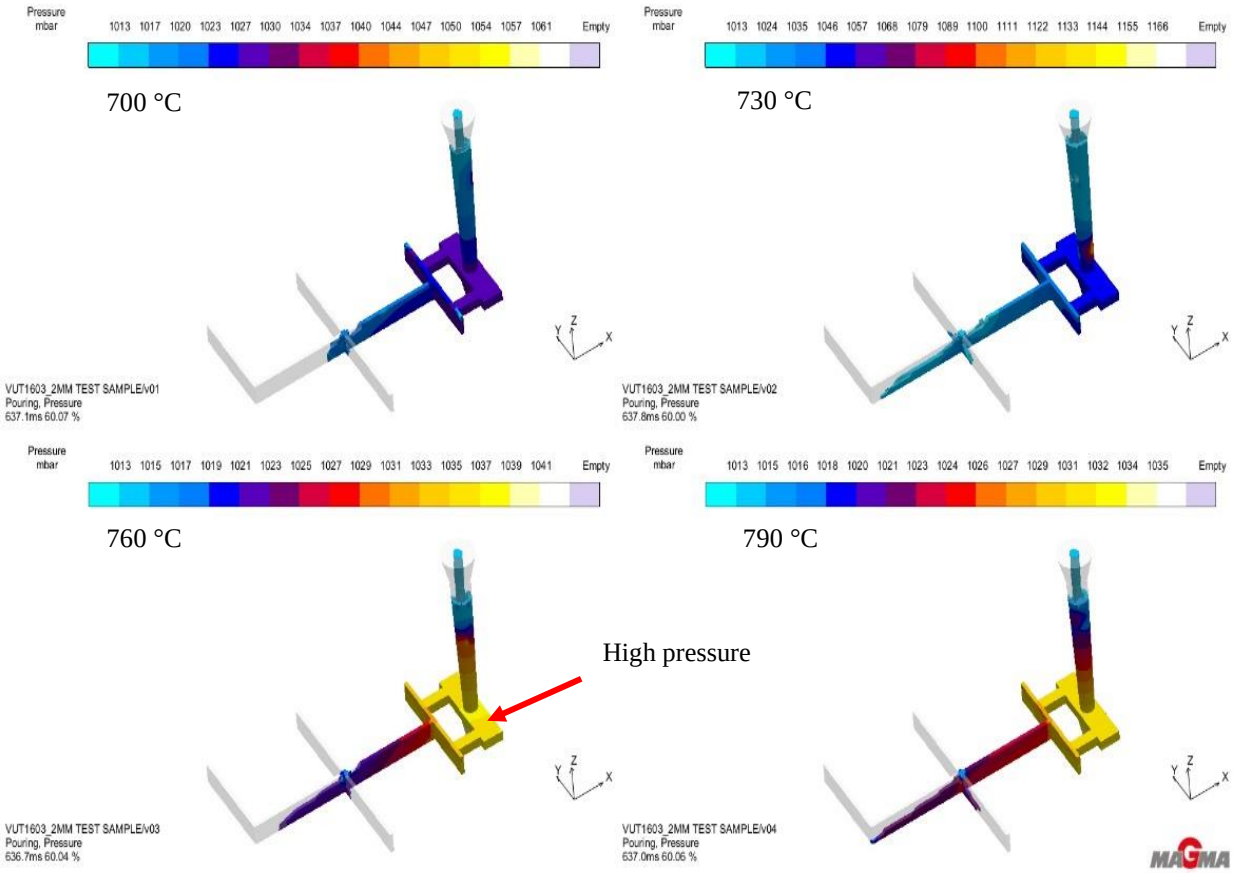

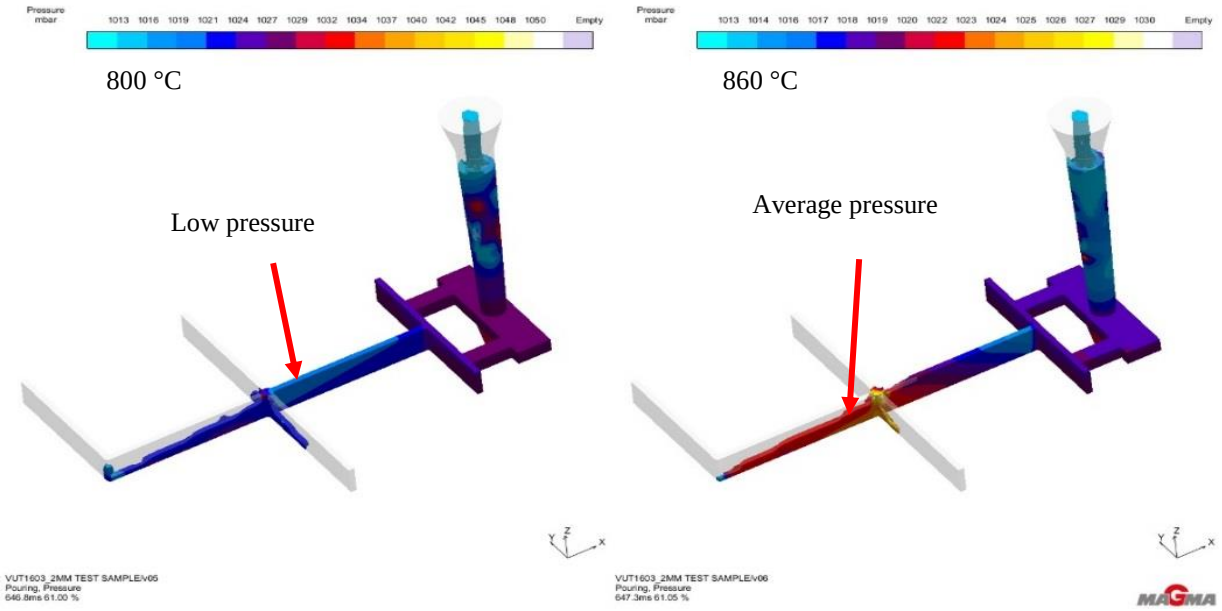

Figure 4.3B: Metal pressure after 640 milliseconds of 2 mm test sample at 700 °C to 860 °C pouring temperature.

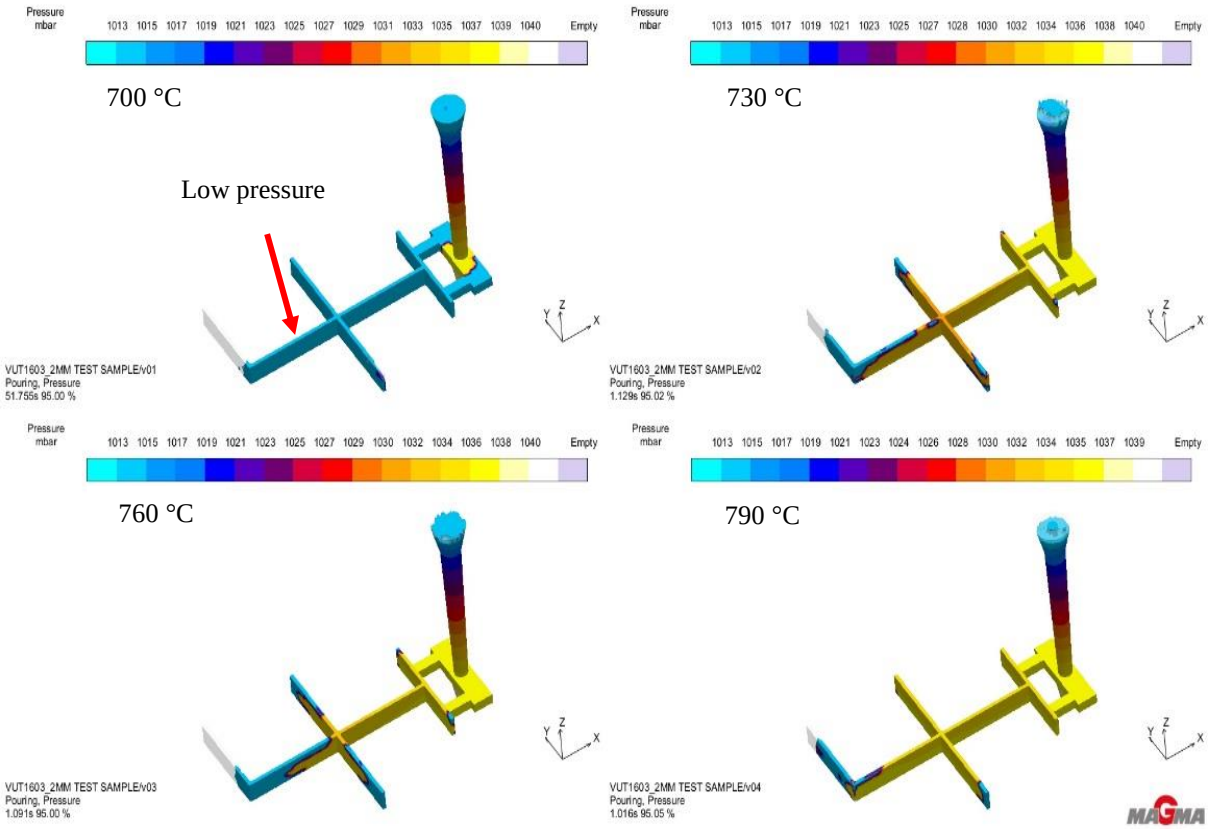

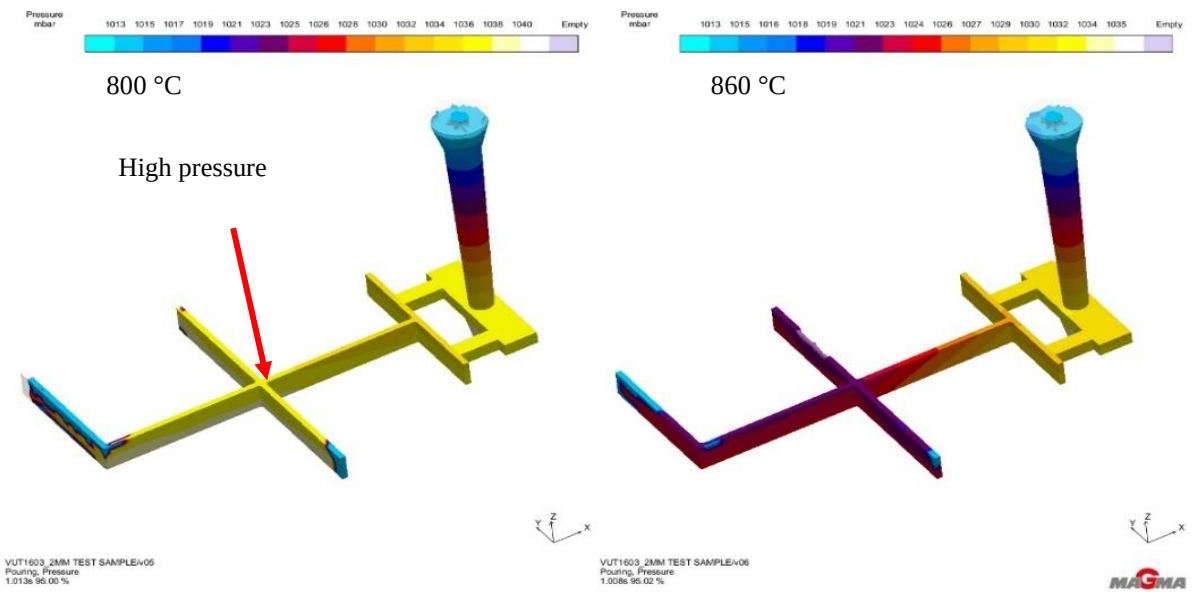

Figure 5.3C: A representation of metal pressure after 1.1 seconds of 2 mm test sample at 700 °C to 860°C pouring temperature.

A solidification simulation was carried out to identify hot spot areas which represents hot islands in the casting which are likely to solidify last (See Figure 4.4). The blue colour represents the first part to solidify followed by red and lastly yellow. At 700°C, hot metal was noted at the sprue well which could promote shrinkage porosity at that location. Clearly, the last part to solidify is represented by the pouring basin area under all the casting conditions investigated. At lower pouring temperatures (from 700 °C to 760 °C), cold metal in the casting was dominant at the tip of the L-junction. However, as the pouring temperatue increases from 760 °C to 860 °C the cold metal was dominant at the cross-junctions. This was due to an increase in section area at the cross-junction making it prone to hot spot (Joshi and Ravi 2010).

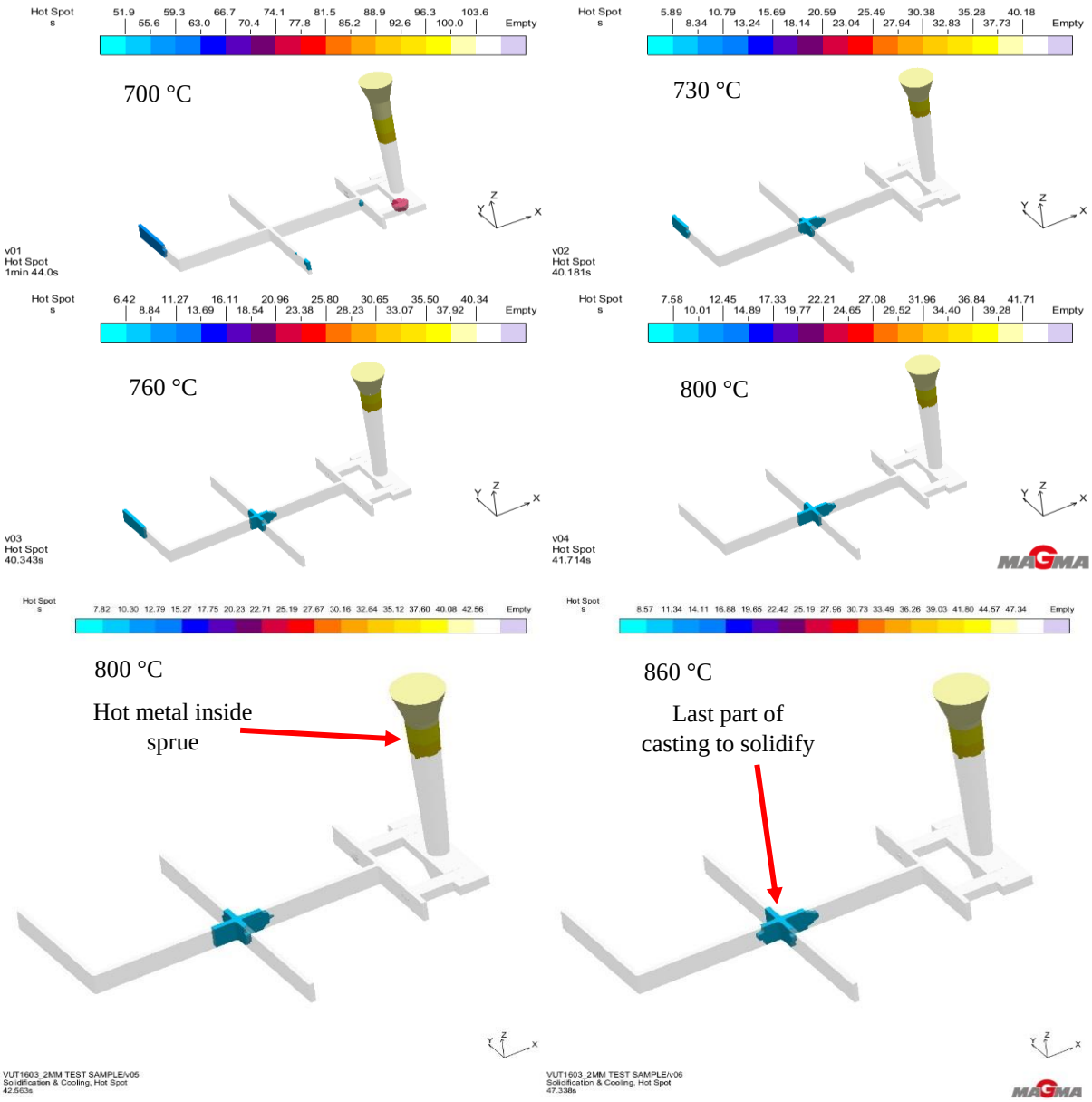

Figure 4.4: Hot Spot results of 2 mm test sample at 700 °C to 860 °C pouring temperature.

In order to elucidate the above hot spot observations, a simulation on the level and location of porosity spots was carried out. Figure 4.5 is colour coded to represent varying severities of porosity with blue colour representing the lowest severity followed by red and lastly yellow. At lower pouring temperatures though (from 700 °C to 760 °C), the possibility of porosity to form was only at the surface of the L-section of the casting. This is the part which is likely to be unfilled during filling process. However, as the casting temperatue increases from 790 °C to 860 °C the possibility of porosity formation shifted to the junctions. This is however confined to very small sections and can promote cracking at the junctions (Li et al. 2015).

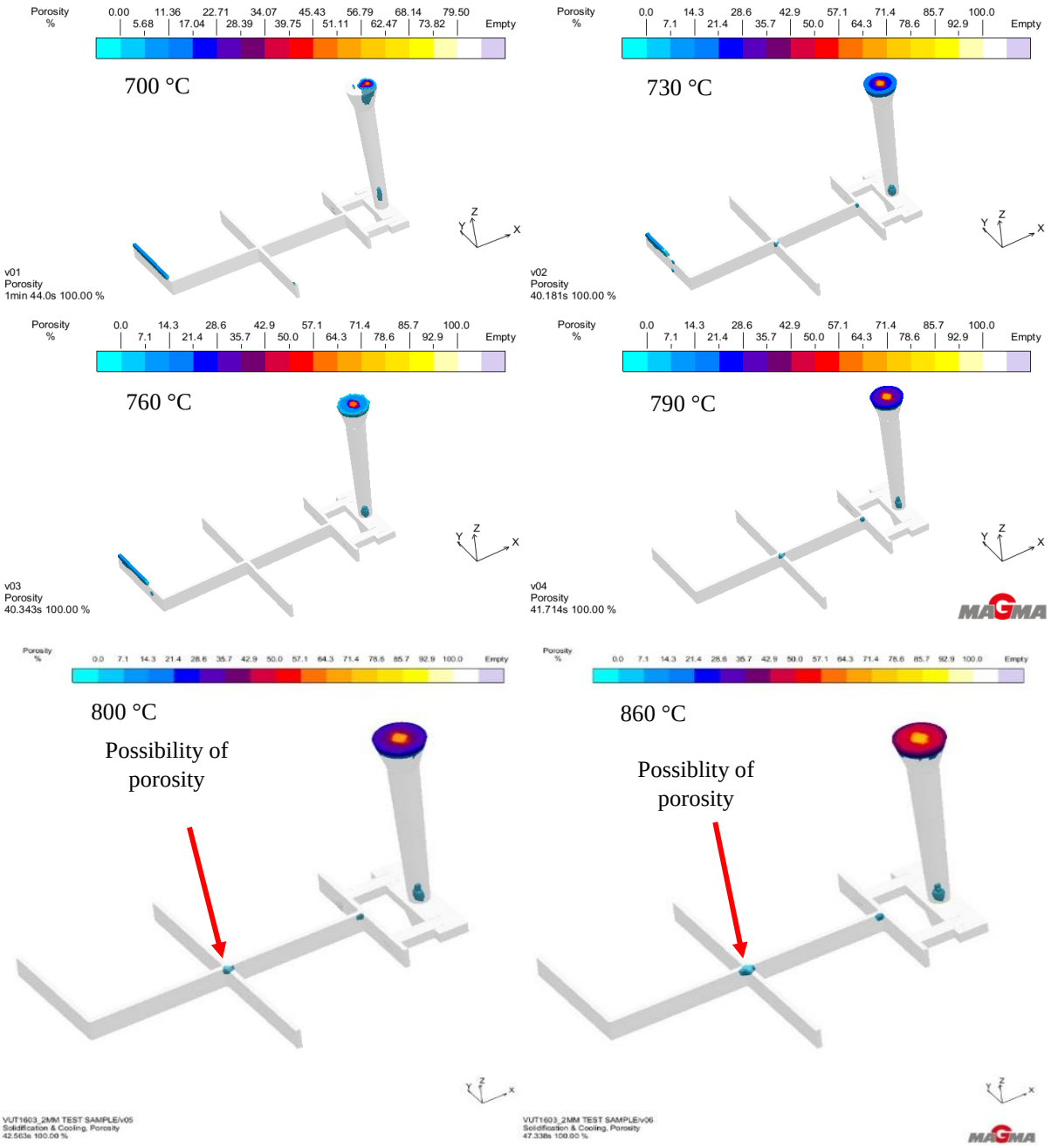

Figure 4.5: Porosity results of 2mm test sample at 700 °C to and 860 °C pouring temperature

4.1.2 Casting results

Figure 4.6 represent the test samples taken after casting at different pouring temperatures. Incomplete mould filling was observed at temperatures of 702 °C and 729 °C. At a temperature of 761°C, the mould was filled completely with flashing. At temperatures of 794 °C, 800 °C and 862 °C cracking was quite pronounced at the cross-junctions (See Figure 4.6D, 4.6E and 4.6F).

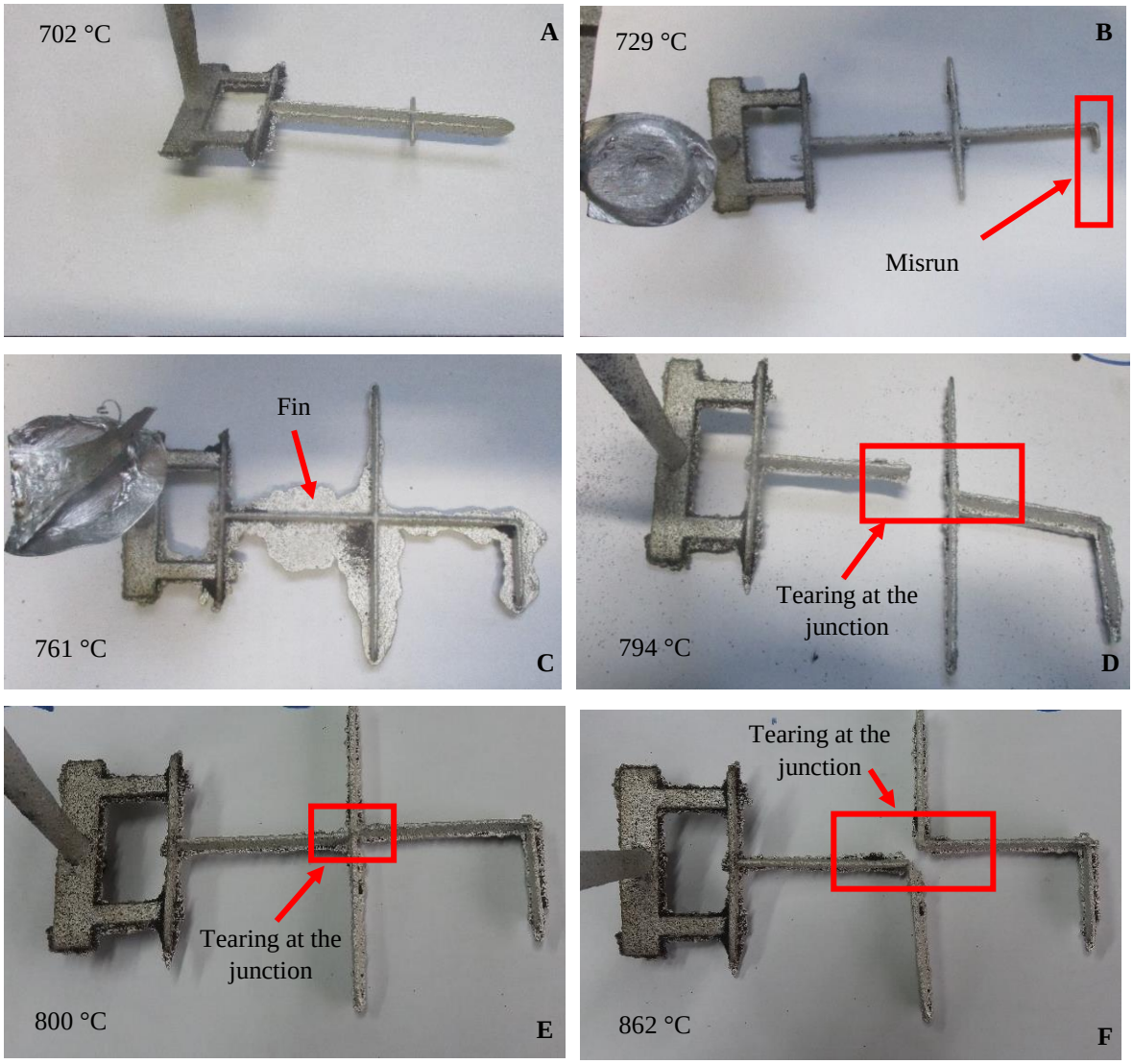

Figure 4. 6: Casting results of 2mm test sample at 702 °C (A), 729 °C (B), 761 °C (C), 794 °C (D), 800 °C (E) and 862 °C (F).

4.1.3 Microstructure

Figure 4.7 shows relationship between pouring temperature and grain size. At 702 °C pouring temperature, short dendrite arms of 103.01 µm were noted. Dendrite arms were measured with the use of the scale bar which is at the bottom of the microstructural samples in Figure 4.8. As pouring temperature increases to 729 °C and 761°C dendrite arms also increase to 119.88 µm and 145.78 µm respectively. However, a further increase in pouring temperature to 794 °C resulted in reduction of dendrite arms to 135.15 µm. The reason for the decrease of dendrite arms is unknown since this sample was cast the same way as the others. There was no change in temperature which could affect solidification rate. The size of dendrite arms increased again

to 141.33 µm when the pouring temperature was increased to 800 °C. There was a sudden decrease in dendrite arms to 95.38 µm when pouring temperature was increased to 862 °C.

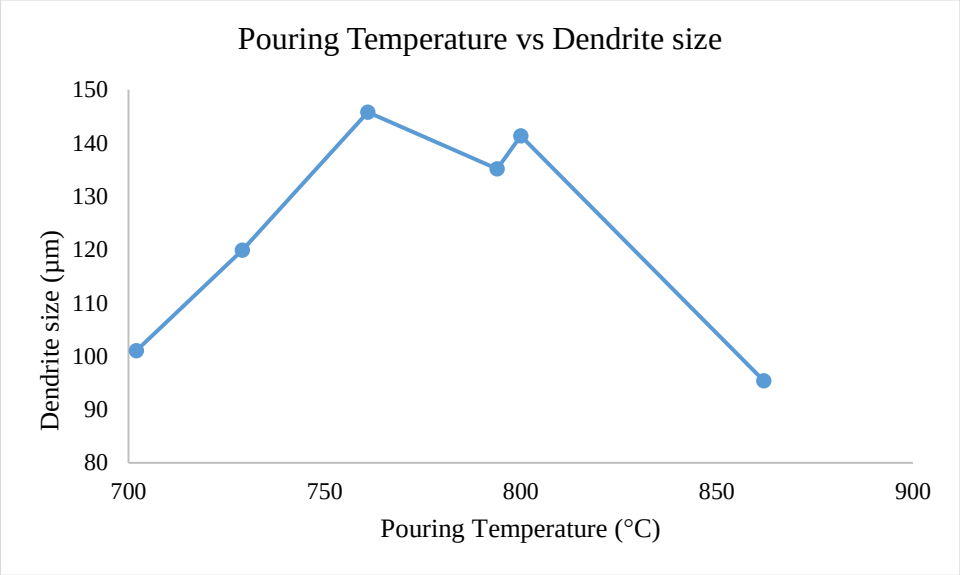

Figure 4. 7: Relationship between pouring temperature and grain size.

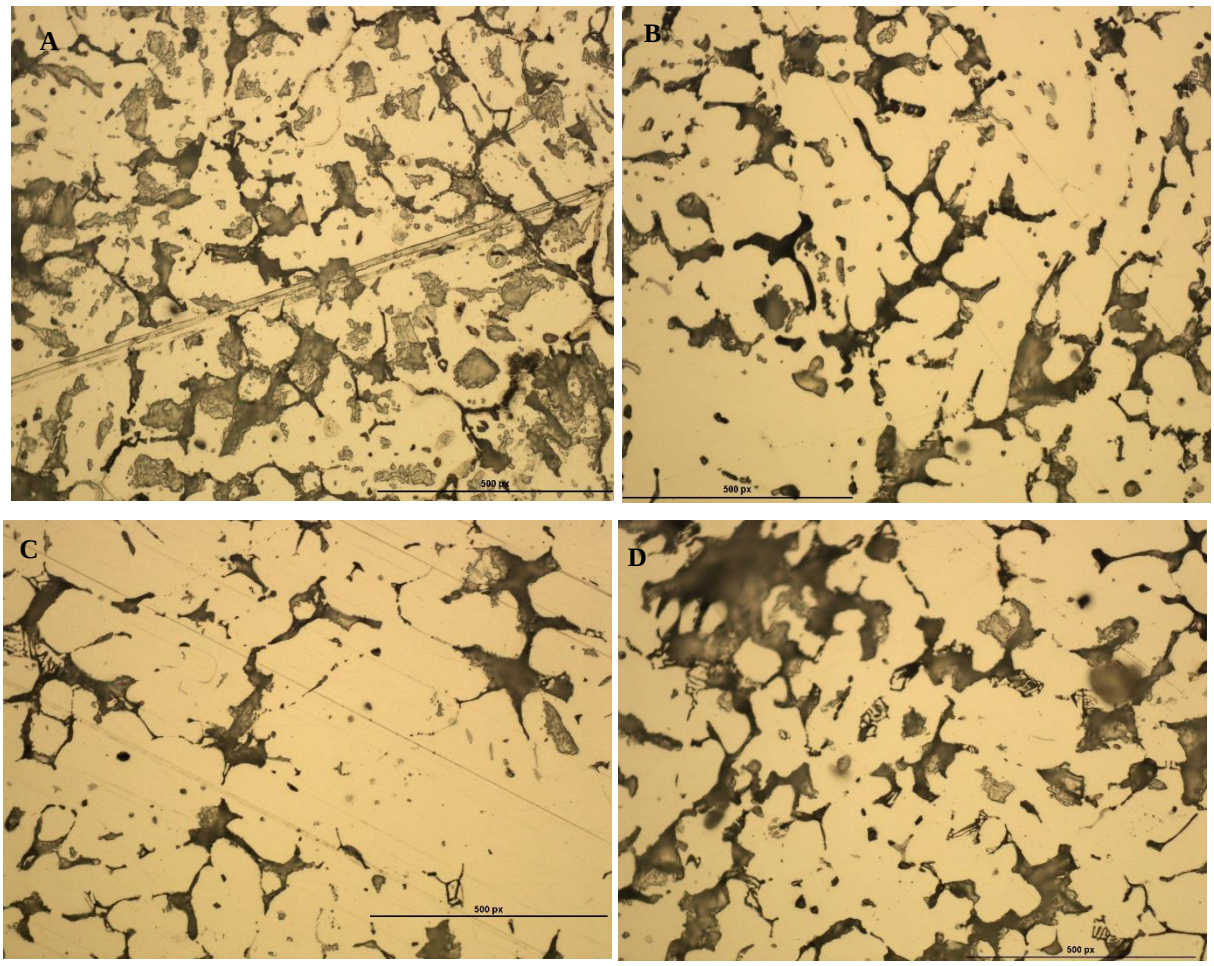

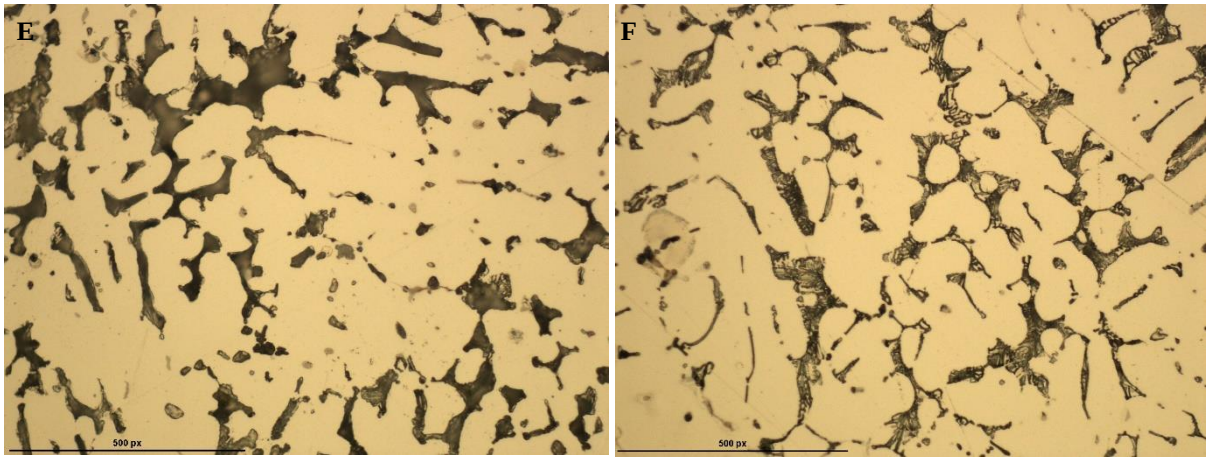

Figure 4. 8: Microstructural results of 2mm test sample at different pouring temperatures at 50X magnification.

4.1.4 Hardness

Figure 4.9 shows Vickers hardness results of the test samples at different pouring temperatures. Samples were taken at the part which filled last during casting process. High hardness value of 77.2 HV_5 was noted at a pouring temperature of 702 °C. As the pouring temperature increases to 729 °C and 761 °C a decline in hardness value to 75.8 HV_5 and 70.1 HV_5 respectively was noted. But, as the pouring temperature further increase to 794 °C, hardness picked up again to 72.9 HV_5. A decline in hardness to 67.3 HV_5 and 66.6 HV_5 was noted as the pouring temperature further increase to 800 °C and 862 °C respectively.

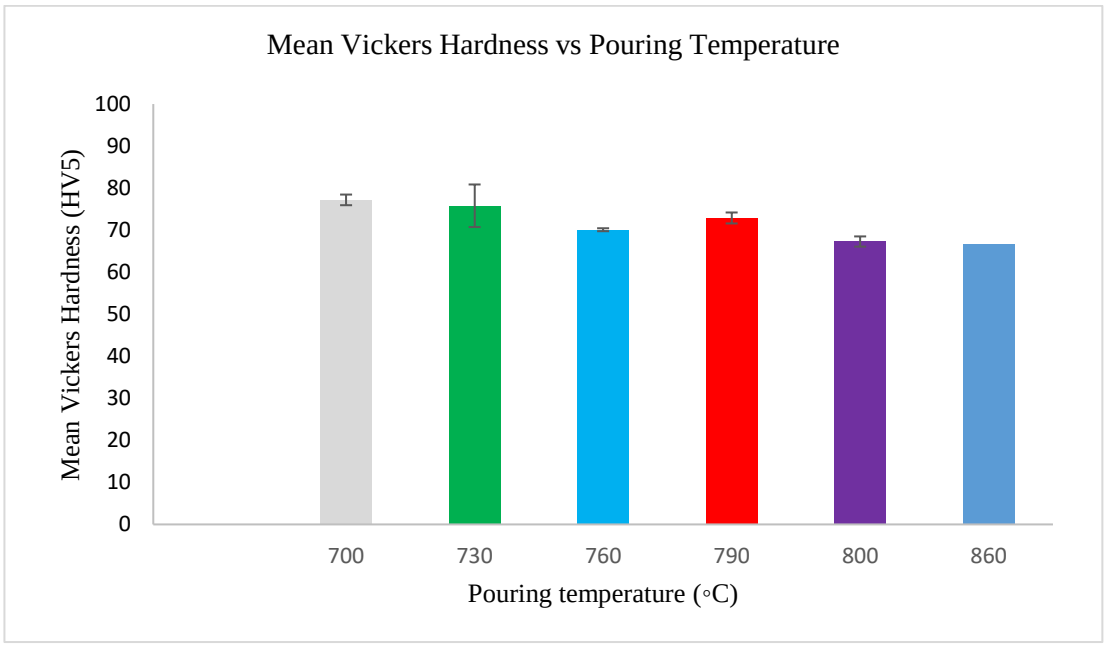

Figure 4. 9: Vickers hardness vs pouring temperature

4.2 Results of experimental study 2

4.2.1 Simulation

Evaluating effect of wall thickness on the filling and feeding of thin-walled aluminium alloy components during sand casting.

The results of numerical simulation are shown in Figure 4.10. and Figure 4.11. The blue colour represents solidified metal whereas the white colour represents incomplete filling. Figure 4.10A shows the simulation results of 1 mm wall thickness at 700 °C pouring temperature with only 32.5 % of the entire mould filled. When wall thickness was increased by at least 0.5 mm a significant increase in filling ability to 52.5 % (approximately 20 % increase) was noted. Figure 4.10B clearly indicate that the filling ability of 1.5 mm was 52.5 % which is approximately 20 % more than that of 1 mm section.

A further increase in the wall thickness by 0.5 mm to 2 mm caused a higher increase in filling ability. Figure 4.10C showed that a 2 mm wall thickness yielded a filling ability percentage of 84.5 % which is 32 % increase in comparison to the 1 mm section. At a wall thickness of 2.5 mm test sample, a high filling ability of 97.5 % was obtained as shown in Figure 4.10D.

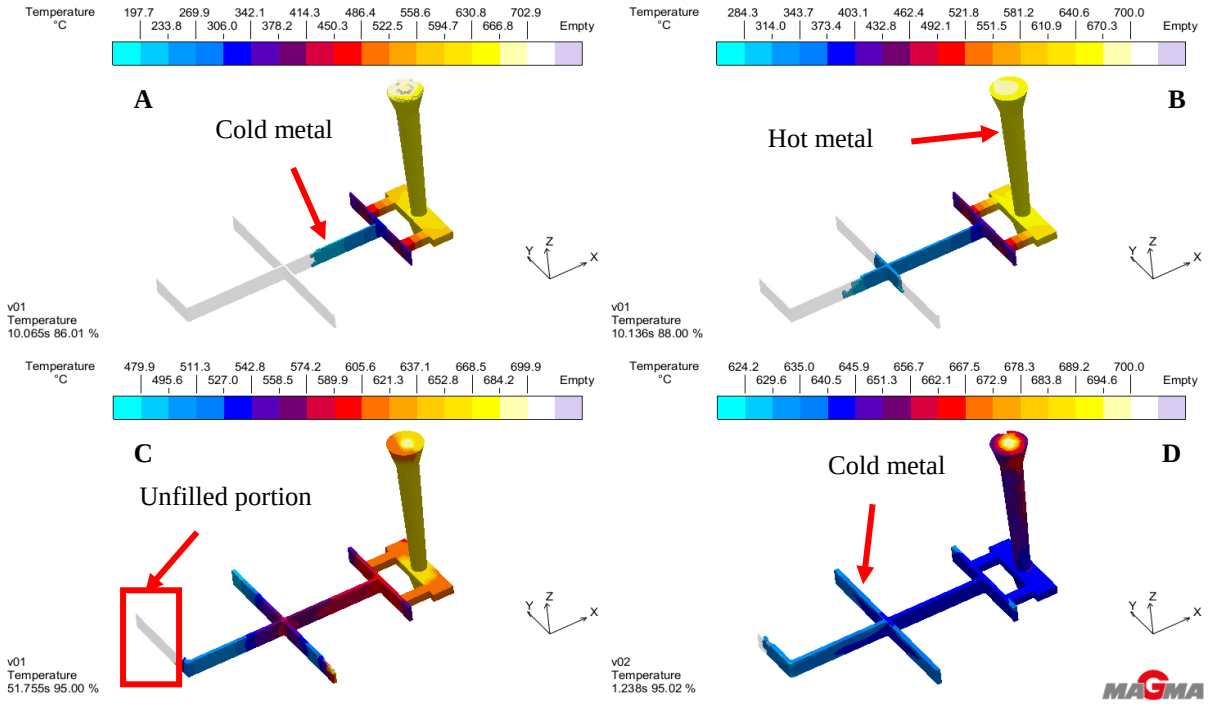

Figure 4. 10: Filling ability of 1 mm (A), 1.5 mm (B), 2 mm (C) and 2.5 mm (D) at 700 °C pouring temperature.

Complete filling ability was only observed when the wall thickness was increased to 3 mm as illustrated in Figure 4.11.

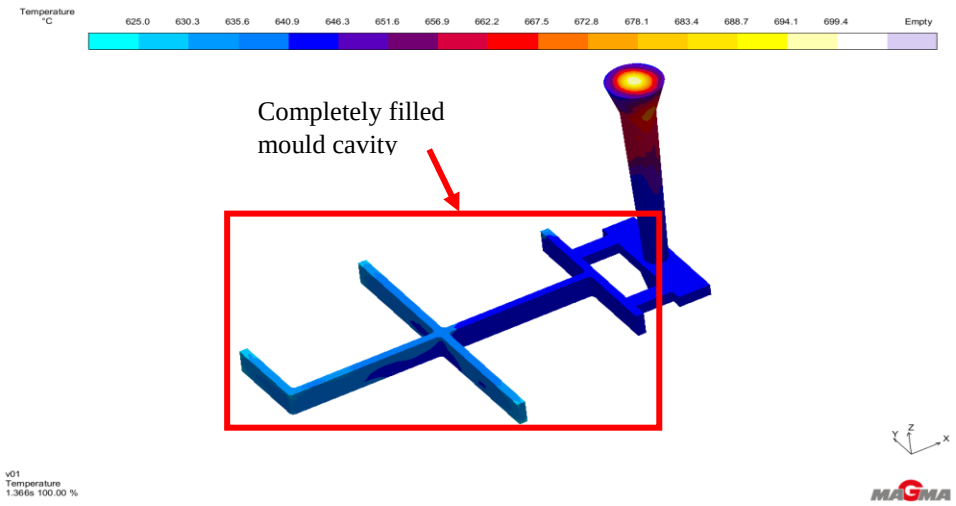

Figure 4. 11: Filling ability of 3 mm test sample at 700 °C pouring temperature

Clearly there is gradual increase in filling ability with increasing mould thickness. Figure 4.12. shows the correlation of filling ability with wall thickness. Filling ability increase was high between 1 mm and 2 mm wall thickness. From 2 mm to 3mm wall thicknessthe increase in filling ability was low.

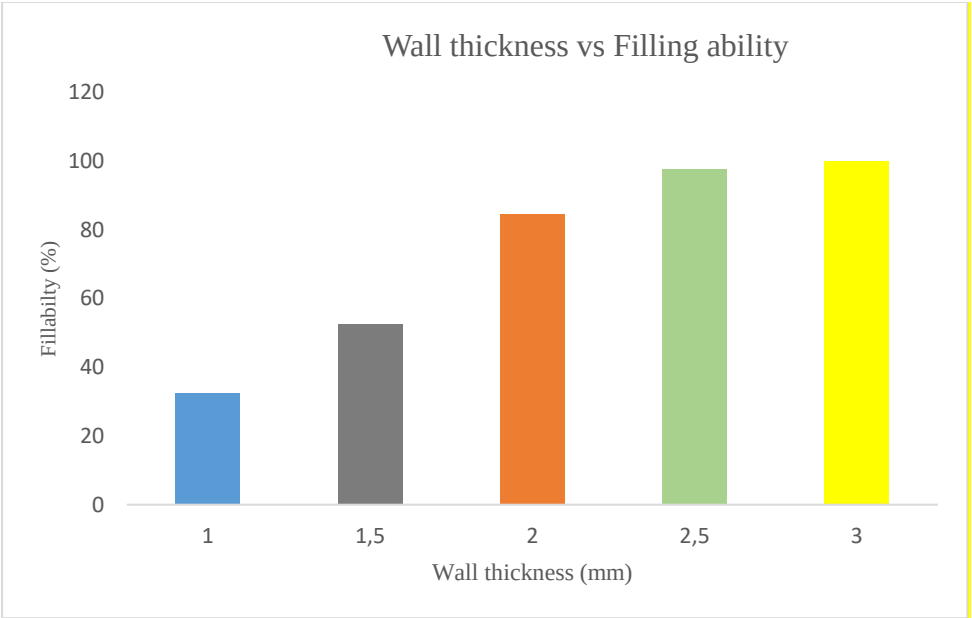

Figure 4. 12: Wall thickness vs filling ability at 700°C pouring temperature

4.2.2 Casting

A summary of pouring temperature and filling ability are shown in Table 4.1. The cast components are shown in Figure 4.13.

Table 4. 1: Summary of casting results for the different wall thicknesses at 700 °C.

Sample designation	Wall thickness (mm)	Actual pouring temperature (°C) (±error)	Observation (% of total length filled)
1	1.0	702	25
2	1.5	695	38
3	2.0	700	65
4	2.5	701	0
5	3.0	699	100

Results after casting of 1 mm wall thickness at 702 °C pouring temperature showed incomplete filling ability of the mould cavity See Figure 4.13A. An increase in wall thickness by 0.5 mm showed an increase in filling ability when the pouring temperature was 695 °C which is 5 °C lower than what it should be. The results showed approximately 13 % increase in filling ability which is 14.5 % less compared to simulation results as shown in Figure 4.13B. Figure 4.13C shows a significant increase in filling ability when the wall thickness was increased to 2 mm. The pouring temperature read as 700 °C which is exactly what was required. Poor results were observed when casting 2.5 mm wall thickness due to mould breakage resulting in poor filling ability (See Figure 4.13D). Pouring temperature was 701 °C. A complete mould filling ability was only observed in figure 4.13E when the wall thickness was increased to 3 mm at a pouring temperature of 699 °C.

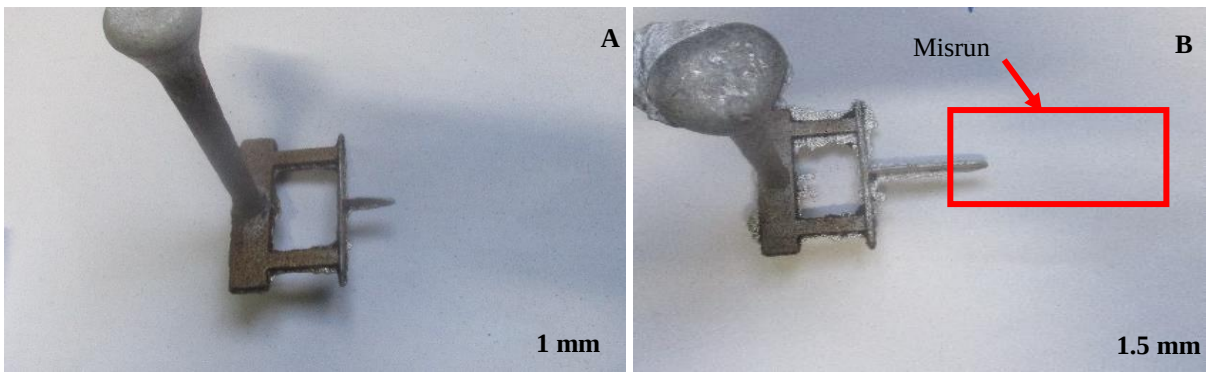

D

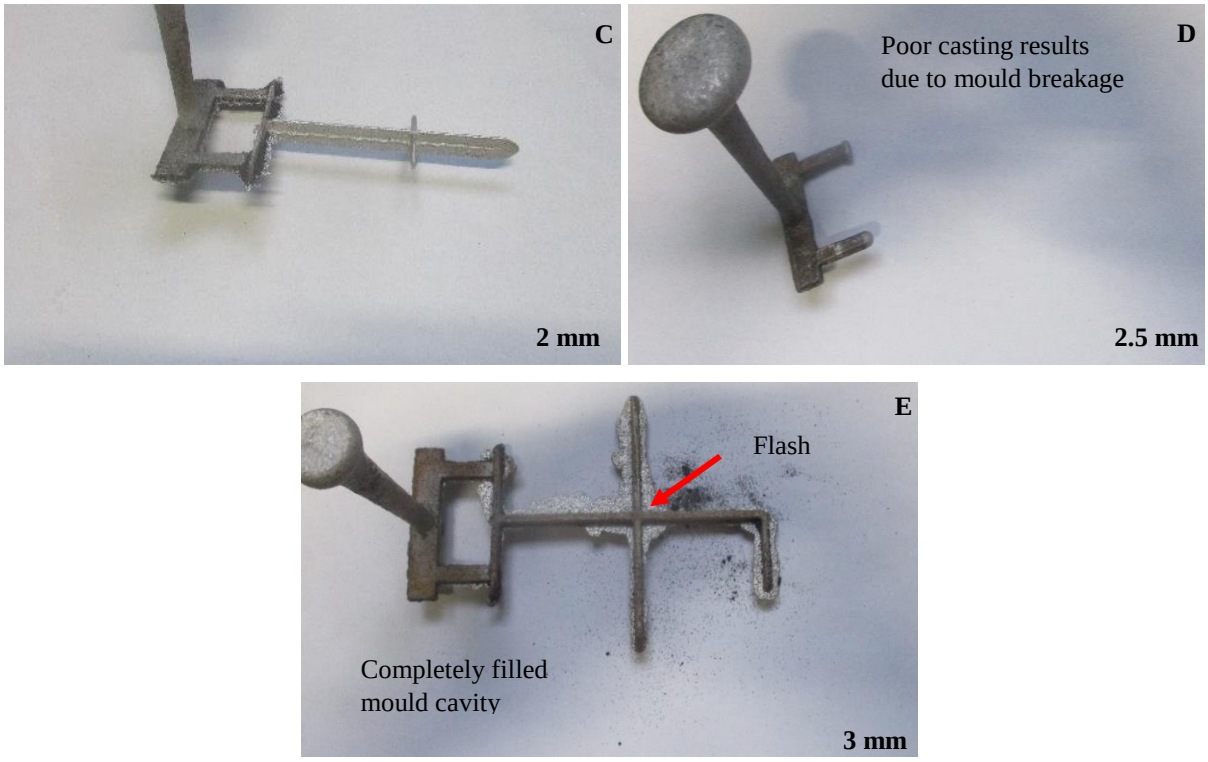

Figure 4. 13: Casting results at 700 °C of 1 mm test sample(A), 1.5 mm (B), 2 mm (C), 2.5 mm (D) and 3 mm (E).

4.2.3 Microstructure

At 1 mm wall thickness, dendrite arms of 86.44 µm were noted as illustrated in figure 4.14A. An increase in dendrite arms was noted when the wall thickness was increased to 1.5 mm, 2 mm, 2.5 mm and 3 mm as illustrated in figures 4.14B to 4.14E. The increase in dendrite arms were 100.22 µm, 103.01 µm, 114.94 µm and 141.86 µm respectively.

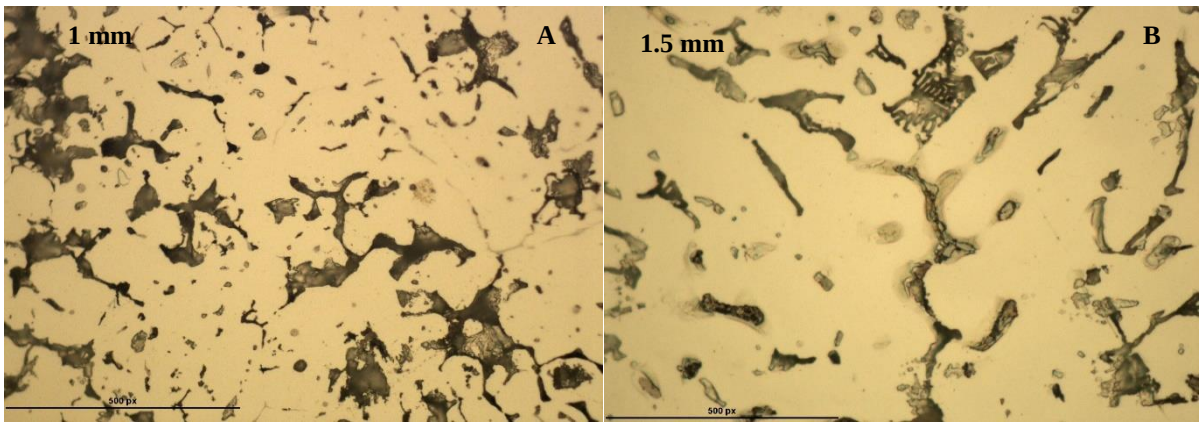

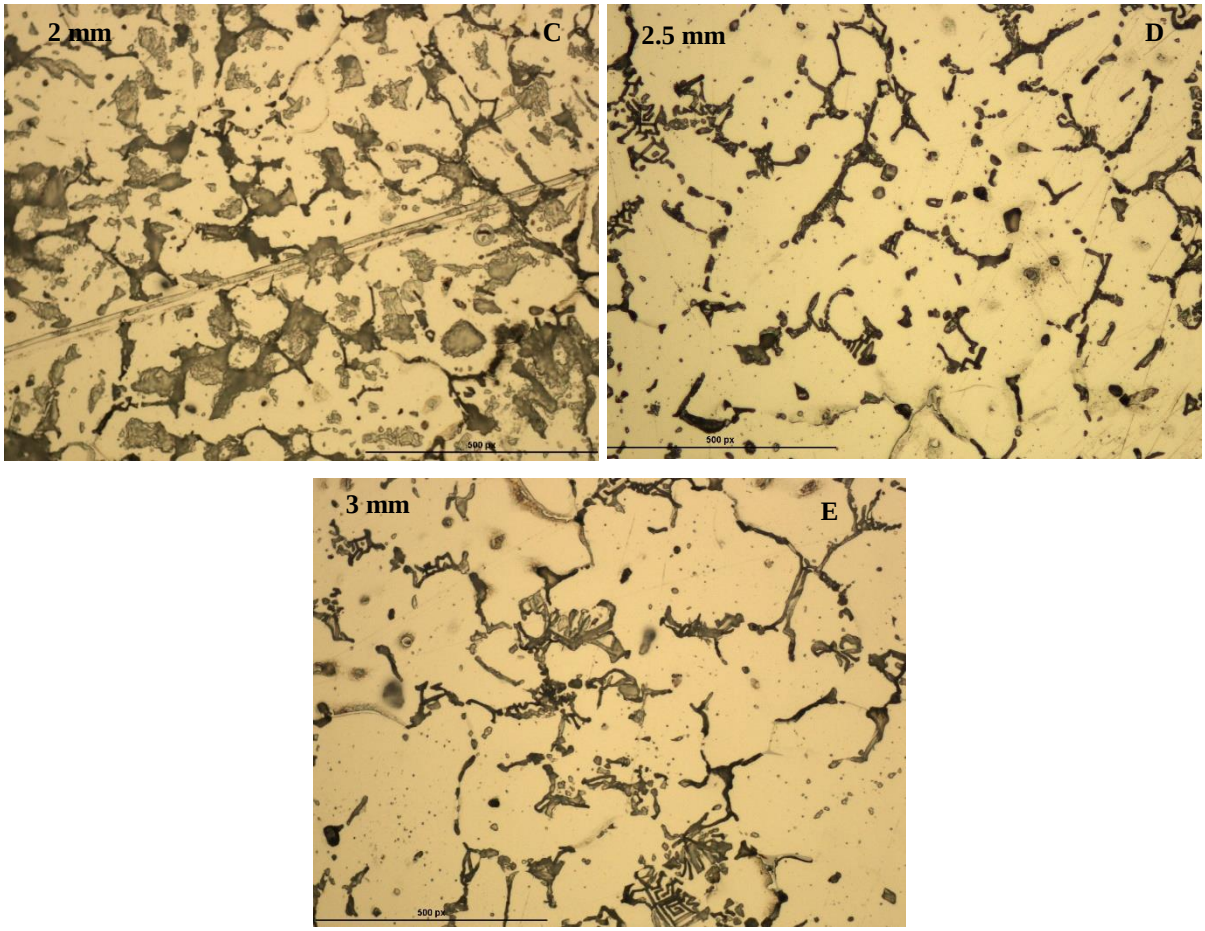

Figure 4. 14: Microstructural results of 1 mm to 3 mm at 50X magnification.

4.2.4 Hardness

Figure 4.15 shows Vickers hardness results of the test samples with different wall thickness. A hardness value of 70.3 HV_5 was obtained for a 1 mm test sample which was cast at 702 °C. As the wall thickness increases by 0.5 mm so did the hardness value to 75.4 HV_5. Hardness value increased further as the wall thickness was increased by 0.5 mm to 77.2 HV_5. A clear correlation between wall thickness and hardness value was then noted when the wall thickness was increased to 2 mm. Beyond 2.5 mm the hardness value declined to 66.3 HV_5 and 63.7 HV_5 respectively.

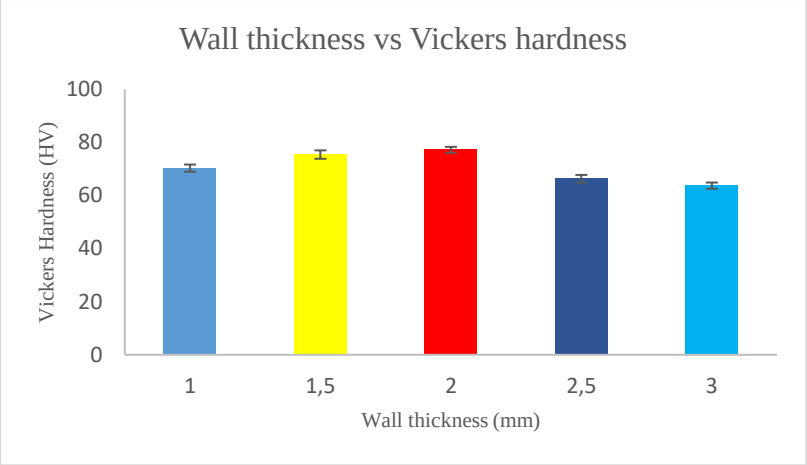

Figure 4. 15: Vickers hardness vs wall thickness

4.3 Results of study 3 (1st Trial): Optimization of filling and feeding of austenitic stainless-steel pump impeller produced by sand casting

4.3.1 Design VX 01

4.3.1.1 Filling Simulation of Design VX01

Design VX 01 used in casting pump impellers is normally bottom gated as shown in figure 4.16. This is for better flow of molten metal into the mould cavity with less splashing and less turbulent flow. Five feeders were placed on the top of the casting to compensate for shrinkage porosity. Figure 4.17 shows filling simulation of design VX 01.

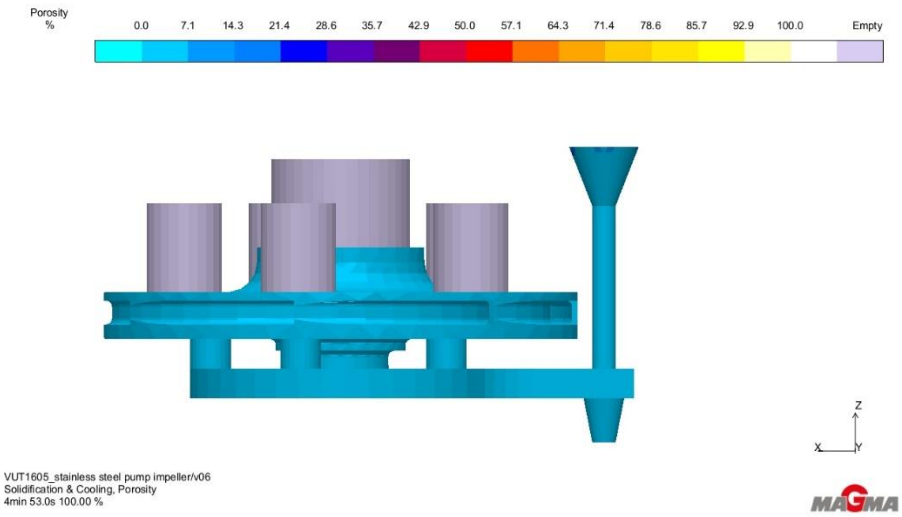

Figure 4. 16: A schematic view of design VX 01 runner system

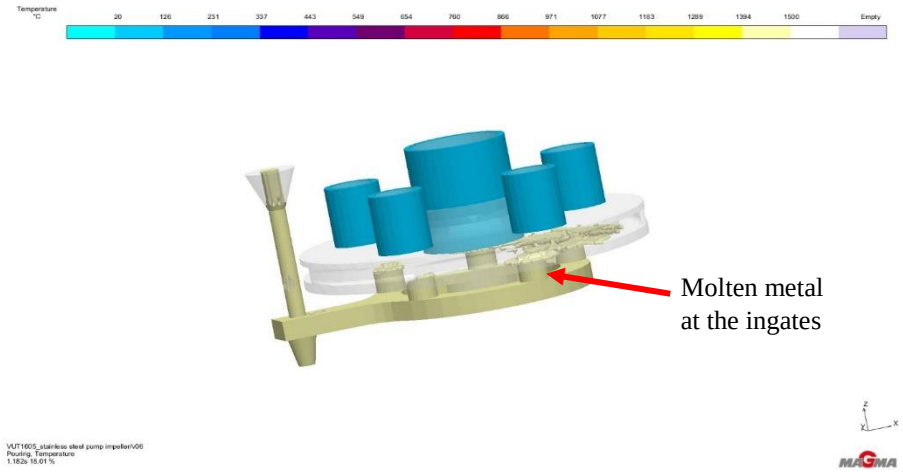

Figure 4. 17: Filling simulation of design VX 01

4.3.1.2 Solidification simulation of Design VX 01 (Hot Spot & Shrinkage Porosity)

Figure 4.18 represent hot island in the casting which are to solidify last during solidification. These islands are susceptible to porosity defects after solidification is complete (Jadeja et al. 2016). From the scale which is at the top of Figure 4.18, blue colour represents lowest solidification time of an island (approximately 30 seconds), red represents the average solidification time (approximtely 160 seconds) and pale yellow indicates highest solidification time (260 seconds). It is important to ensure that all the hot spots are completely outside the casting because they form shrinkage porosity when they solidify. Figure 4.18 shows lowest possibility of hot spots inside the casting at the point of junction between ingate and the casting. And these hot spots are at the exact location of porosity defects because they are located at the junctions of ingate and casting.

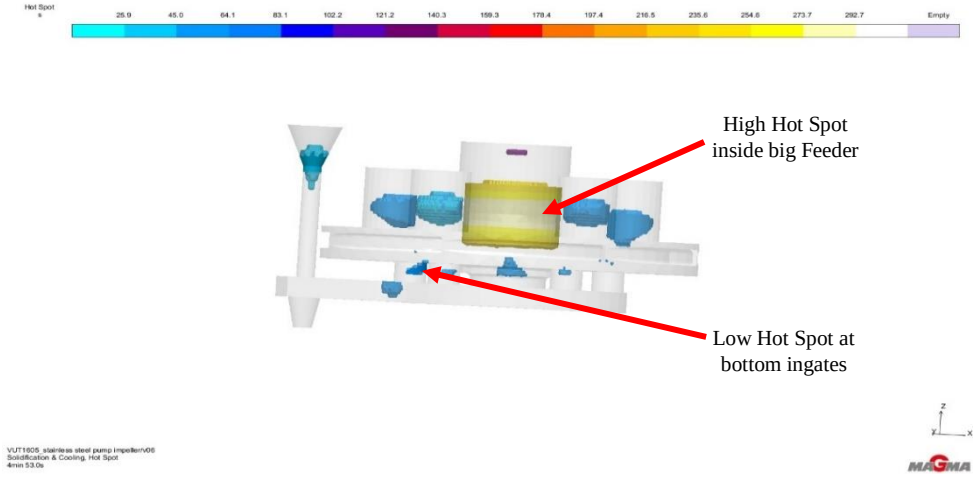

Figure 4. 18: 3D view showing hot spot results at junctions made by bottom ingates and casting.

The scale on top of Figure 4.19 and Figure 4.20 shows the possibility of porosity formation in percentage (%). The blue colour shows the lower possibility of porosity formation (approximately 10%), red colour shows the average possibility of porosity formation (approximately 50%) and the pale yellow colour shows high possibility of porosity formation (approximately 70%-100%). High amount of shrinkage was noted after solidification at the junction between ingates and the casting. The increase in section thickness at the junctions promoted the possibility of shrinkage porosity. High shrinkage was also noted at the junction where thin-walled blade connects to the pump impeller body and ingate (See Figure 4.20). The metal at the junction took a lot of time to solidify promoting shrinkage porosity.

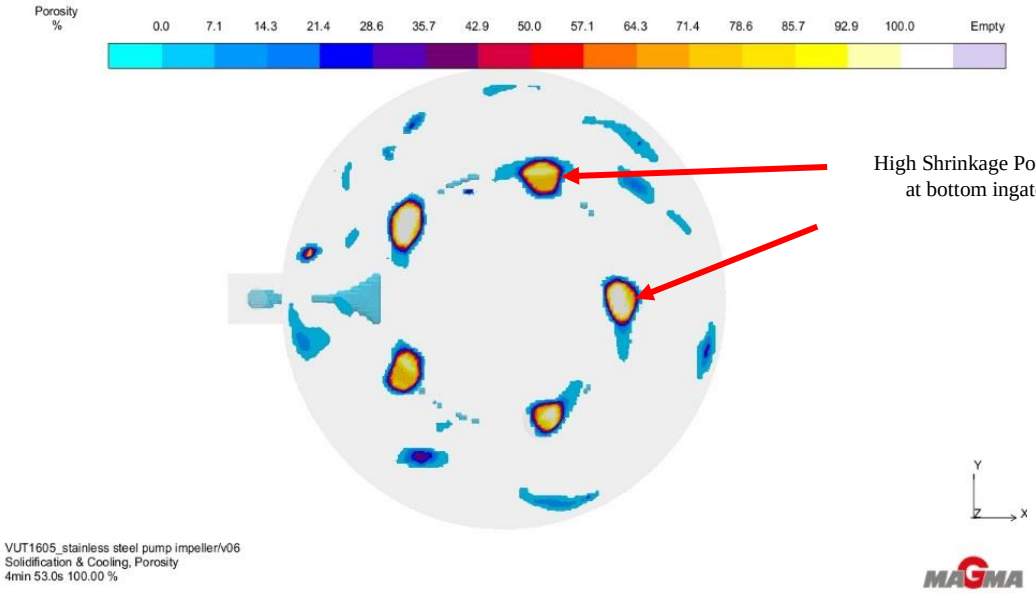

Figure 4. 19: Top-view showing shrinkage porosity at bottom ingates

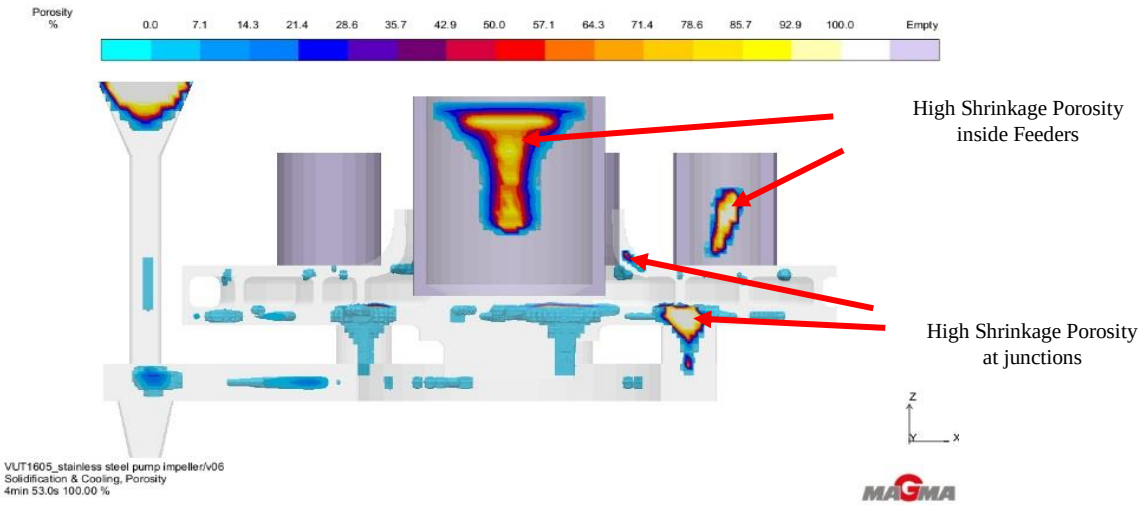

Figure 4. 20: Side-view showing shrinkage porosity at junctions

4.3.2 Design VX 02

4.3.2.1 Solidification simulation of design VX 02

Since Design VX01 (shown in figure 4.21A) had high shrinkage porosity at the junctions, a new Design VX02 was proposed with the ingates at the side of the casting as illustrated in figure 4.21B & 4.22B. Small feeder size caused shrinkage porosity at the top and bottom part of the casting (See Figures 4.21B & 4.22B). The size of the feeders was increased and shrinkage porosity at the top of the casting were removed as shown in Figures 4.21C and 4.22C. Although the feeders were big, they were not able to feed the bottom part of the casting hence one bottom feeder was introduced as shown by (Figures 4.21D and 4.22D). A modification of Design VX 02 was done by introducing bottom feeders (5X) to compensate for shrinkage at the bottom part of the casting. The introduction of bottom feeders showed positive results as the shrinkage porosity at the bottom part of the casting were removed. With this design, the quality of the casting was improved since shrinkage porosity was reduced. However, casting yield was sacrificed since a lot of material was used to compensate for shrinkage porosity both at the top and bottom of the casting.

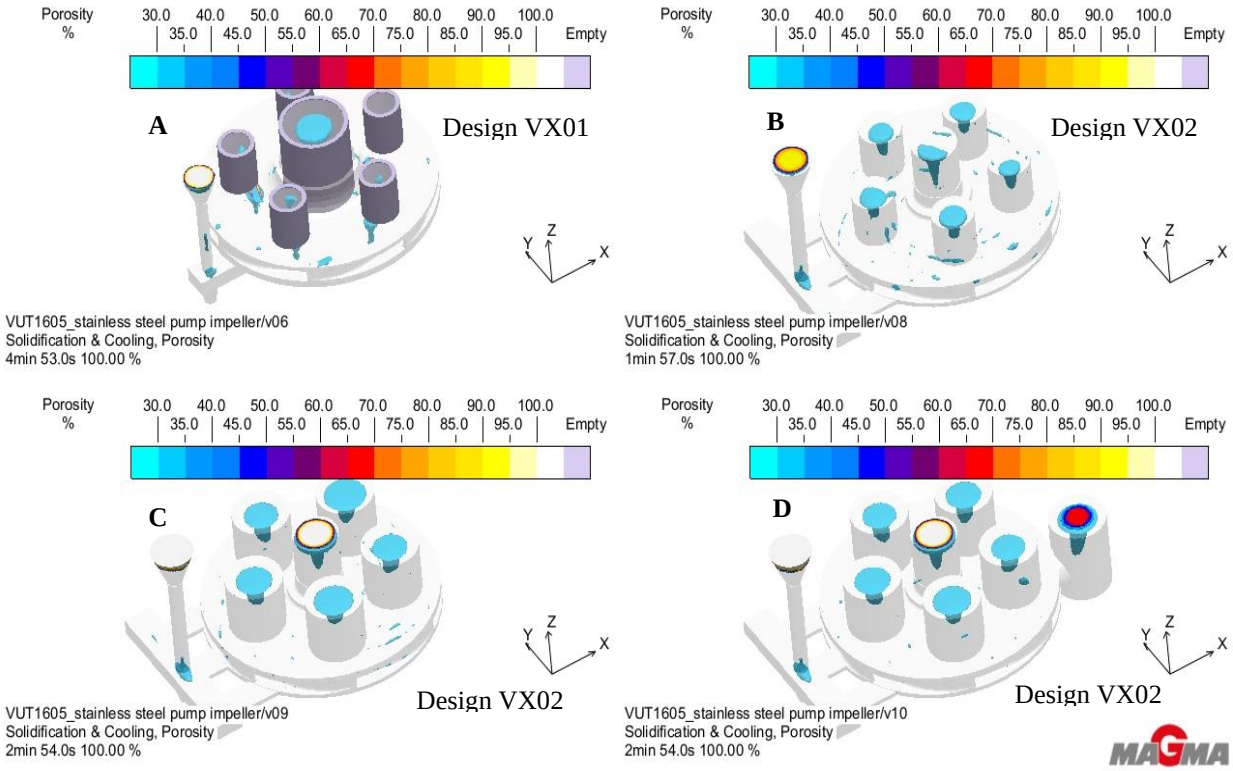

Figure 4. 21: 3D view showing porosity results of different runner system designs

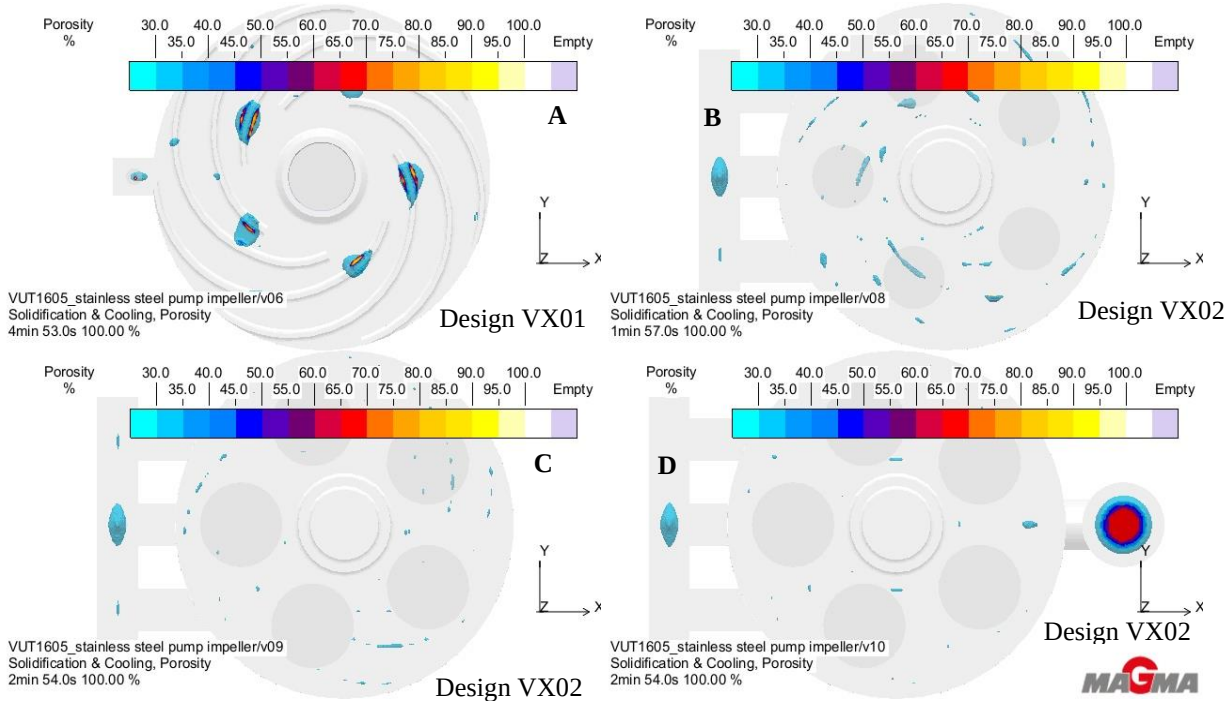

Figure 4. 22: Top view showing porosity results of different runner system designs

4.3.2.2 Optimization simulation of design VX 02

Optimisation simulation uses design variables specified in Table 3.5 under section 3.3.1. The simulation software matched all design variables against each other and have different possible designs. After optimisation simulation, approximately 30 different designs were obtained as illustrated in figure 4.23. It is clear from Figure 4.23 that the highest yield value which can be obtained from all the designs is 24%. Depending on the objectives needed which in this case it was low porosity and micro-porosity, four best designs out of 30 possible designs were selected as illustrated in figure 4.24. The four designs have almost the same amount of porosity and micro-porosity. From the four best designs selected, the one with highest yield was selected (Design 24). Design 24 consists of feeder radius of 18 mm, feeder height of 35 mm and number of feeders which is 5 (as shown in figure 4.25). The design also shows 1% increase in casting yield from 21% to 22%.

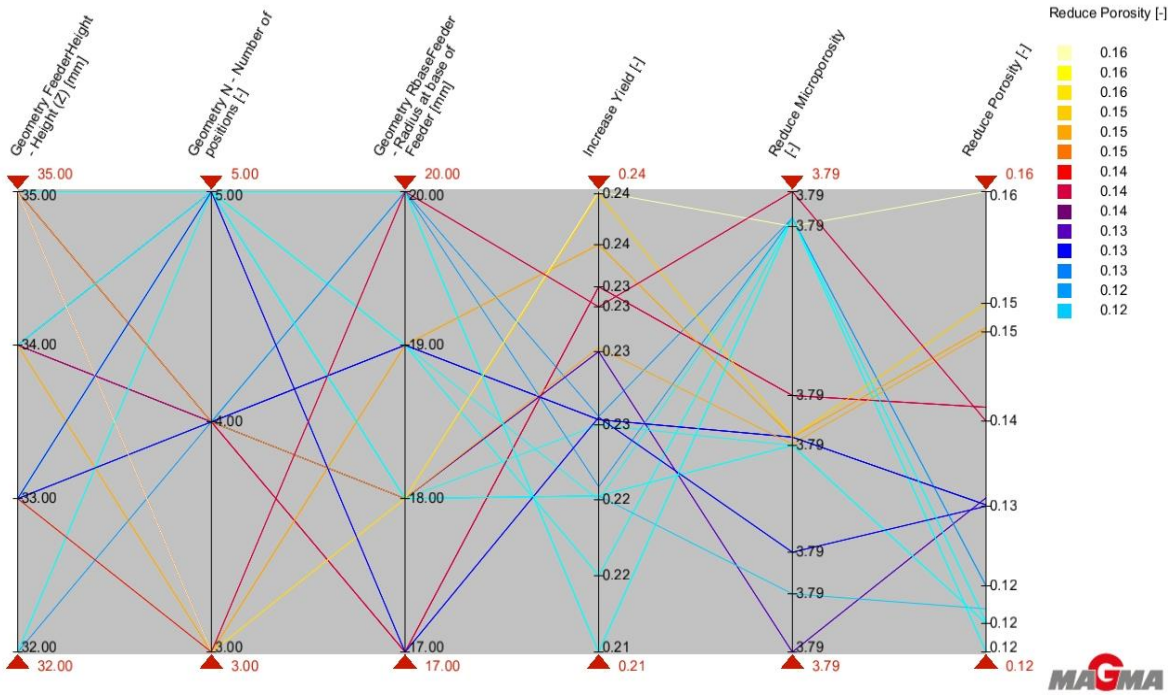

Figure 4. 23: Parallel coordinates results after optimisation simulation (30 different designs)

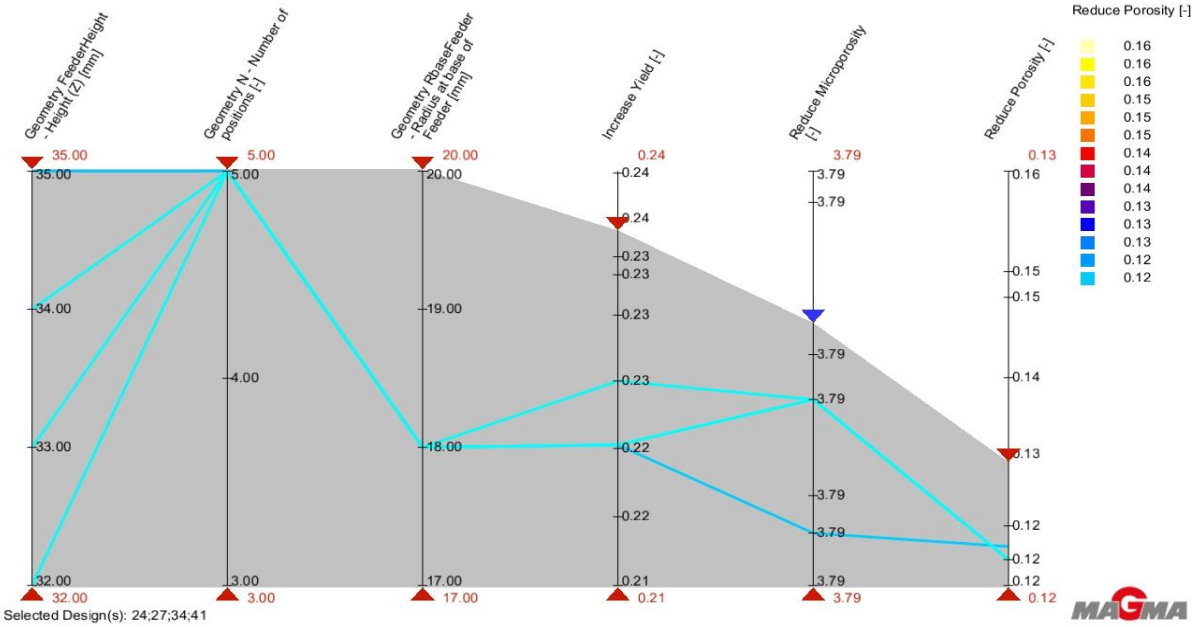

Figure 4. 24: Parallel coordinates results after optimisation simulation (4 best designs)

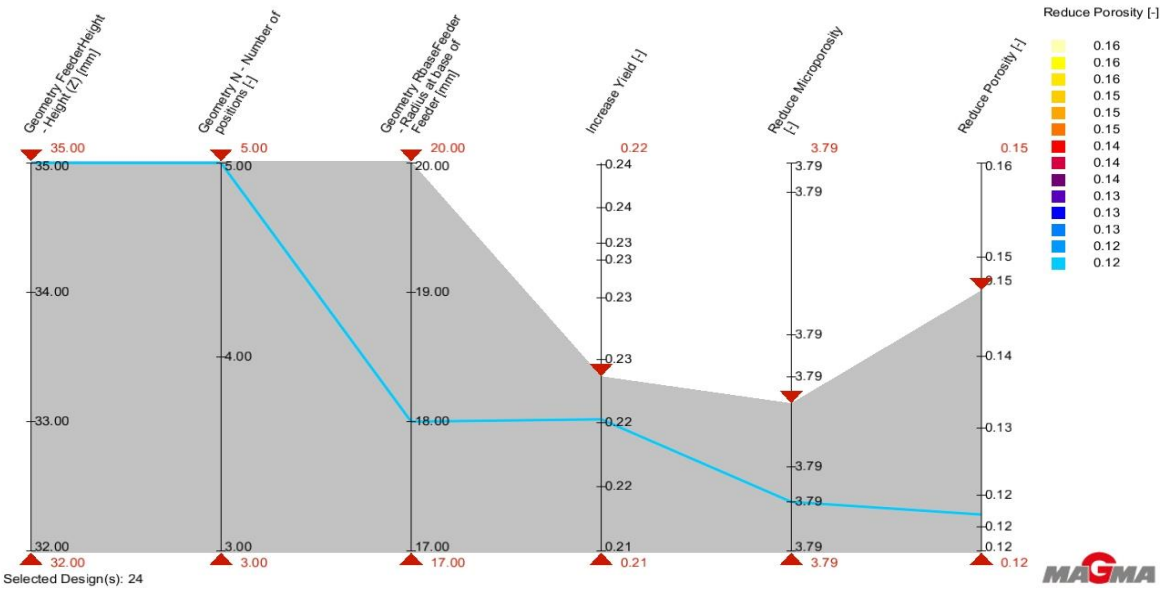

Figure 4. 25: Parallel coordinates results after optimisation simulation (1 best design)

Optimisation simulation also showed how each variable affects the specified objective (low hot spot, low porosity and high yield). Design variables used are specified in Table 3.5 under section 3.3.1. Figure 4.26 showed how hot spot is affected by specified variables. When feeder height was increased from 32 mm to 35 mm there was a slight increase in the size and number of hot spot islands (See Figure 4.26). An increase in the feeder radius (from 17 mm to 18 mm) also increased the number and size of hot spot islands. From 18mm to 19mm increase in feeder radius there was no effect on the number and size of hot spot. From 19mm to 20mm increase in feeder radius there was a slight decrease in the size and number of hot spot islands. These results are normal since the increase was negligible. Increasing the number of feeders from 3 to 4 resulted a noticeable decrease in size and number of hot spot island. This is normal since increasing the number of feeders provide excess metal which reduces hot spots in the casting. But when the number of feeders were increased from 4 to 5 there was a slight increase in the size and number hot spot results.

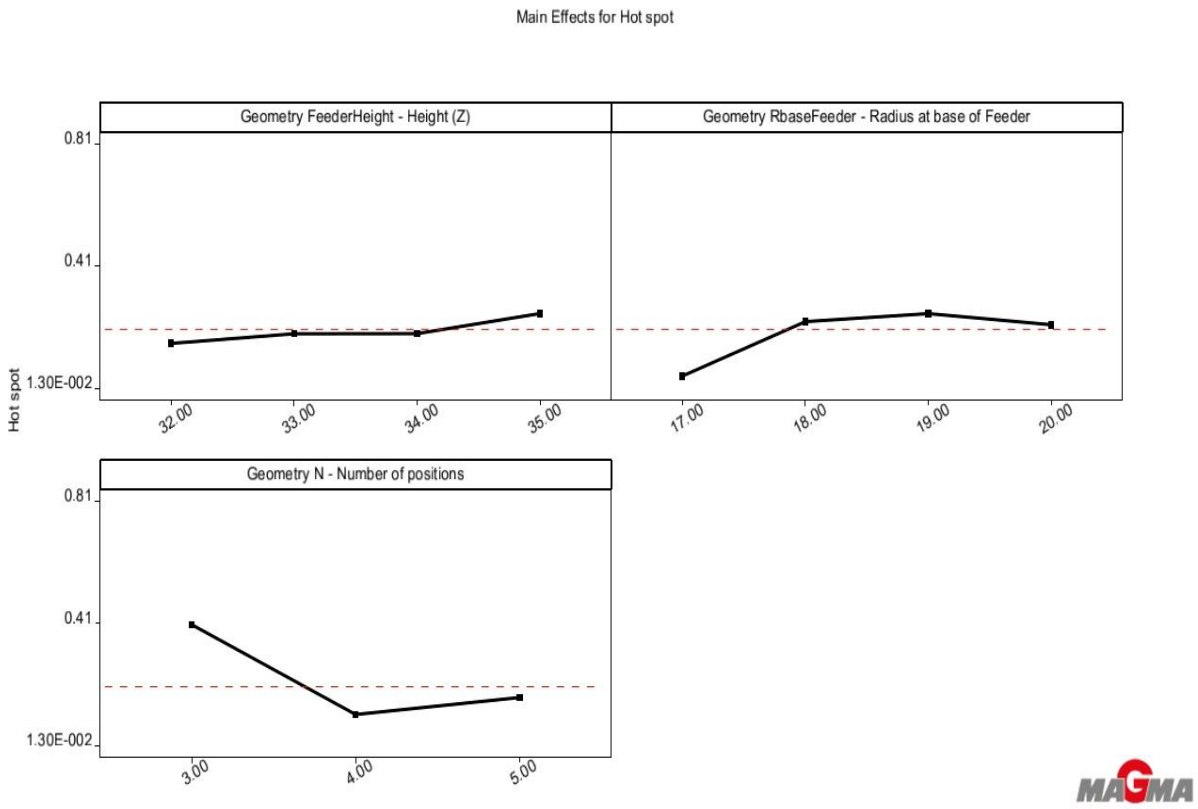

Figure 4. 26: Relationship between hot spot and different variables

Different results were noted when analysing the main effects of different variables on the porosity results as shown in figure 4.27. An increase in feeder height from 32 mm to 33 mm showed an increase in possibility of porosity formation inside the casting. A further increase in feeder height showed only a small increase in possibility of porosity formation inside the casting. There was a slight decrease in possibility of porosity formation inside the casting as feeder radius was increased from 17 mm to 18 mm. A further increase in feeder radius from 18 mm to 20 mm showed a noticeable decrease in possibility of porosity formation inside the casting. A decrease in possibility of porosity formation inside the casting was noted as the number of feeders were increased from 3 to 5.

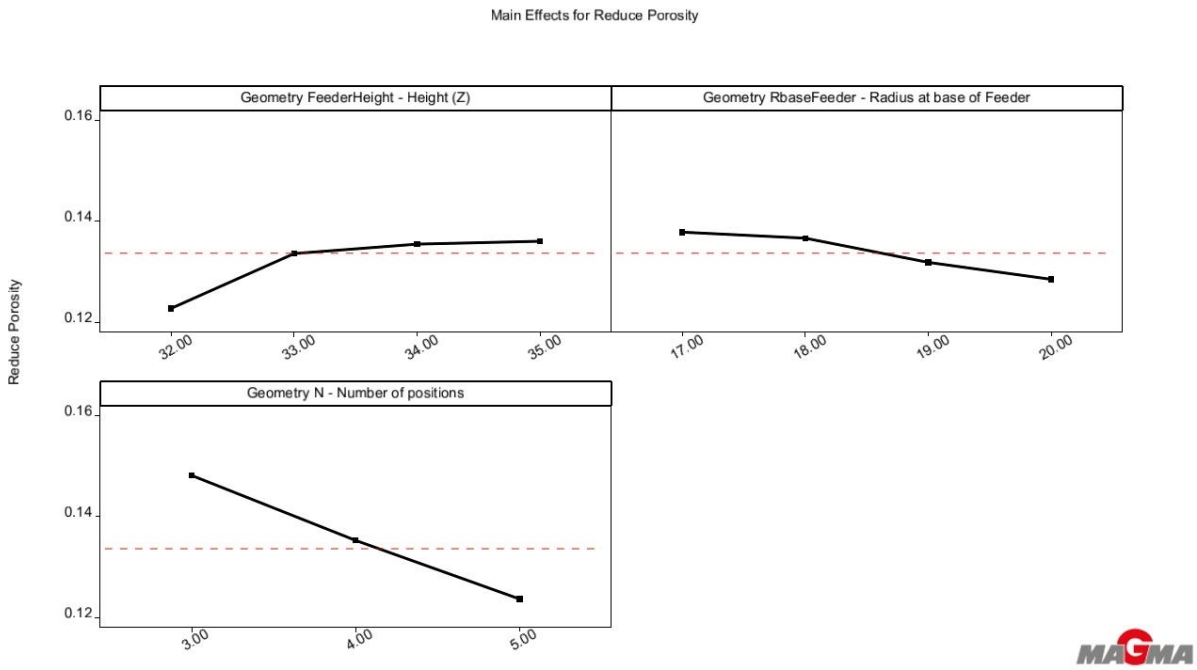

Figure 4. 27: Relationship between porosity and different variables

The change in casting yield as the feeder height increases from 32 mm to 35 mm was negligible (Figure 4.28). This was due to small change in feeder height. An increase in feeder radius from 17 mm to 18 mm caused a slight decrease in casting yield. A further increase in feeder radius from 18 mm to 20 mm showed a decrease in casting yield. A sharp decrease in casting yield was noted when the number of feeders were increased from 3 to 5. All these results are normal since increasing amount of metal reduce casting yield.

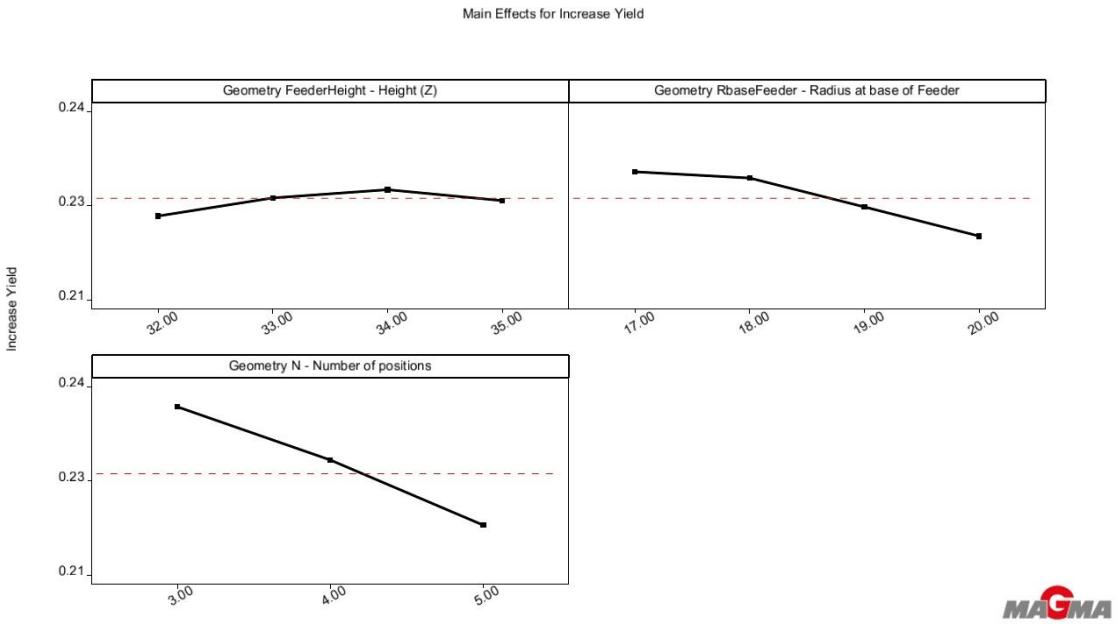

Figure 4. 28: Relationship between casting yield and different variables

The relationship between quality of the cast (in terms of porosity results) and casting yield was recorded in Figure 4.29. The orange curve shows the results of casting yield while the blue curve showed the amount of porosity. It is clear from the curve that when the porosity increases (i.e. poor quality) the casting yield increases. Thus, when improving the casting quality, the casting yield was found to decrease.

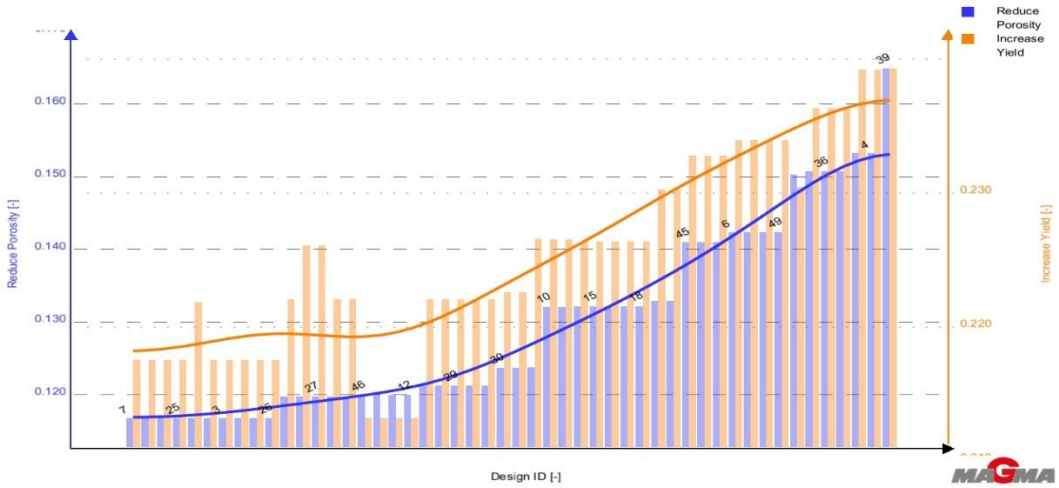

Figure 4. 29: Relationship between casting yield and porosity

The best design (Design 24) was then further analysed to evaluate filling and solidification results. A 3D view of an optimised runner system design of austenitic stainless steel is shown in Figure 4.30.

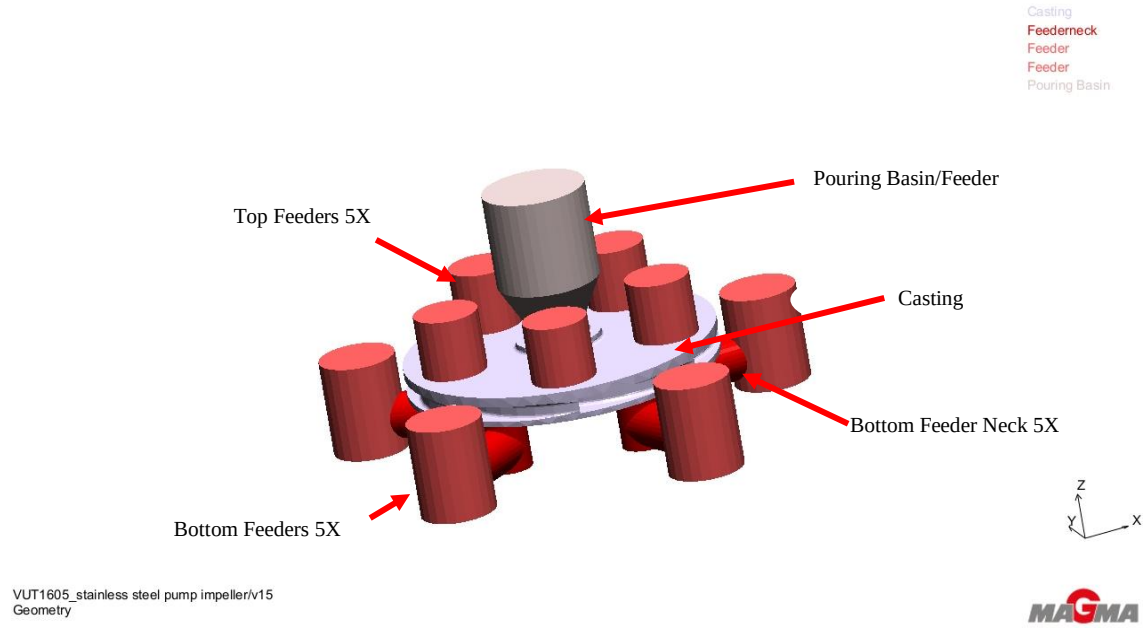

Figure 4. 30: 3D view of the best design chosen (d24)

Figure 4.31 showed the filling simulation of a pump impeller. The scale on the right-hand side was set from solidus temperature to liquidus temperature. The blue colour showing solidus temperature (1399 °C) and yellow colour showing liquidus temperature (1454 °C). Figure 4.31 shows the filling results where 36 % of the mould cavity was filled. Figure 4.32 shows filling results where 70 % of the mould cavity has been filled.

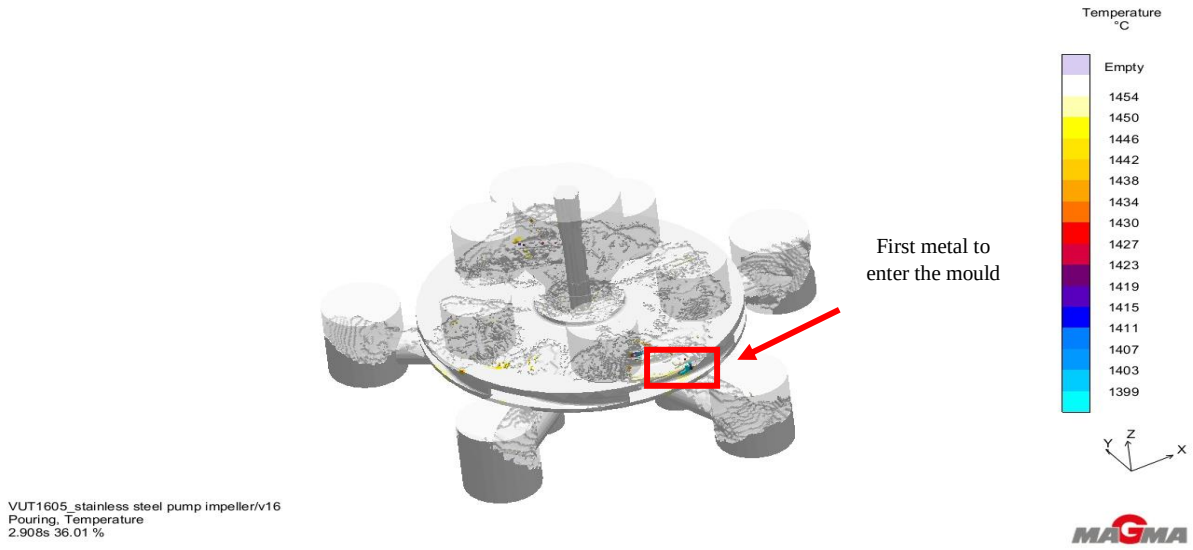

Figure 4. 31: Filling simulation of casting after 2.9 seconds

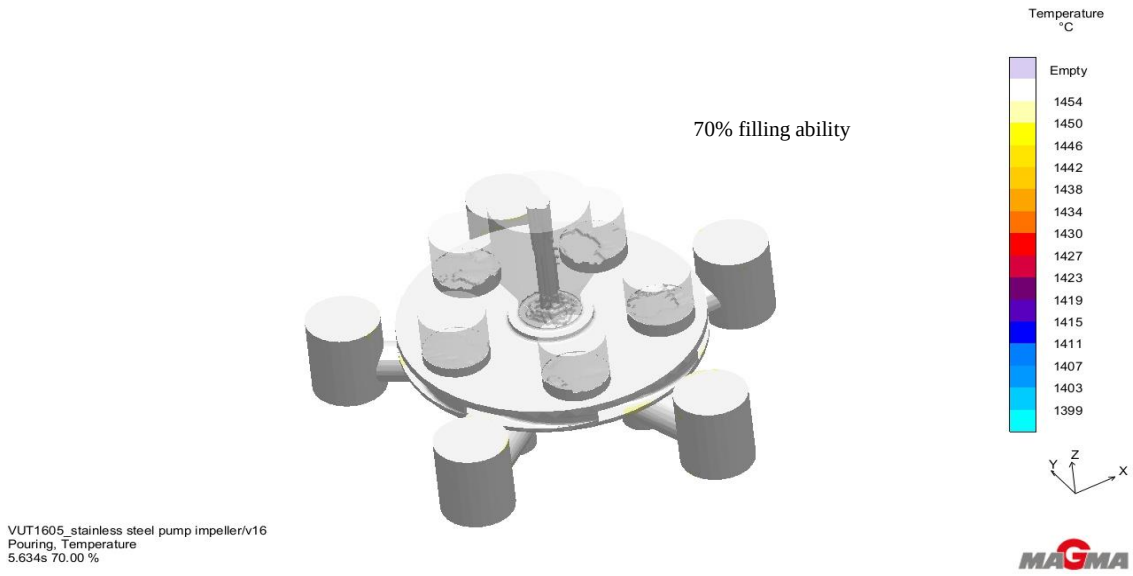

Figure 4. 32: Filling simulation of the casting after 5.6 seconds

Figure 4.33 showed hot spot results where the yellow colour shows the last part to solidify during solidification. There were no hot spot inside the casting, all the hot spots were moved into the feeders. Figure 4.34 showed porosity results with the scale on the right-hand side of the casting. The scale of porosity results showed the possibility of porosity formation in percentage

(%). The blue colour shows low possibility (approximately 20 %) of porosity, red showing approximately 60 % possibility and yellow showing 90 % possibility. All the porosity shifted from the casting to the feeders (See Figure 4.34).

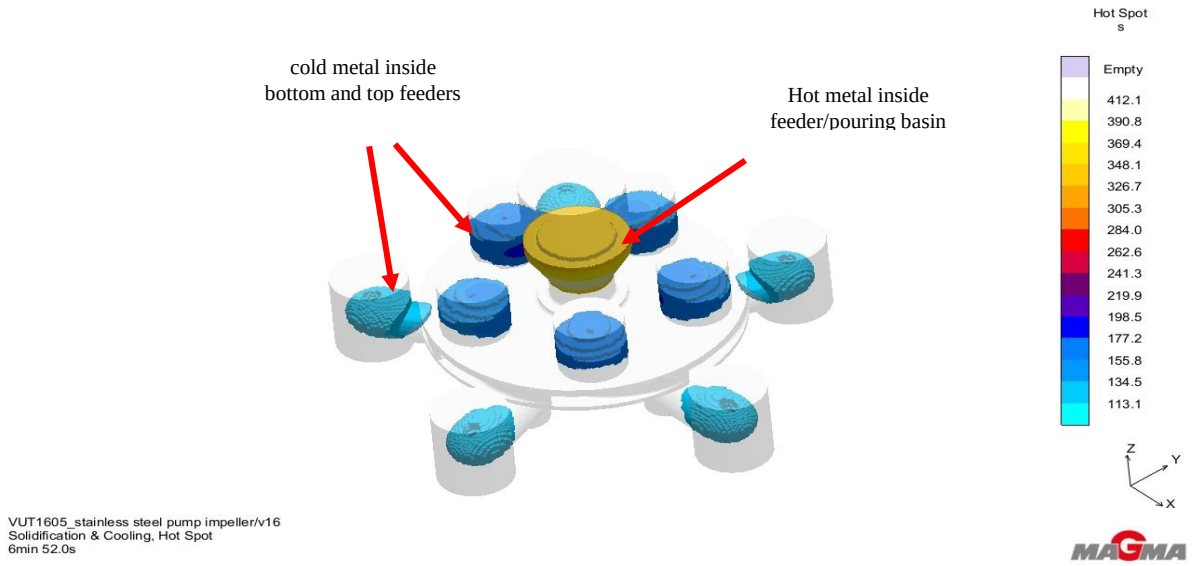

Figure 4. 33: Hot spot results of the best design

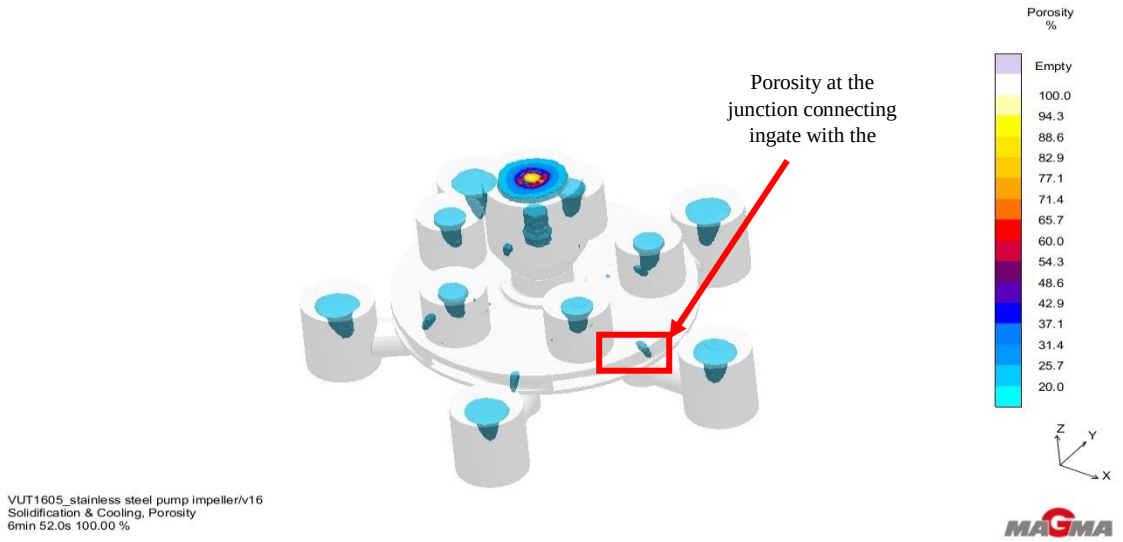

Figure 4. 34: Porosity results of the best design

4.3.2.3 Chemical analysis and temperature reading of design VX 02

Table 4.2 shows chemical composition of different samples taken during melting process before casting. Sample 1 showed Mn content being low by 0.27 with Ni and Cr high by 0.07 and 0.09 respectively as compared to the targeted aim. Minor Mn additions were made to pick up Mn

content and sample 2 showed it low by 0.01. A final sample with the chemical composition close to the targeted chemical analysis was then taken before tapping the furnace. Table 4.3 showed temperature reading during melting and casting process. The furnace was tapped at 1518 °C which is 2 °C below targeted tapping temperature. A massive temperature drops of 12 °C was noted in the ladle temperature. The ladle temperature was 4°C below the ladle temperature aim. Casting was done at a temperature 3 °C below the targeted temperature (1497 °C).

Table 4. 2: Chemical composition of austenitic stainless-steel (Design VX02) after casting

Element	C	Mn	Si	P	S	Ni	Cr	Mo
Aim	0.05	1.5	1	0.04	0.03	10	18	2.5
Sample 1	0.06	1.23	0.98	0.021	0.022	10.07	18.09	2.51
Sample 2	0.06	1.49	0.99	0.021	0.022	10.08	18.09	2.51
Final sample	0.055	1.51	0.99	0.021	0.022	10.07	18.09	2.50

Table 4. 3: Temperature readings during casting of austenitic-stainless steel (Design VX02)

Temperature (°C)	Aim	Reading
Tapping temperature	1520	1518
Ladle temperature	1510	1506
Pouring temperature	1500	1497

4.3.2.4 Casting results of design VX 02

Figure 4.35 (A and B) shows a defective austenitic stainless-steel pump impeller after casting at 1497 °C. Approximately 50 % of the entire mould cavity was filled with the remaining 50 % unfilled. Simulation results on the other showed completely-filled casting. Cold laps which form due to metal being cold were observed at the top part of the casting whereas simulation showed no indication of cold laps. Incomplete filling of impeller blades at the bottom part of the casting was also observed. Top feeders were still full indicating quick solidification which left feeders ineffective.

Figure 4. 35A and 4.35B: Defective austenitic stainless-steel pump impeller cast at 1497 °C.

4.3.2.5 Microstructural analysis of design VX 02

Figure 4.36 shows microstructural analysis of the test samples which was cast at 1497 °C. Microstructure showed austenitic matrix (γ) with delta ferrite (δ) precipitates (Rundman 2005). A fully austenitic matrix could have been promoted by Ni content which was at the higher level. With the low C (0.05 %) content, no indications of martensite or carbides were noted.

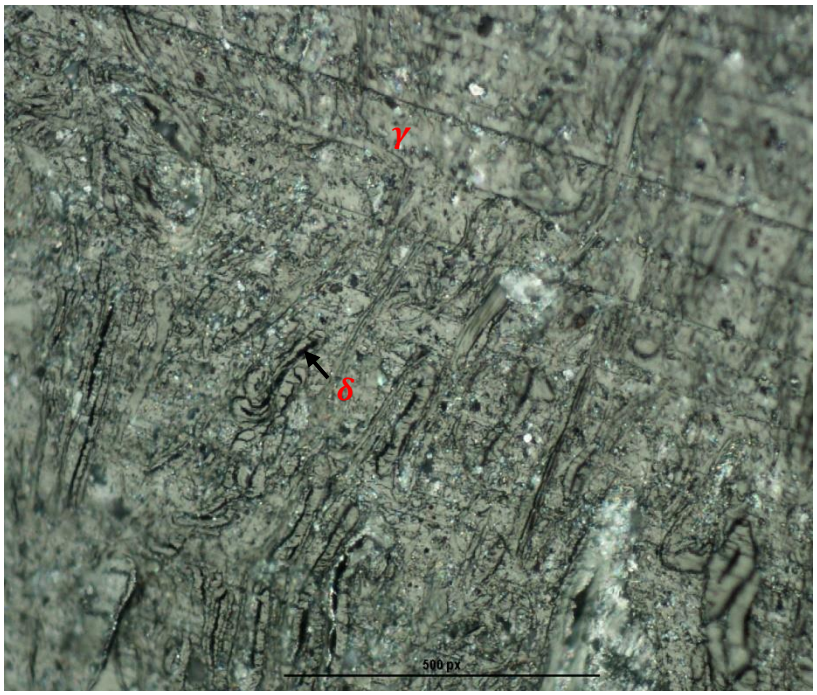

Figure 4. 36: As cast microstructure of an austenitic stainless steel pump impeller at 50X magnification

4.3.2. 6 Hardness of design VX 02

Vickers hardness results of the sample was taken and plotted in Figure 4.37. Hardness was taken at five different positions showing different results. Position 1, 2, 3, 4 and 5 have 271 HV_5, 351 HV_5, 285 HV_5, 404 HV_5 and 258 HV_5 hardness values respectively. It was noted that the hardness value was not consistent. The average hardness obtained was 313.8 HV_5 with the standard deviation of 61.8 and a standard error of 27.63.

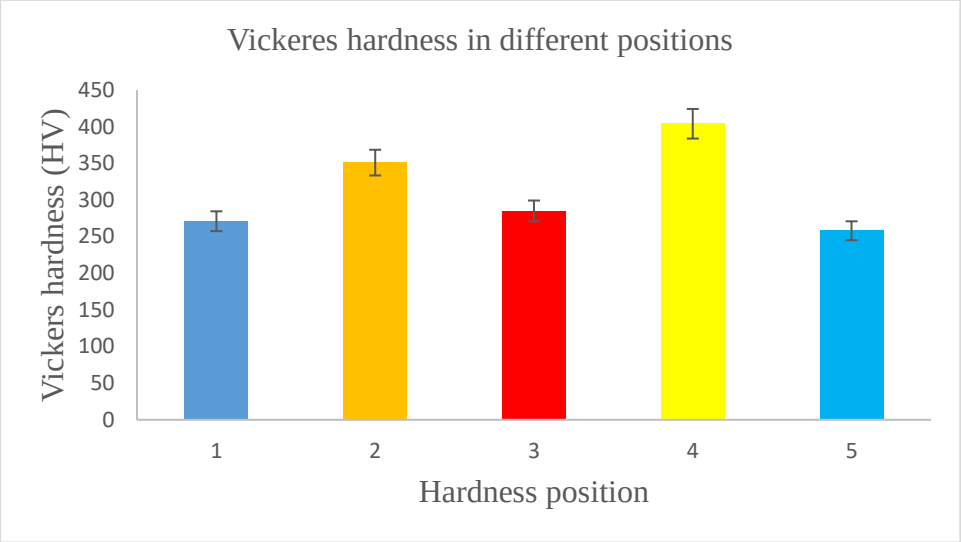

Figure 4. 37: Vickers hardness results of an as cast austenitic stainless steel at different positions

4.4 Results of study 4 (1st of 2nd Trial): Optimization of filling and feeding of nodular cast iron pump impeller produced by sand casting.

4.4.1 Design VX03

4.4.1.1 Optimization simulation

Design variables used for optimisation simulation are specified in Table 3.6 under section 3.3.2. After simulation software matched all design variables against each other, the best design of them all was chosen. The decision was made based on the objectives required (low hot spot, low porosity and high yield). The best design consists of 17mm feeder radius, 32mm feeder height, 3 number of feeders and casting yield of 48% as illustrated in figure 4.38.

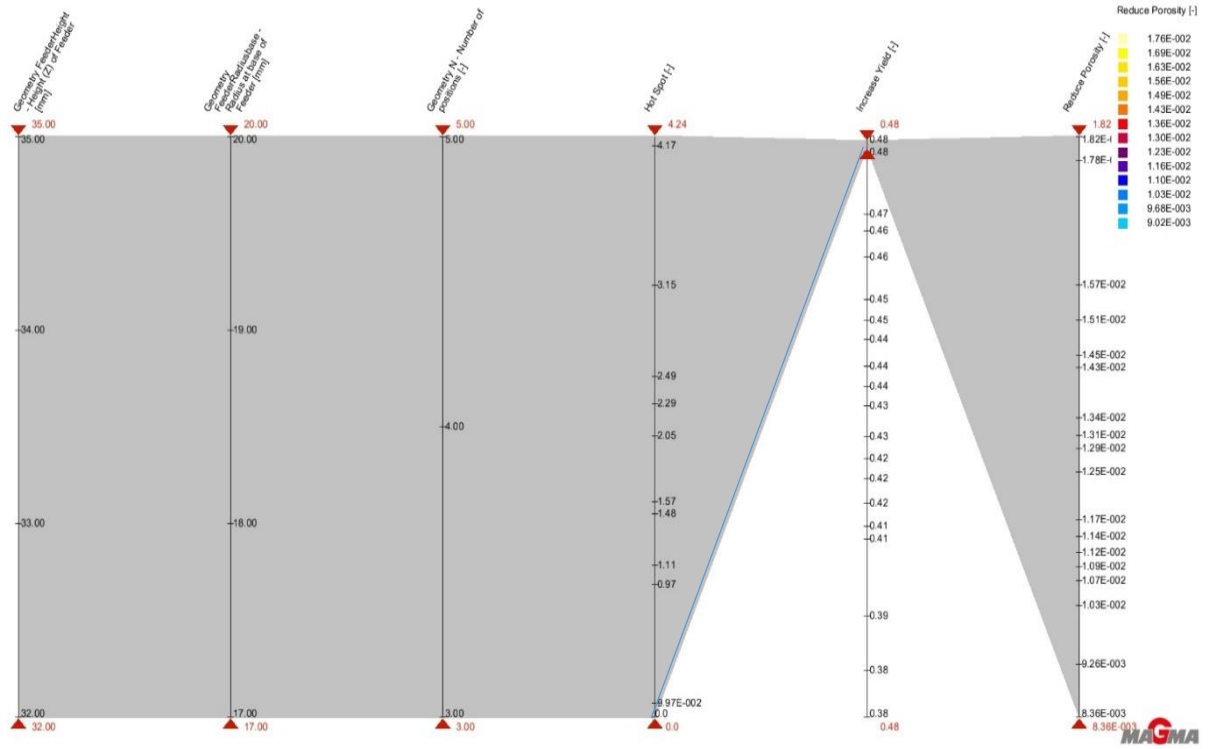

Figure 4. 38: Parallel coordinates results after optimisation simulation (1 best design)

Optimisation simulation also showed how different selected variables affect the quality of the casting. Figure 4.39 shows that there was no significant change of hot spot with feeder height increase. A linear increase of hot spot was noted as the number of feeders increase from 3 to 5. An increase in hot spot was also noticed when the feeder radius was increased from 17mm to 20mm.

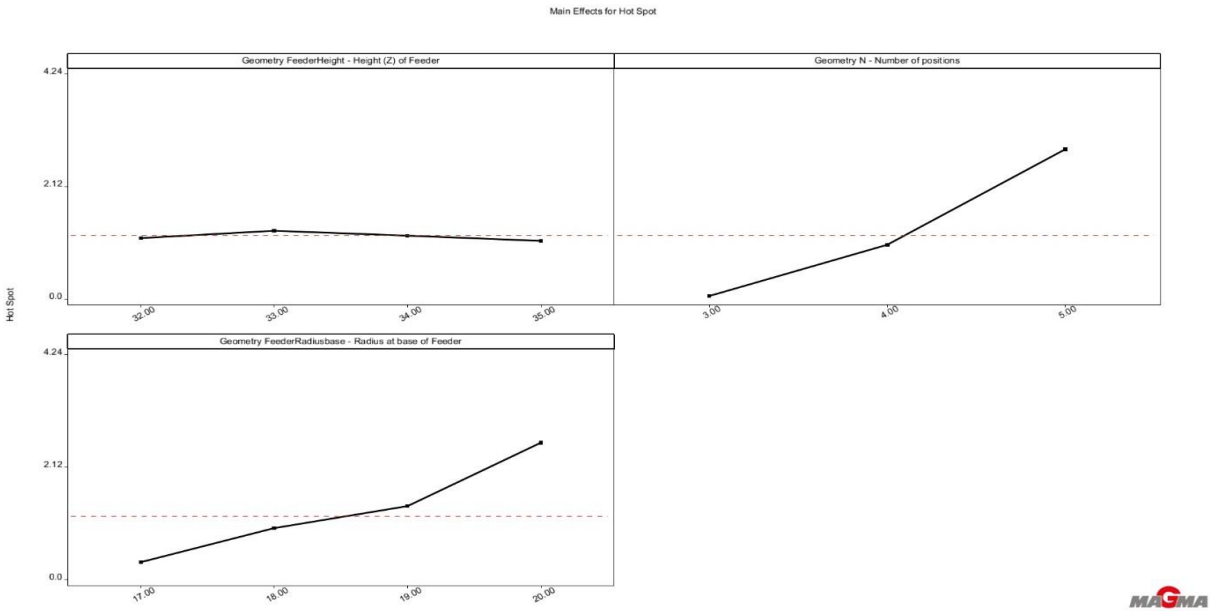

Figure 4. 39: Relationship between hot spot and different variables

An increase in feeder height from 32mm to 34mm shows an increase in porosity results (Figure 4.40). However, this increase was followed by a decline when the feeder height was increased to 35mm. When the number of the feeders were increase from 3 to 5, porosity results increased. Figure 4.39 also showed a decline in porosity results when the feeder radius was increased from 17mm to 20mm.

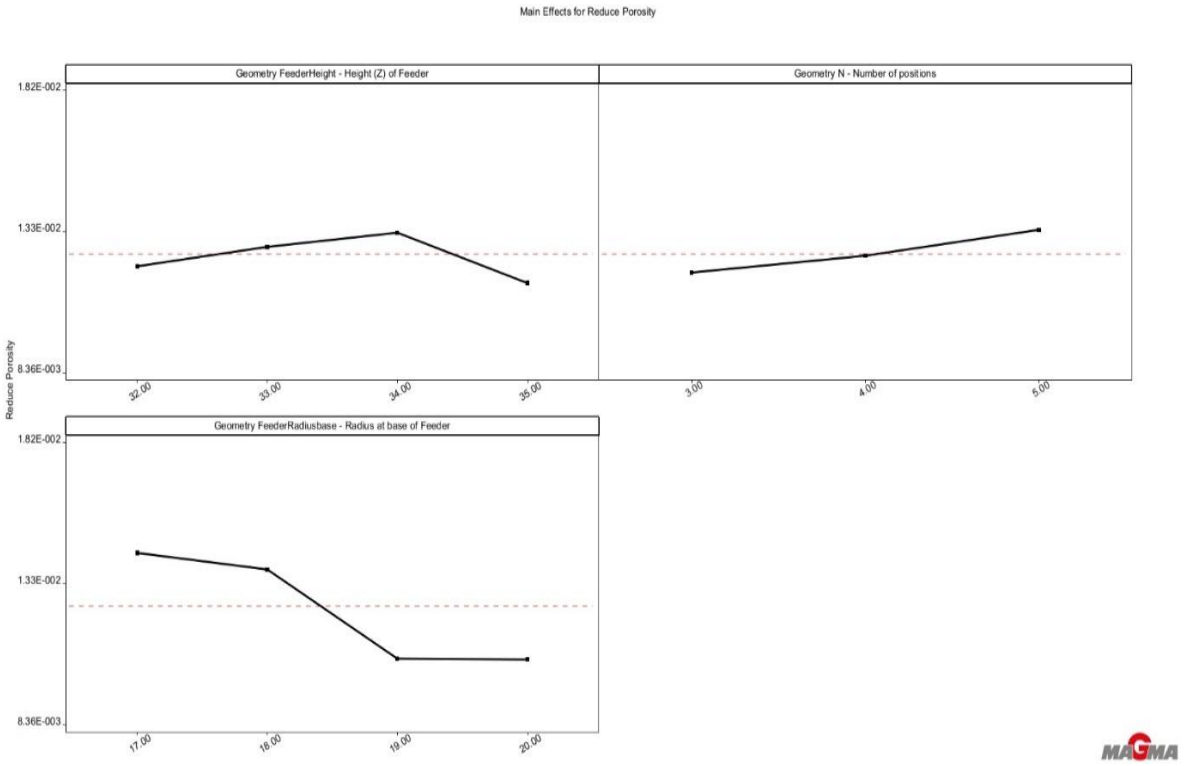

Figure 4. 40: Relationship between porosity and different variables

Increasing feeder height from 32mm to 35mm shows a marginal decrease in casting yield according to Figure 4.41. A decline in casting yield was observed when the number of feeders were increased from 3 to 5. A decline on casting yield was again noticed when the feeder radius was increased from 17mm to 20mm.

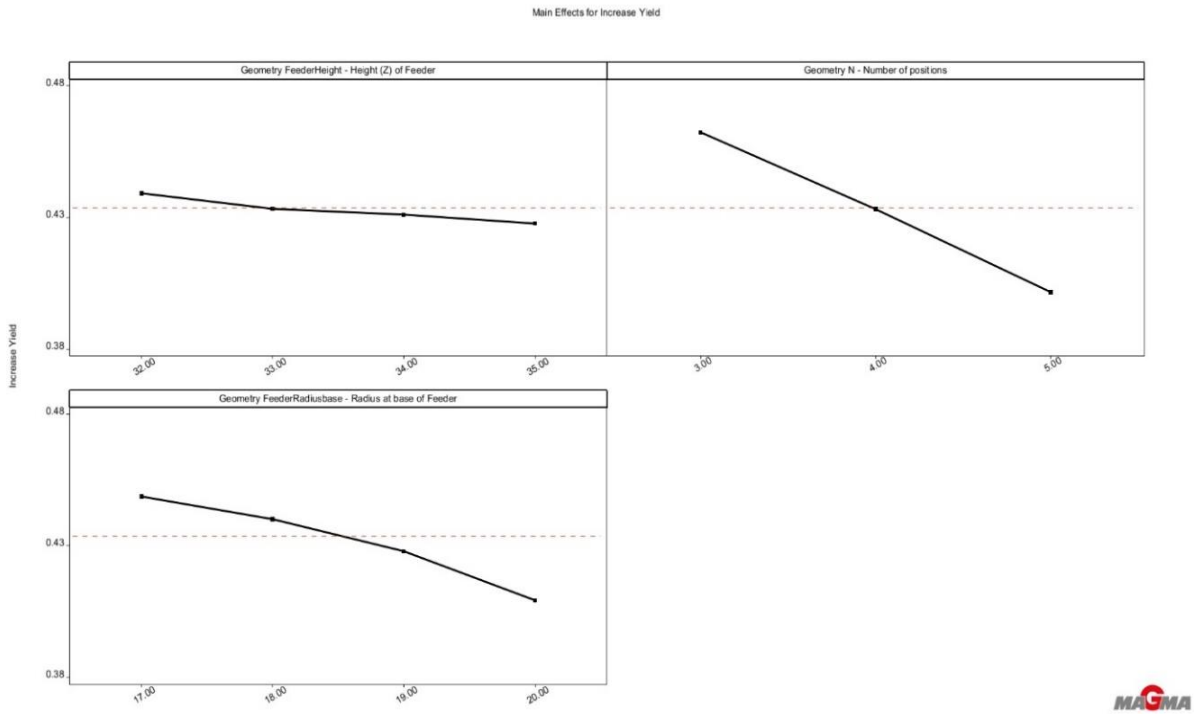

Figure 4. 41: Relationship between casting yield and different variables

From the best optimisation design (d20), changes were made to increase casting yield from 48% to 56% while maintaining quality of the casting. The changes made were reducing feeder radius from 17mm to 15mm and feeder height from 35mm to 30mm. This was expected since the modulus of the reduced feeders was still higher than of the casting making feeders last part to solidify.

Figure 4.42 showed hot spot results after solidification of Design VX 03. The scale above this figure showed that after 78 seconds the material represented by blue colour will be solid. Material represented by purple colour will be solid after 300 seconds and the one represented by yellow colour will take approximately 550 seconds. This means that the material represented by yellow colour will be the last to solidify followed by purple and lastly blue. Thin walled blades were first to solidify followed by the junctions where blades connect to the casting. Minimal indications of shrinkage porosity at this location was noticed. Small side feeders solidified later than the casting but faster than the pouring basin. Figure 4.42 showed feeder/ pouring basin being the last part to solidify. However, there was a delay in solidification at the top part of the casting.

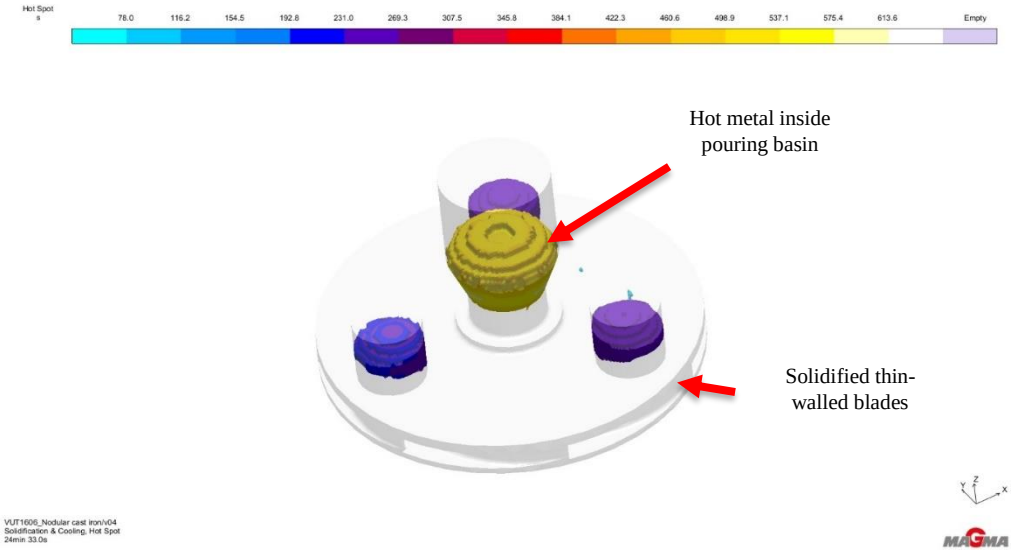

Figure 4. 42: Hot spot results of the best design

From the scale at the top of Figure 4.43, blue colour showed the lowest possibility of porosity formation (0-20%), red colour shows the average possibility of porosity formation (40-50%) and yellow colour showed the highest possibility of porosity formation (70-100%). Casting showed no indication of porosity defect. Small feeders showed minimal possibility of porosity formation. Porosity was high inside the big feeder/pouring basin which is a good indication of quality casting.

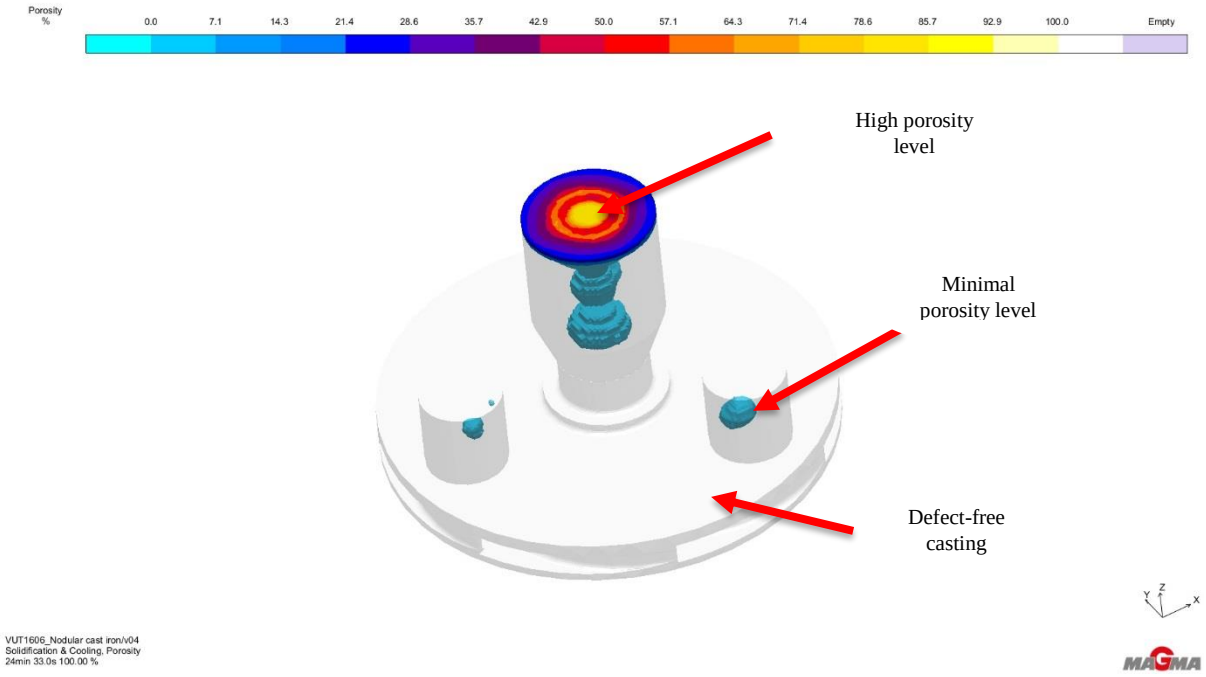

Figure 4. 43: Porosity results of the best design

4.4.1.2 Chemical analysis and temperature reading of Design VX03

Chemical composition of different samples taking during melting of nodular cast iron are shown in Table 4.4. Sample 1 showed C and Mn content below aim by 0.26 and 0.07 respectively. After additions, sample 2 showed all alloys close to the targeted composition. A final sample which had almost the same chemical composition as sample 2 was taken before tapping of the furnace. Tapping was done at a temperature lower than the aim by 3°C (See Table 4.5). After tapping, temperature inside the ladle was higher than its aim by 1 °C.

Table 4. 4: Chemical composition of nodular cast iron after casting

Element	C	Cu	Mg	Mn	P	S	Si
Aim	3.40	0.03	0.03	0.25	0.01	0.02	2.2
Sample 1	3.14	0.02	0.01	0.18	0.01	0.01	2.19
Sample 2	3.41	0.02	0.02	0.24	0.02	0.01	2.21
Final sample	3.41	0.03	0.01	0.24	0.02	0.01	2.19

Table 4. 5: Temperature readings during casting of nodular cast iron

Temperature Reading at	Targeted Temperature (◦C)	Actual Temperature (◦C)
Tapping	1520	1517
Ladle	1510	1511
Pouring	1500	1501

4.4.1.3 Casting results of Design VX03

A completely-filled nodular cast iron pump impeller which was cast at 1501°C as shown in Figure 4.44A. It was observed that the mould cavity with thin-walled blades of 2 mm was completely-filled during casting and visual observation showed no indication of misrun or cold lap defect. Minor shrinkage defect on the top surface of pump impeller were noted. These surface defect can typically be repaired with the use of welding process. The bottom part of the casting showed no indication of defect (Figure 4.44B).

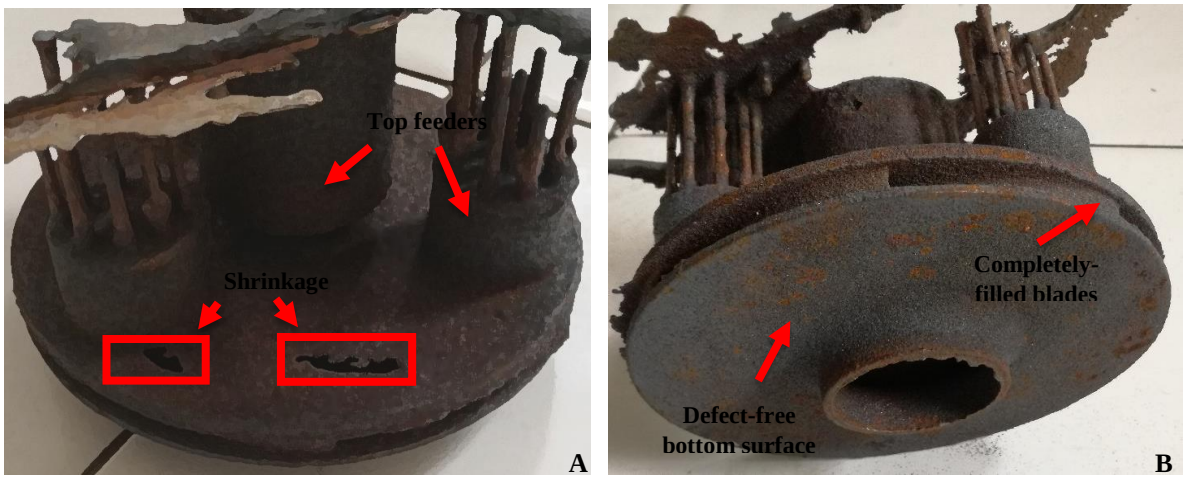

Figure 4. 44A and 4.44B: Completely-filled nodular cast iron pump impeller with minor shrinkage defects cast at 1501 °C.

4.4.1.4 Microstructural results of Design VX03

Solidification started when the temperature reaches a liquidus line with the formation of austenite in the liquid metal (Rundman 2005). This structure remained the same until the temperature drops below eutectic line. Below this eutectic line, the whole microstructure transforms to austenite with the formation of pearlite, martensite and ledeburite matrix as illustrated in Figure 4.45. Figure 4.45 also showed retained austenite which was surrounded by cementite inside the pearlite and ledeburite matrix. A variety of phases (pearlite, martensite, ledeburite and retained austenite) were noted in this structure which could affect its mechanical properties.

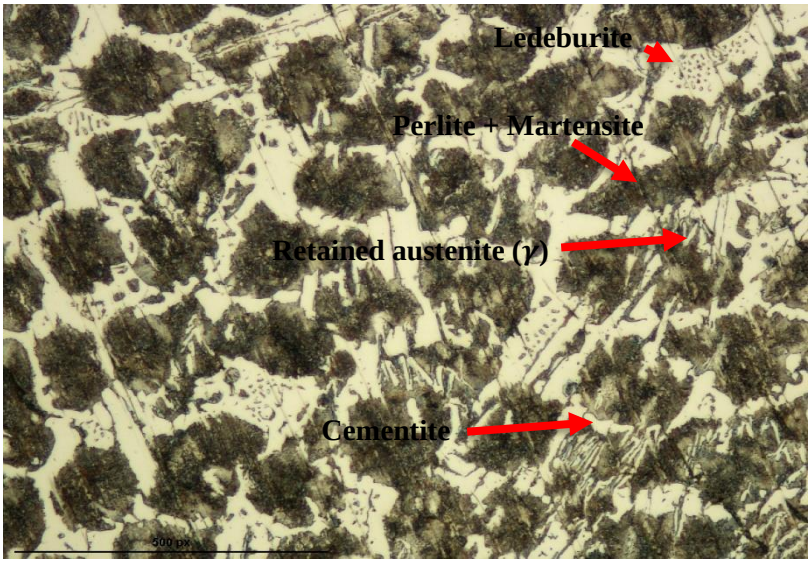

Figure 4. 45: As cast microstructure of a nodular cast iron pump impeller at 500X magnification

4.4.1.5 Hardness results of Design VX 03

An average of three indentations were taken at five different positions (1, 2, 3, 4 and 5). In position 1, the hardness value was 271 HV_5. The hardness value picked up to a high value of 474 HV5 after changing position from position 1 to position 2 as shown in Figure 4.46. Hardness dropped to 292 HV_5 and 247 HV_5 when moving to position 3 and 4 respectively. Position 5 showed an increase in hardness of 438 HV_5. The average hardness obtained was 345 HV_5 with the standard deviation of 103 and a standard error of 46.06.

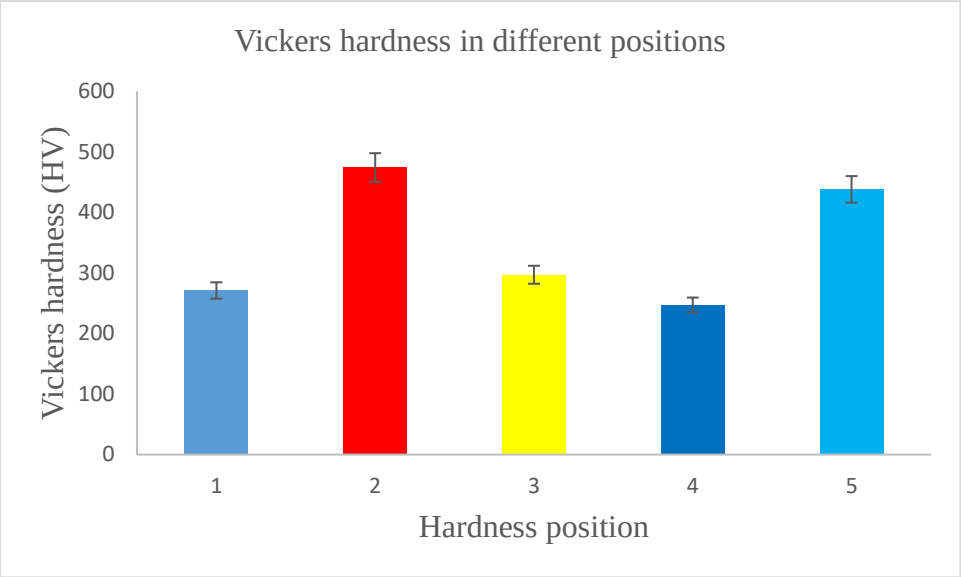

Figure 4. 46: Vickers hardness results of a nodular cast iron pump impeller at different positions

4.5 Results of study 5 (2nd Trial): Optimization of filling and feeding of austenitic stainless-steel pump impeller produced by sand casting.

4.5.1 Design VX04

4.5.1.1 Filling Simulation of Design VX04

A new design (VX04) of runner system was developed to improve filling and solidification of austenitic stainless-steel pump impeller in Design VX02. The design consists of a tapered circular runner bar with tapered sprue well and 7x tapered ingates (See Figure 4.47). Pouring was done at 1550 °C and the metal enters the mould cavity a temperature of approximately 1525 °C indicating temperature loss of approximately 25 °C from pouring to the ingates. On

the right-hand side of Figure 4.47, Figure 4.48 and Figure 4.49 there is a colour coding temperature scale.

When the mould cavity was 42 % filled, simulation results showed cold metal at the end part of the runner bar (opposite pouring location) as shown in figure 4.47. Figure 4.48 also showed cold metal at the bottom part and the walls of the casting. The temperature of the cold colder metal indicated a loss of approximately 100 °C from the pouring temperature. At 70 % filling ability, the mould was filled except for the sleeve which was still filling. The metal inside the casting was cold with only runner system left with hot metal. Though the cold metal inside the casting, the mould cavity was filled with no indications of misrun defect.

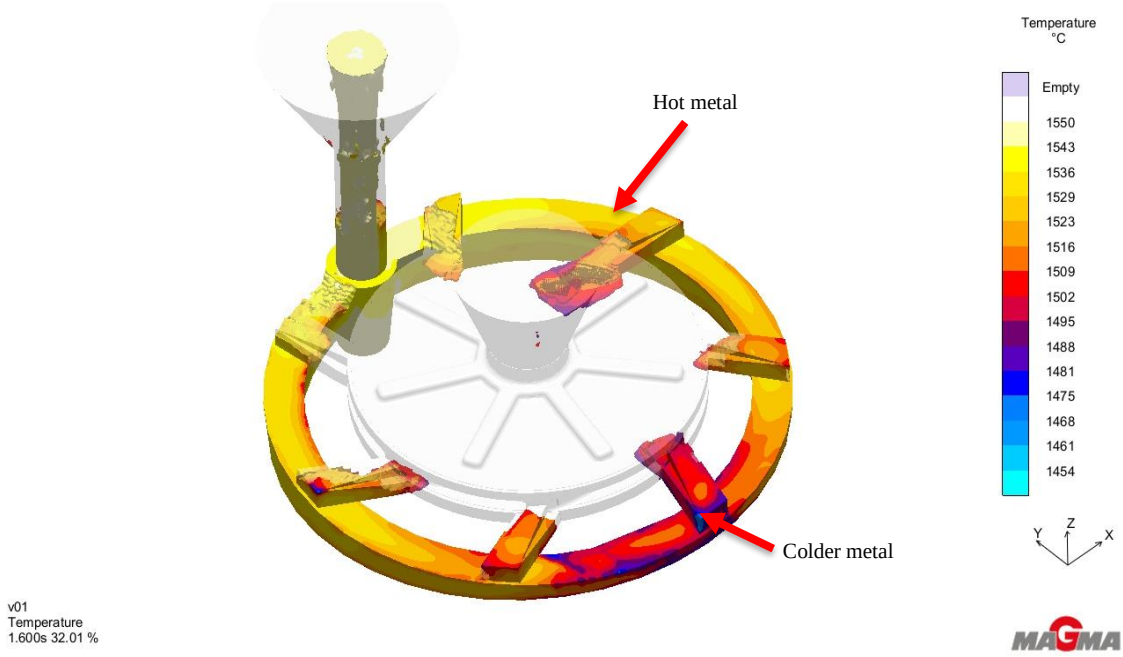

Figure 4. 47: Filling simulation of design VX04 at 32 % filling ability

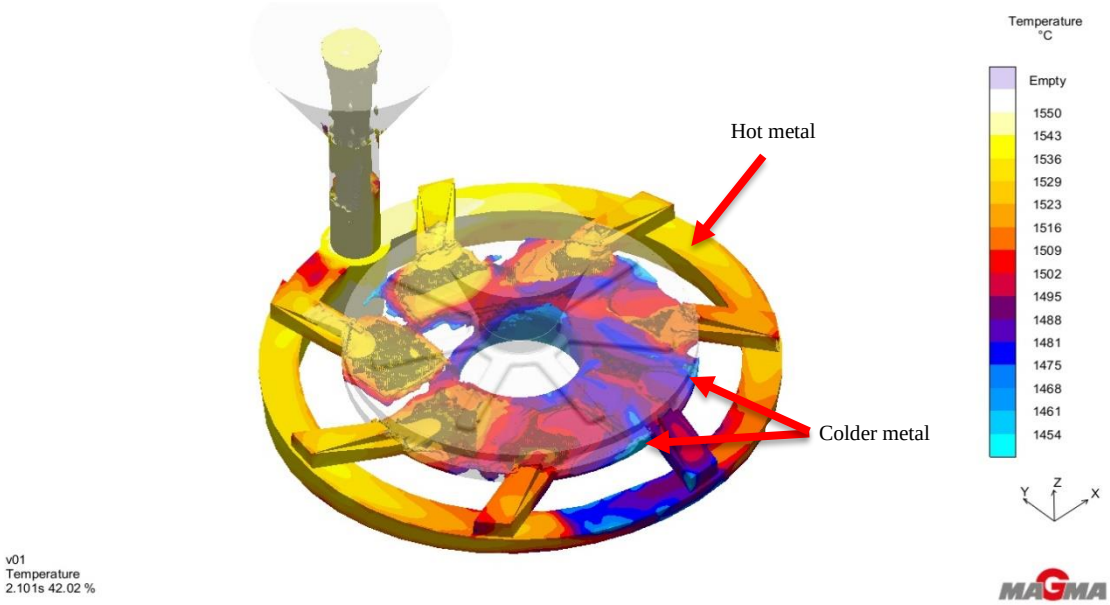

Figure 4. 48: Filling simulation of design VX04 at 42% filling ability

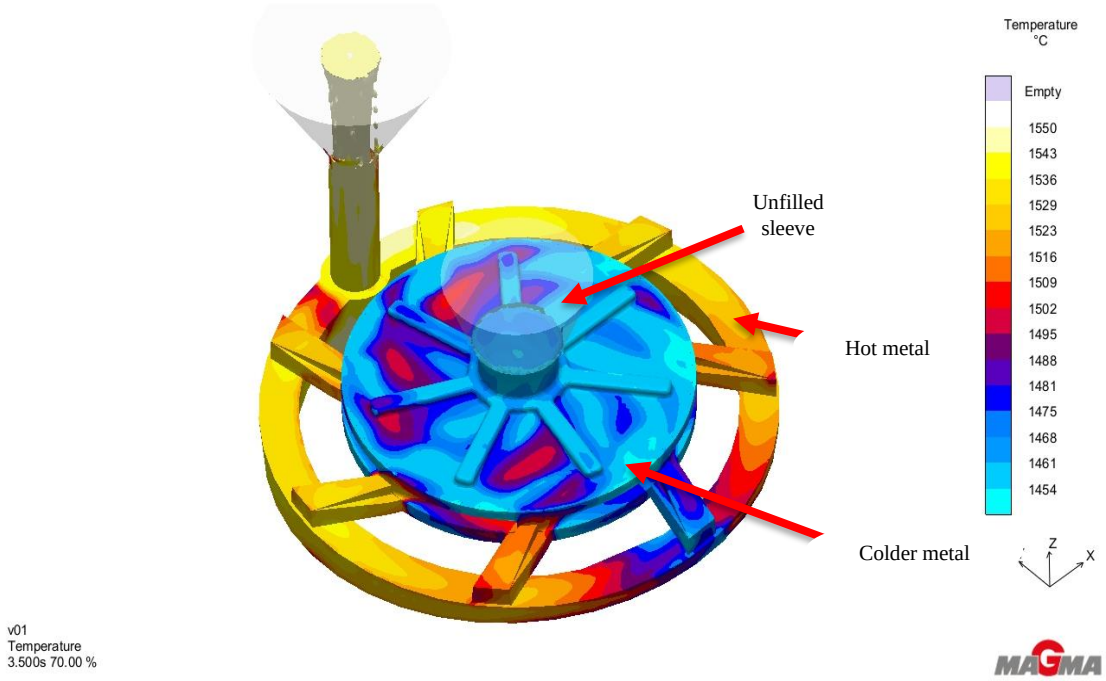

Figure 4. 49: Filling simulation of design VX04 at 70% filling ability

4.5.1.2 Solidification of Design VX04

From the scale on the right-hand side of Figure 4.50 and Figure 4.51, pale yellow colour represents 70 to 100% of liquid metal, white represents solidified metal and red represent 40 to 69% of liquid metal. Figure 4.50 shows solidification results when 31% of the metal had solidified after 16.7 seconds. Solidification started at the bottom part and the walls of the

casting. It then followed thinner section of the runner bar and bottom part of the ingates. Solidification then proceed to the middle part of the casting which consist of the thin-walled blades after 22.6 seconds (Figure 4.51). The feeding from the ingates was cut off as solidification proceed. Hot islands were noted at the junctions between thin-walled blades and bottom part of the casting showing possibility of porosity at those locations.

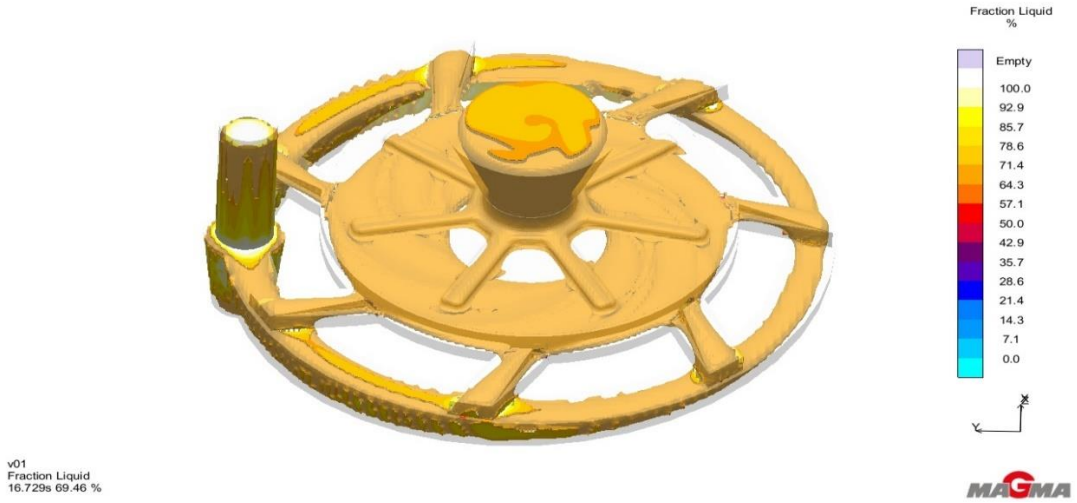

Figure 4. 50: Solidification simulation of design VX04 after 31% solid at 16.7 seconds

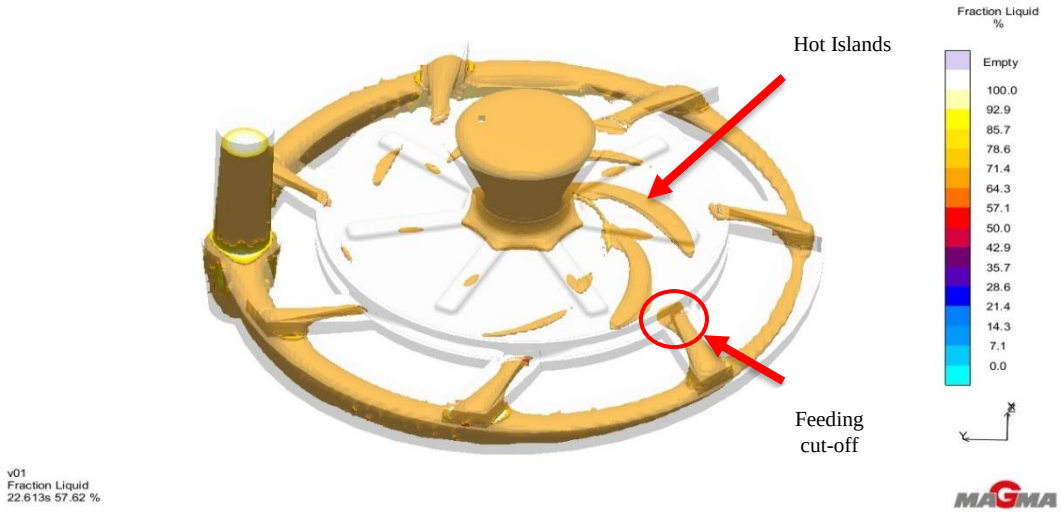

Figure 4. 51: Solidification simulation of design VX04 after 53% solid at 22.6 seconds

From Figure 4.52, the colour coding scale on the left-hand side shows the possibility of porosity formation (where pale yellow colour shows a high possibility and dark blue shows low possibility of porosity formation). In accordance to Joshi and Ravi (2010), and experimental study 1 reported here (in section 4.1), shrinkage porosity were noticed at the I-junctions of the casting. The other parts of the casting showed no indication of porosity formation.

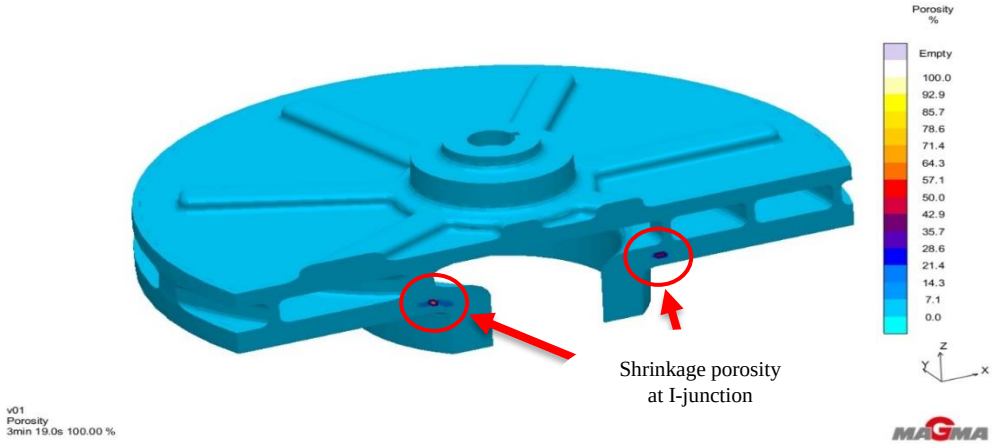

Figure 4. 52: Porosity results of design VX04 after solidification

4.5.1.3 Chemical analysis and temperature reading of design VX 04

Three different samples were taken before casting. The chemical composition of all three samples are shown in Table 4.6 below. The results show that the composition of the scrap charged was close to the target composition (comp). The final sample showed Mn, Si and Mo below the target by 0.15, 0.31 and 0.27 respectively. Cr on the other hand was above the aim by 0.39. Tapping temperature, ladle temperature and pouring temperature were all close to the target composition by -4 °C, +2 °C and +3 °C respectively as illustrated in Table 4.3.

Table 4. 6: Chemical composition of austenitic stainless steel after casting (in wt.%)

Element	C	Mn	Si	P	S	Ni	Cr	Mo
Targeted comp	0.05	1.50	1.00	0.04	0.03	10.00	18.00	2.50
Sample 1	0.01	1.36	0.66	0.022	0.008	10.02	18.21	2.26
Sample 2	0.03	1.33	0.62	0.027	0.003	10.01	18.17	2.29
Final sample	0.01	1.35	0.69	0.028	0.008	10.02	18.39	2.23

Table 4. 7: Temperature readings during casting of austenitic stainless steel

Temperature Reading at	Targeted Temperature (°C)	Measured Temperature (°C)
Tapping	1580	1576
Ladle	1560	1562
Pouring	1550	1553

4.5.1.4 Casting results of design VX 04

The results after casting showed a pump impeller which was not completely-filled (see Figure 4.53A). Indication of misrun was noted at the top of the casting. Figure 4.53A also shows indications of metal flash at the parting line. Some of the thin-walled blades were filled with some showing misrun defect. There was no slag in the casting or feeder noticed. Misrun defect was also noticed at the bottom surface of the casting as illustrated in figure 4.53B and figure 4.53C. However, misrun at the bottom surface was minor as compared to the one on the top surface. Approximately 80% of the entire mould cavity was filled with the remaining 20% unfilled.

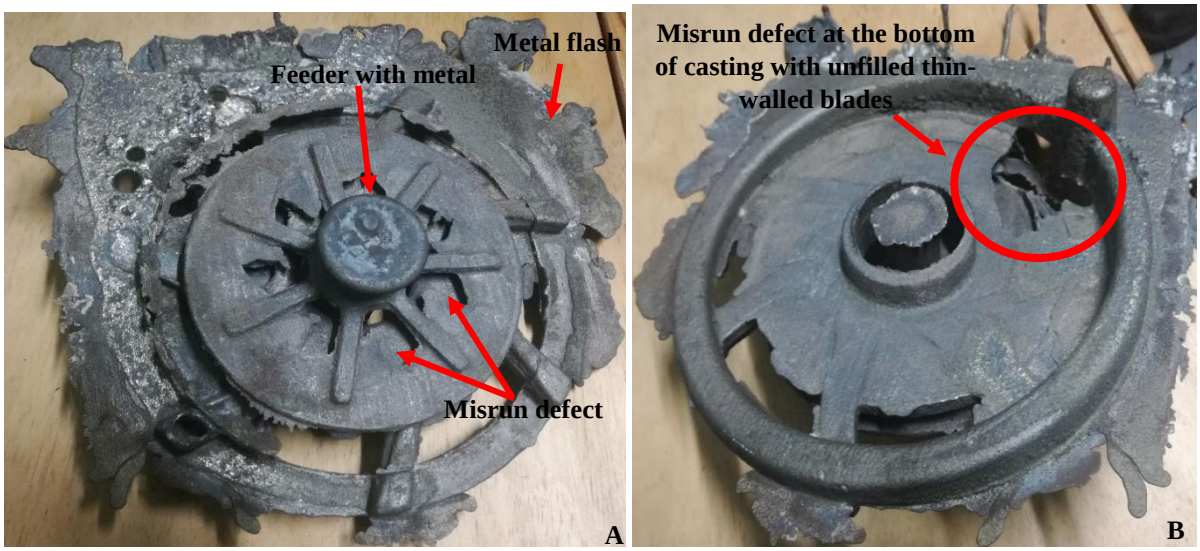

Figure 4. 53A, 4.53B & 4.53C: Misrun defect on an austenitic stainless-steel pump impeller cast at 1497°C.

4.5.1. 5 Microstructural analysis of design VX 04

As-cast microstructure of austenitic stainless steel (figure 4.54A and 4.54B) showed a fully austenitic matrix (γ) with sigma ferrite (δ) uniformly distributed. The structure showed no indication of carbides.

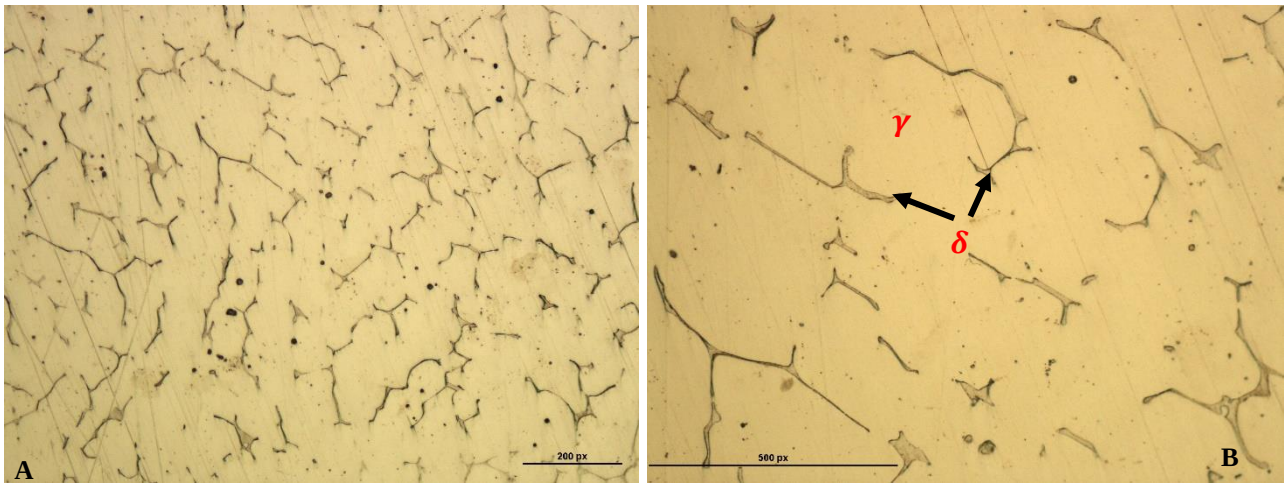

Figure 4. 54A and 4.54B: As cast microstructure of an austenitic stainless steel pump impeller at 20X (A) and 50X (B) magnification.

4.5.1.6 Hardness of design VX 04

An average of three indentations were taken at five different positions with position 1 having a hardness value of 149 HV_5 as shown in figure 4.55. The hardness was more consistent from the 1st till the 5th position as illustrated in Figure 4.54. The average hardness obtained was 156 HV_5 with the standard deviation of 11.4 and a standard error of 5.11.

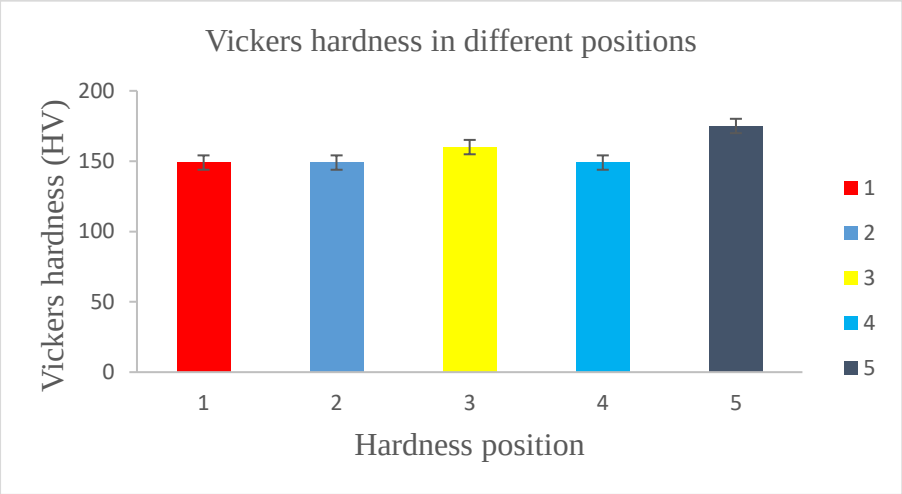

Figure 4. 55: Vickers hardness results of an as cast austenitic stainless steel at different positions

4.6 Results of study 6 (2nd Trial): Optimization of filling and feeding of nodular cast iron pump impeller produced by sand casting

4.6.1 Design VX05

4.6.1.1 Filling Simulation of Design VX05

Based on the simulation and experiments of Design VX03, a runner system was developed to further improve filling and solidification of nodular iron pump impeller. Design VX03 had minimum shrinkage porosity at the top surface of the casting.

Tapered circular runner bar with tapered sprue well and untampered 7x ingates was the new runner system of nodular cast iron pump impeller. The ingates were located at the bottom part of the casting allowing the bottom part to fill first followed by middle and lastly the top part of the casting as illustrated by Figure 4.56. A colour coded scale on the right-hand side of Figure 4.56, Figure 5.57 and Figure 5.58 have a yellow colour indicating a low temperature range (1330 °C to 1390 °C) and blue colour shows a high temperature range (1168 °C to 1390 °C).

Figure 4.57 shows filling after 1.6 seconds, figure 5.58 shows filling after 2.1 seconds and figure 4.58 shows filling after 3.5 seconds. Pouring temperature used was 1390 °C. There was no heat loss noticed from pouring to the ingates, the metal enters the mould cavity at 1390 °C. However, it was noted in the ingates that the metal did not enter the mould cavity at the same time which could have been caused by design change as illustrated in figure 4.56.

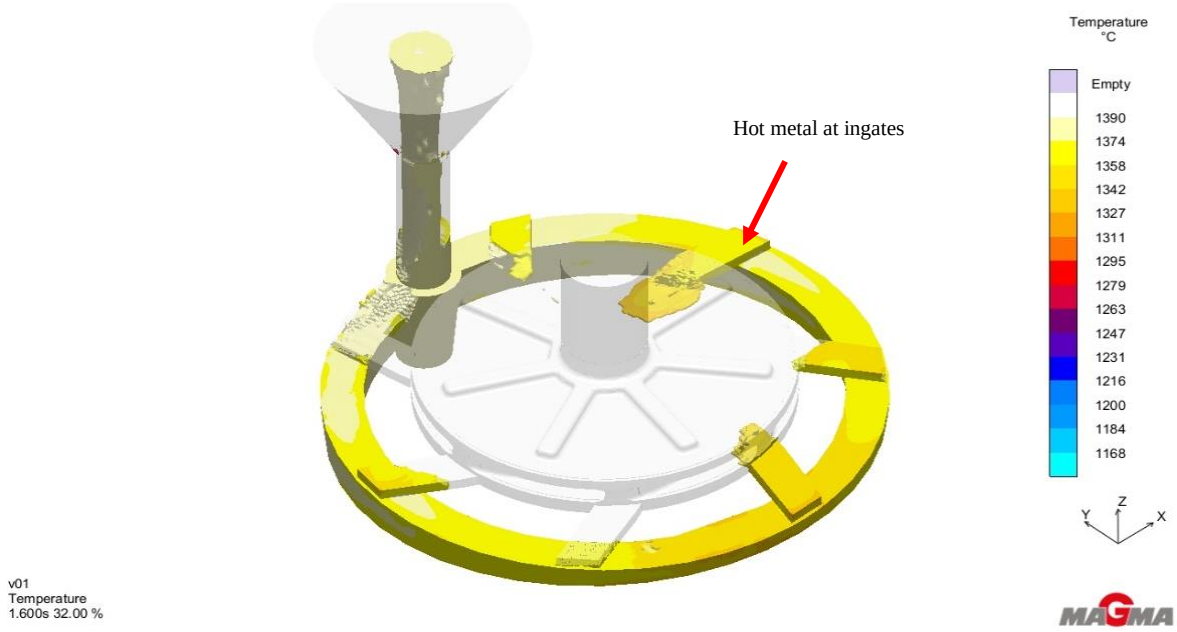

Figure 4. 56: Filling simulation of design VX05 at 32% filling ability after 1.6 seconds

The bottom part of the mould cavity was filled with less temperature variations in different locations of the casting as shown in figure 4.57. When 70% of the mould cavity was filled, some minor temperature variations were noted at the top surface of the casting indicating the first metal to enter the mould cavity (see Figure 4.58). Complete mould filling ability was noted with no risks of misrun or cold-shut defects.

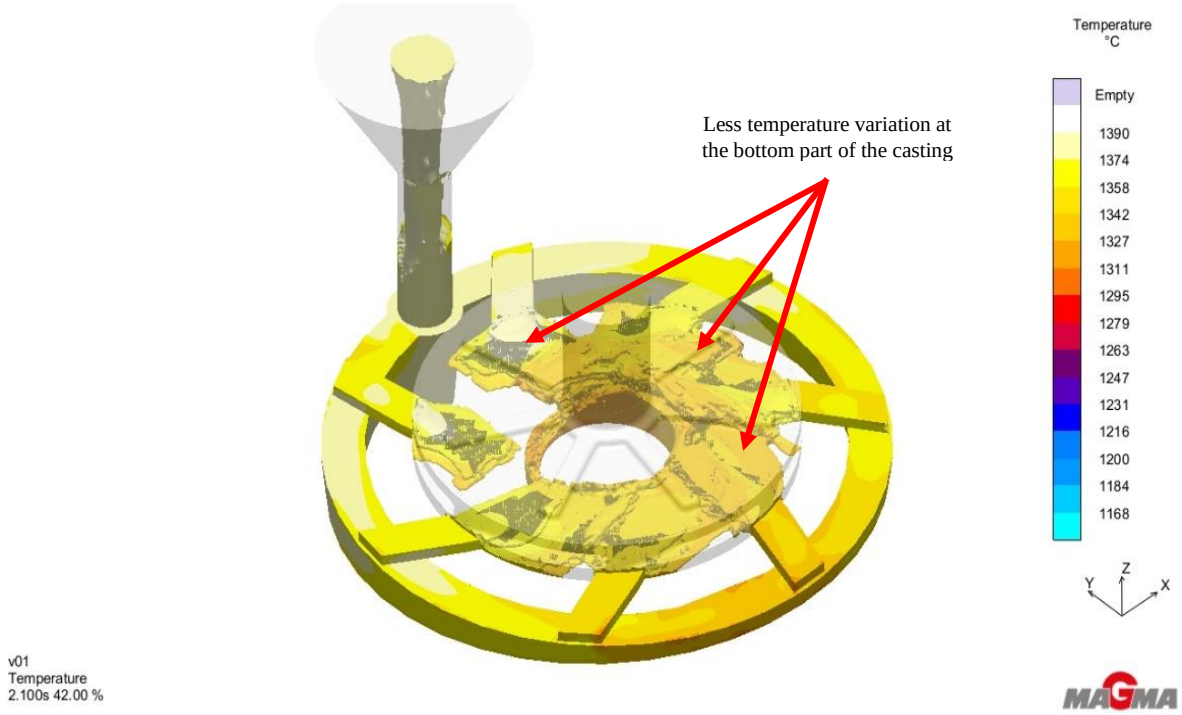

Figure 4. 57: Filling simulation of design VX05 at 42% filling ability after 2.1 seconds

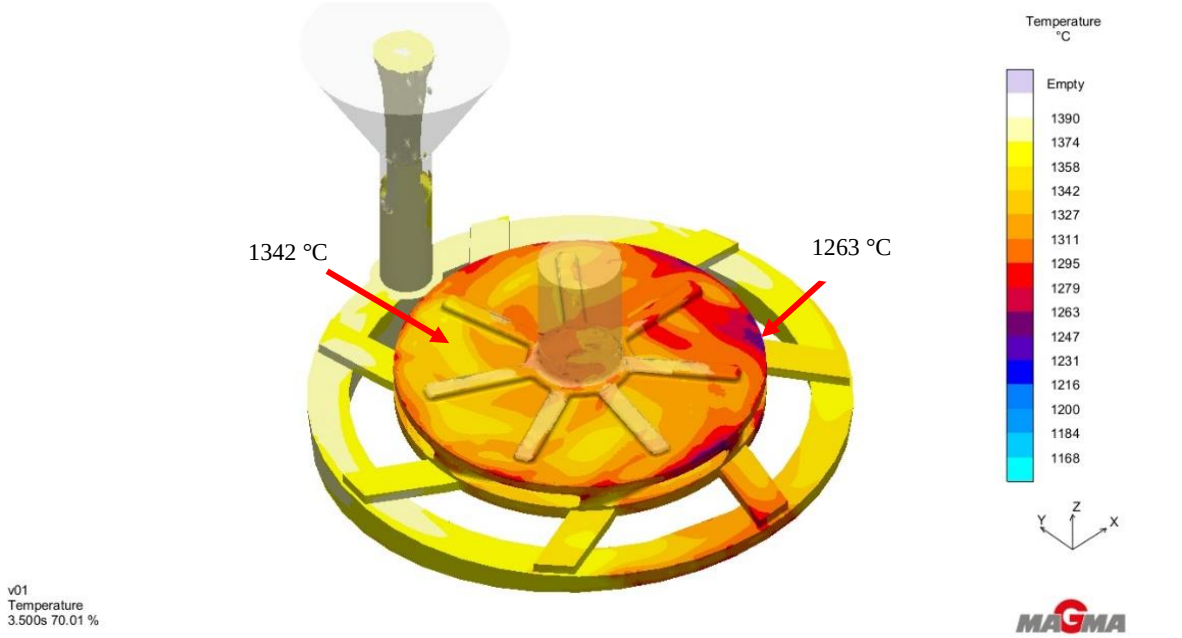

Figure 4. 58: Filling simulation of design VX05 at 70.01% filling ability after 3.5 seconds

4.6.1.2 Solidification Simulation of Design VX05

Solidification started at the bottom of casting after 57 seconds. It started at the sides of the casting and ingates due to their wall thickness which was thinner than the other parts of the

casting as shown in figure 4.59. It is clear from Figure 4.59 that even after 30% of solidification there is still a constant supply of metal to the casting from the feeder and the runner system. After 42% solidification (after 71 seconds), the necking at the ingates increased showing a reduction in metal supply from the runner bar as indicated in figure 4.60. Thus, the only metal supply will be from the feeder which is located at the top of the casting. As solidification continues after 130 seconds, the ingates solidified preventing any metal supply from the runner bar as illustrated in figure 4.61. No indication of isolated hot islands which promote porosity defects were noted.

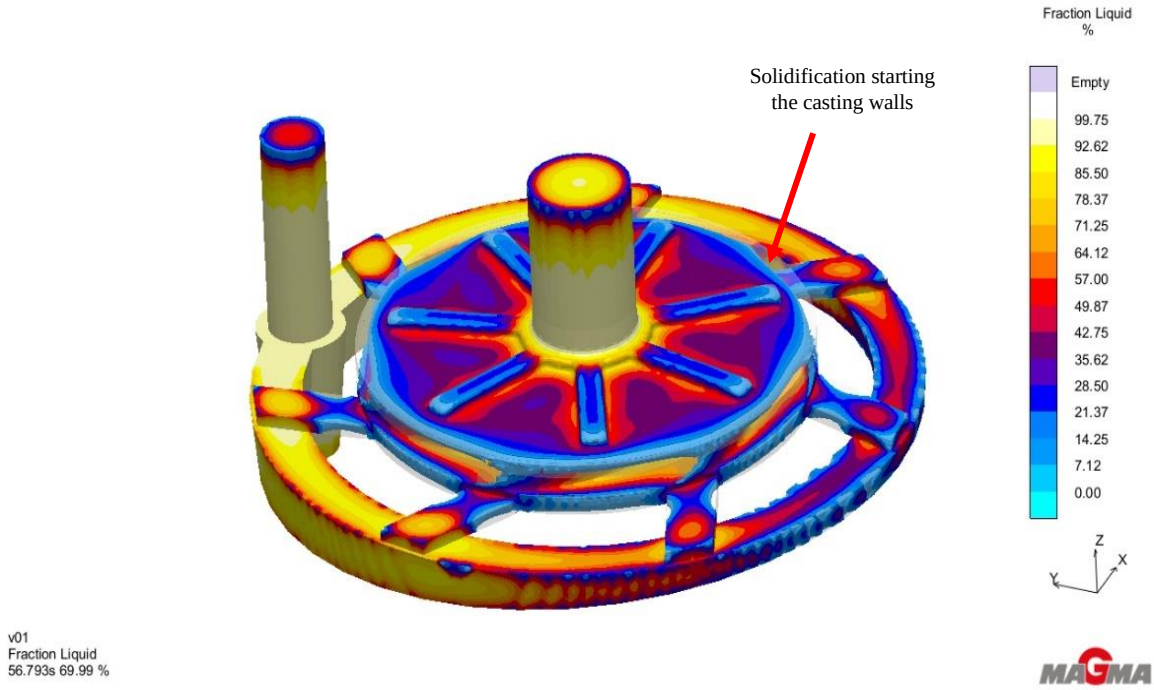

Figure 4. 59: Solidification simulation of design VX05 after 30% solid in 57 seconds

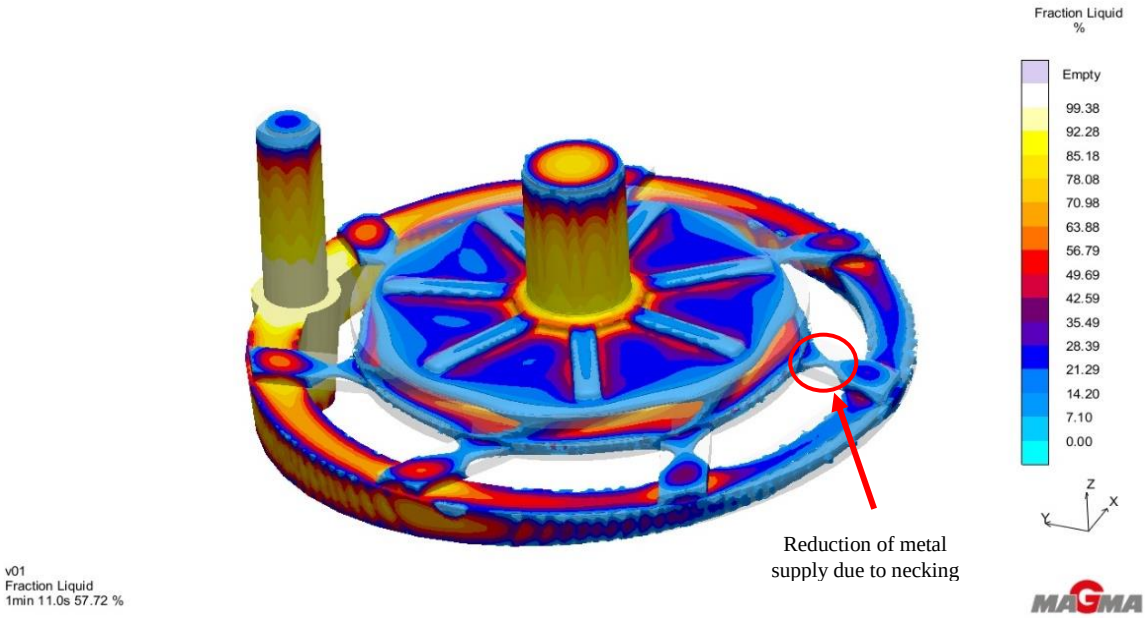

Figure 4. 60: Solidification simulation of design VX05 after 42.3% solid in 71 seconds

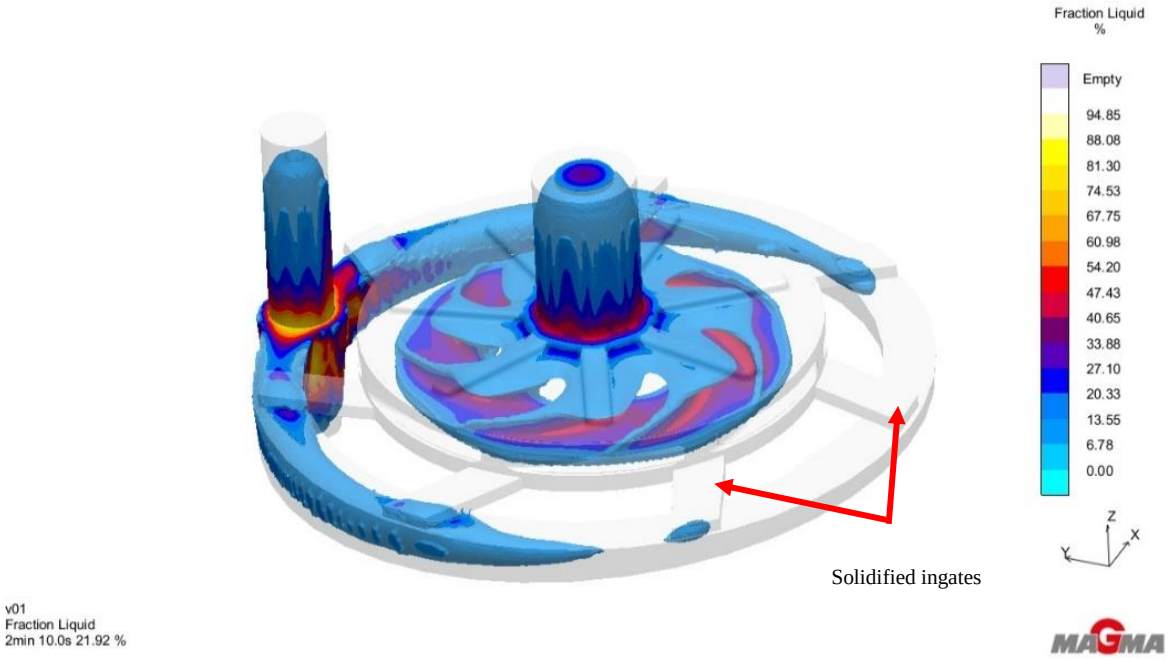

Figure 4. 61: Solidification simulation of design VX05 after 78.1% solid in 130 seconds

From Figure 4.62 and Figure 4.63, yellow colour shows high possibility (70 to 100%) and blue shows low possibility (0-40%) of porosity formation. Minimal porosity were noted at the bottom I-junction of the casting as illustrated in figure 4.62 and figure 4.63 (Joshi and Ravi 2010). The other parts of the casting showed no indication of porosity formation.

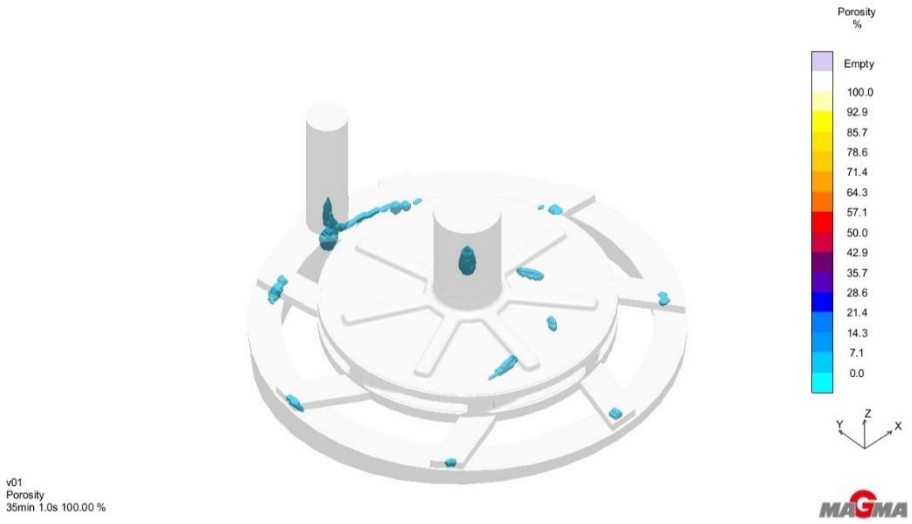

Figure 4. 62: Porosity results of design VX05 after 2100 seconds solidification

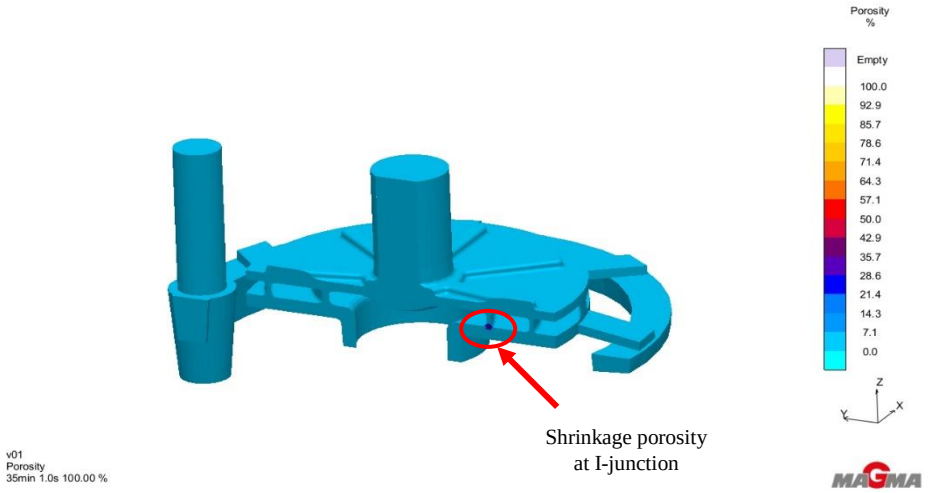

Figure 4. 63: Porosity results of design VX05 after 2100 seconds solidification

4.6.1.3 Chemical analysis and temperature reading of Design VX05

Three samples were taken during melting operation before casting process. Two batch samples (sample 1 and sample 2) and one final sample. First batch sample showed C above by 0.48 and Si below by 0.06 as shown in Table 4.4. Though other elements were either above or below targeted chemistry, their variations are largely negligible. The second batch sample showed a drop in C content to 3.81 which is still above aim by 0.41. Si remained constant at 2.14. Final sample was taken which showed a further drop in C content to 3.77 which is still above aim by 0.37. The final sample also showed drop in Si content to 2.11 (below targeted aim by 0.09). All

samples showed no Mg content. The change in other elements were negligible. Manganese treatment was not done due to unavailability of material.

Table 4. 8: Chemical composition of nodular cast iron after casting

Element	C	Cu	Mg	Mn	P	S	Si
Targeted chemistry	3.40	0.03	0.03	0.25	0.01	0.02	2.2
1st batch sample	3.88	0.02	0.00	0.28	0.04	0.05	2.14
2nd batch sample	3.81	0.04	0.00	0.28	0.04	0.03	2.14
Final sample	3.77	0.02	0.00	0.22	0.04	0.03	2.11

Tapping temperature, ladle temperature and pouring temperature were (1454 °C, 1403 °C and 1385 °C respectively) all slightly above and below aim by +4 °C, +3 °C and -5 °C respectively. Their variation was negligible.

4.6.1.4 Casting results of Design VX05

Figure 4.64A shows a completely-filled pump impeller with minor short cast indication at the top ring of the casting. Slag indication were noted at the feeder, pouring cup and the top surface of the casting as illustrated in figure 4.64A and figure 4.64B. Thin-walled blades were completely-filled with no indication of misrun defects. The bottom surface of the casting showed no sign of defect. Except for the minor fin which was noted in figure 4.64B and figure 4.64C at the bottom opening of the casting. Flashing was also noted at the parting line where cope and drag joined as illustrated in Figure 4.64B.

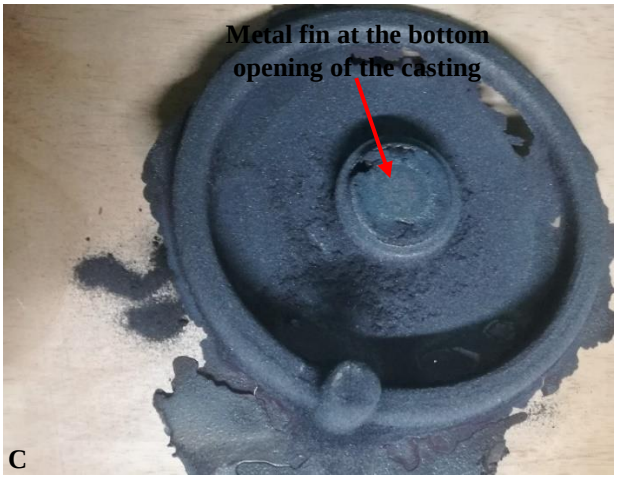

Figure 4. 64A, 4.64B & 4.64C: Completely-filled nodular cast iron pump impeller with minor slag entrapment at the top surface of the casting and the feeder and metal fin at parting line.

4.6.1.5 Microstructural results of Design VX05

Figure 4.65A and Figure 4.65B shows a complete pearlitic gray cast iron with a clear pearlitic matrix. Graphite flakes were distributed all over pearlitic matrix as illustrated in figure 4.65A. Some minor ferrite was also noted around the graphite flakes as shown in figure 4.65B.

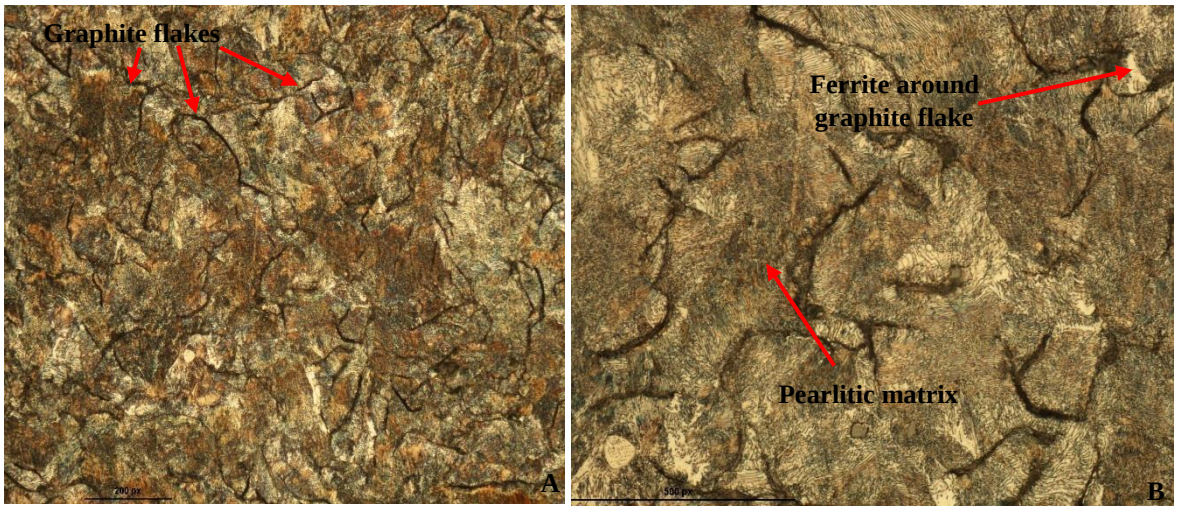

Figure 4. 65A & 4.65B: As cast microstructure of a nodular cast iron pump impeller at 20X (A) and 50X (B) magnification

4.6.1.6 Hardness results of Design VX05

An average of three indentations were taken at five different positions with position 1 having a hardness value of 180 HV_5 as shown in figure 4.66. The hardness was more consistent from the

1st till the 5th position as illustrated in figure 4.66. The average hardness obtained was 196 HV_5 with the standard deviation of 17.42 and a standard error of 7.79.

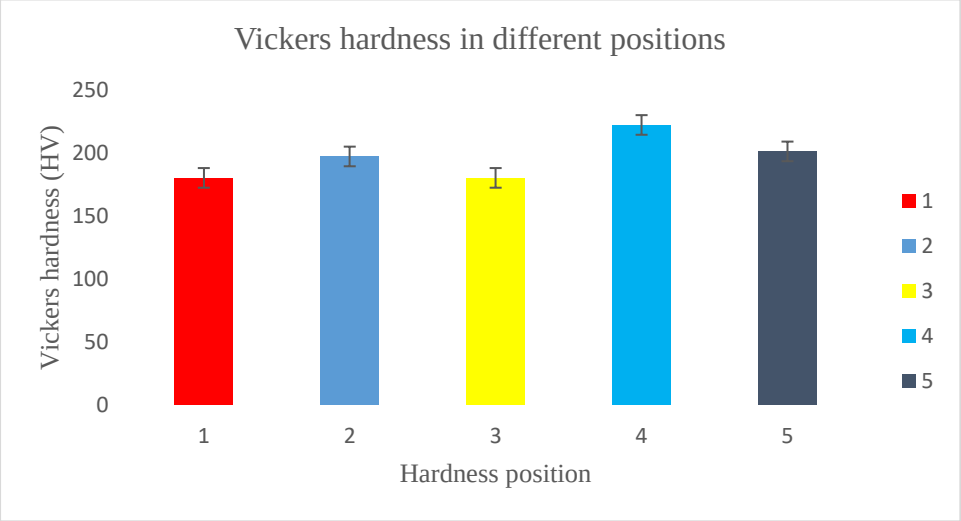

Figure 4. 66: Vickers hardness results of a nodular cast iron pump impeller at different positions

CHAPTER 5

DISCUSSION

5.1 Discussion of study 1: To optimise filling and feeding of thin-walled aluminium alloy component with complex geometry during sand casting.

5.1.1 Simulation

High viscosity of the molten metal at low pouring temperature (700 °C) contributed to low filling ability of the 2 mm test sample. Viscosity was reduced as the pouring temperature increases and this reduction in viscosity caused filling ability to increase (Zhang et al. 2009). A minimum of 100 °C was required to induce enough viscosity to achieve complete filling ability of the 2 mm test sample. There is a clear indication that at temperatures below 800 °C the mould is not fully filled thus there is high probability of misrun formation. The unfilled mould cavity was caused by high viscosity at the temperature below 800 °C (Ding et al. 2013).

Mould cavity backpressure which is high at low temperature opposes the metal flow and reduce filling ability. The pressure of the molten metal must be high enough to overcome backpressure inside mould cavity for complete filling ability. The test samples with temperatures below 800 °C still contain unfilled portions signifying substantial amount of backpressure opposing metal flow at this stage as also observed by Voigt (2002).

After complete solidification (from 794 °C, 800 °C and 86°C), hot spots were noted at the +-junctions of the test samples. An increase in surface area at the junctions promote the possibilities of hot spots (Kumar and Ravi 2006). Hot spots are susceptible to porosity defects after solidification is complete, this is a result of shrinkage of metal. They increase with an increase in pouring temperature because of reduction in solidification rate as the pouring temperature increase (Li et al. 2015). The wall thickness of the test sample promoted quick solidification hence the last part to solidify was in the pouring basin. The possibility of porosity formation is very low for all conditions (approximtely 10 % and less possibility). This is because of quick solidifcation of the test sample. The possiblity of porosity formation at the junctions increase with increase in pouring temperature. This is due to an increase in solidification time which promote shrinkage porosity. Porosity was noted at the same spot with the hot spot results.

5.1.2 Casting

Metal fin formation signifies possibility of high metal fluidity or mould cracking due to low strength. Metal fin could also be caused by poor mould assembly which leave spaces between the cope and drag. Porosity at cross junctions promote cracking. This observation is consistent with the simulation results presented in section 5.1.1 above. Thus, the simulation results and casting results are in correlation to each other. There was some slight deviation in pouring temperature of range 1°C to 4 °C due to temperature measurement error.

5.1.3 Microstructure

The quick solidification which occurs at lower pouring temperature prevents the growth of dendrite arms. Smaller dendrite arms result in higher hardness value. The microstructural results were not in correlation with the simulation results due to the reduction in dendrite arms at 794 °C and 862 °C.

5.1.4 Hardness

Quick solidification and small dendrite arms have promoted high hardness value. A decline in hardness as the pouring temperature increases is an indication of grain growth which happens when pouring temperature increases (Li et al. 2015). These results are in correlation with the microstructural results except for the pickup in hardness value at 794 °C pouring temperature.

Increasing pouring temperature reduces viscosity and increases the filling ability. However, increasing pouring temperature also increase chances of hot spots which result in shrinkage porosity. Poor mould assembly cause metal fin at the parting line.

5.2 Discussion of study 2: Evaluating effect of wall thickness on the filling and feeding of thin-walled aluminium alloy components during sand casting.

5.2.1 Simulation

It is evident from 1 mm test sample that solidification occurred before the mould cavity was completely-filled thus preventing further flow of metal. As the wall thickness was increased from 1 mm to 1.5 mm, the filling ability was also increased. Although the increase was

significant, solidification rate was still high enough to cause a misrun defect. Filling ability continues to increase as the wall thickness increase because of an increase in solidification time as the wall thickness increase as was also observed by Voigt (2002). Complete mould filling ability was only observed when the wall thickness of the test sample was increased to 3 mm.

5.2.2 Casting

The quick solidification of the molten metal of 1 mm test sample prevented further flow of molten metal resulting in only 25 % of the mould cavity filled. A difference in filling ability increase between simulation and casting of 1.5 mm test sample was due to 5 °C deviation in pouring temperature. Solidification occurred while still filling when the metal approaches the middle +-junction whereas in simulation results solidification occurred just after middle +-junction. Though there was significant increase in filling ability of 2 mm test sample, misrun defect was still observed as approximately 65 % of the mould cavity was filled with remaining 35 % unfilled mould cavity. Casting results of 2.5 mm test sample was not correlating with the simulation results because of mould breakage which result in poor filling ability. Casting also showed complete mould filling ability when the wall thickness was increased to 3 mm. Overall, casting results were in correlation with the simulation results although there were some deviations in the filling ability percentage predictions.

5.2.3 Microstructure

Short dendrite arms which were observed in 1 mm test sample were caused by quick solidification which hinders the growth of the arms. These dendrite arms promote high hardness value (Rundman 2005). An increase in dendrite arms as wall thickness increase might be an indication of delay in solidification time which happens in thicker sections than thinner sections. A delay in solidification promoted dendritic growth.

5.2.4 Hardness

As the wall thickness increases, hardness is expected to decrease because of an increase in grain size which lowers hardness value (Rundman 2005). However, the opposite was the case when wall thickness was increased from 1 mm to 1.5 mm. This might be caused by reduction in dendrite arms. The decrease in hardness from 66.3 HV_5 to 63.7 HV_5 (from 2.5 mm to 3 mm)

was caused by an increase in dendrite arms which happened when wall thickness increase. Hardness results were in correlation with the microstructural results except for 2 mm wall thickness.

Wall thickness and filling ability have a direct relationship. A complete mould filling ability was only observed when the wall thickness was increased to 3 mm. Simulation results and casting results were in correlation with each other.

5.3 Discussion of study 3 (1st Trial): Optimization of filling and feeding of austenitic stainless-steel pump impeller produced by sand casting

5.3.1 Simulation

Design VX 01 shows feeders which were placed at the top of the casting only compensated for shrinkage porosity at the top of the casting. These feeders were not effective enough to feed the bottom part of the casting hence there was shrinkage porosity at the bottom part of the casting. This was because of high pressure which was present at the thin-walled blades (2 mm). Thin-walled sections are known for high backpressure which opposes the direction of metal flow. On the other hand, junction increases the surface area at the point of connection thus reducing the solidification time and increasing the chances of shrinkage porosity. During solidification, the molten metal at the junction took time to solidify leaving hot spots/island which when finally solidifies it creates shrinkage porosity. High amount of shrinkage was located at the junctions which effectively acts as stress concentration spots that are prone to failure during service. The small bottom sized ingates solidifies faster as compared to the casting blocking the way for molten metal to continue feeding the casting which result in misrun defect.

Design VX02 was done to eliminate defects encountered in Design VX01. Several designs were proposed with the final one having a yield percentage of 21 % selected due to objectives required (low hot spot, low porosity and high yield). The yield of this design was relatively low because of a lot of material used to compensate shrinkage porosity.

There is an inverse relationship between the material used and casting yield. Casting yield is normally inversely proportional to the quality of the cast produced. However, the yield was increased to 22 % after optimisation simulation was performed.

Feeder height has less effect on both the quality of the casting and the casting yield. Feeder radius on the other hand showed an increase in the number and size of hot spot results inside

the feeder and a decrease in possibility of porosity formation inside the casting. The decrease in the possibility of porosity formation inside the casting was due to approximately 2.9 kg of material (increased feeder radius) which was used to compensate for shrinkage porosity. Hence the casting yield was also reduced when feeder radius was increased. When 10X feeders were used, enough material was available to compensate for possible defects like shrinkage porosity. This resulted in a low yield due to high amount of material used to produce casting.

The mould cavity was filled with no indications of misrun and cold-shut defects. The last part to solidify (hot spot) is susceptible to shrinkage porosity after solidification is complete. It is therefore important to make sure that the last part to solidify is inside the feeders and runner system and not in the casting. This ensures that the shrinkage porosity is completely shifted out of the casting into the feeders.

5.3.2 Casting

The combination of chemical composition, thin-walled blades and pouring temperature promote quick solidification and lowered filling ability of the metal. Simulation and casting results are not in correlation to each other. A top filling runner system was used. It allows top part of the impeller to be filled followed by thin-walled blades and lastly the bottom part of the impeller. During casting, the molten metal managed to fill the top part of the pump impeller. Thin-walled blades solidified faster and block the way for the metal to fill the bottom part of the pump impeller. Cold laps and misrun defects resulted due to the poor design promoting poor filling ability.

The chemical composition which consist of high Cr and Ni content played a role in reducing the filling ability of this alloy. These defects were also promoted by pouring temperature which was lower than the targeted pouring temperature. The presence of the thin-walled blades (2 mm) also promoted quick solidification of the molten metal which prevented metal to penetrate through them. Therefore, another experiment must be conducted.

5.3.3 Microstructure

The presence of Ni content ensured that the structure remained austenite even at room temperature (Rundman 2005). This matrix is a soft and ductile phase which normally promote low hardness value. The microstructure also consists of delta ferrite precipitates. This phase is

very brittle and hard. Due to low C content, the possibility of carbides formation was very low hence there were no carbides noticed in the microstructure.

5.3.4 Hardness

The inhomogeneity of the microstructure which consist of austenite matrix (soft) and sigma ferrite (hard) contributed in variety of hardness values at different positions. Lower hardness values which were noticed in position 1, 3 and 5 showed soft phase whereas hard phases are shown in position 2 and 4.

5.4 Discussion of study 4 (1st Trial): Optimization of filling and feeding of nodular cast iron pump impeller produced by sand casting.

5.4.1 Simulation

After optimisation simulation of Design VX03, best design was selected due to its results which showed low hot spot, porosity and high casting yield. Only 3X feeders at the top of the casting were enough to compensate for shrinkage defects. No indications of hot spots and shrinkage defect were noted which is an indication of sufficient metal to feed the casting as it solidifies. The fluidity of the nodular cast iron showed complete filling ability of the casting (including 2 mm blades). The use of less number of feeders to compensate for shrinkage defects result in a casting yield of 48 %. The increase in casting yield to 56 % was due to less material used in the feeders since the feeder size was reduced. This was also evident in the simulation results where feeder radius and number of feeders showed inverse relationship with the casting yield.

5.4.2 Casting

A top filling gating system was adopted when casting a nodular cast iron pump impeller. The molten metal managed to fill up the entire mould cavity including thin-walled blades. Solidification only starts when the entire mould cavity was filled. The use of the chemical composition which was very close to the targeted aim and pouring temperature which was slightly higher than the aim promotes flowability of the molten metal. The presence of high Si content also played a role in improving flowability of the molten metal metal (Di Sabatino et al. 2005). Minor shrinkage defects on top of the casting were caused by presence of junction which connects the top part of the casting with the thin-walled blades. Shrinkage was minimum

and the casting could be repaired with the use of welding techniques. Simulation and casting results were largely in correlation to each other.

5.4.3 Microstructure

The presence of high C content in this alloy promote the formation of a hard and brittle tetragonal structure called martensite. This structure is supersaturated in C and it is clear enough that with the high C content of the present alloy it is likely to form (Askeland & Phule 2006). The microstructure showed stick-like structures with sharp ends. The presence of high C content also promotes the formation of ledeburite. A complete transformation to ledeburite occurs at 4.3 %C, however with the current 3.2 %C, low percentage of ledeburite managed to form (Rundman 2005). Some islands of ledeburite were noted across the entire sample. Though Si is known to improve filling ability, it also promotes formation of retained austenite (Rundman 2005). Retained austenite is known to be a soft phase which can reduce hardness value of the casting. The presence of Mg promotes precipitation of cementite from austenite. During cooling, C will precipitate in form of cementite from austenite reducing the C content in the austenite phase (Rundman 20050.

5.4.4 Hardness

The lower hardness values which were noticed in position 1, 3 and 4 showed possible location of the soft phases (retained austenite and pearlite). Position 2 and 5 showed possible location of hard phases like cementite.

The use of less number of feeders reduces the amount of metal used therefore improving the casting yield. There is an inverse relation between the amount of metal used and the casting yield. Si content improves the filling ability of the nodular cast iron.

5.5 Discussion of study 5 (2nd Trial): Optimization of filling and feeding of austenitic stainless-steel pump impeller produced by sand casting.

5.5.1 Simulation of Design VX04

A new design (Design VX04) with a tapered runner bar to improve the filling process by ensuring that the metal enters the mould cavity at the same time in different ingates was

conducted. The ingates were aligned in such a way that they are connected to the top part, middle and bottom part of the casting to ensure that the metal fills the top, middle and the bottom part of the casting at the same time. Alloy type, travelling distance and section thickness could have played a role in the temperature loss which was noted from the pouring to the ingates.

The quick solidification which was observed at the end part of the runner system could be due to taper angle which made this part thinner than the other parts of the runner system. The travelling distance from the pouring to the last part of the runner bar also played a role in this quick solidification. Other factors which contributed to this situation was the section thickness and material age inside the mould cavity since this was the first metal to enter the mould cavity. The constant supply of hot metal from the runner system which was still hotter than the casting, heat up the cold metal inside the casting and improve complete filling ability of mould cavity. Nevertheless, it can be assumed that there might be a possibility of cold-shut defect in some areas during real casting practice. Only one sleeve was used which was designed as part of the casting having a cone-like shape. This sleeve was enough to provide enough metal to compensate for any possible shrinkage. The casting yield of Design VX04 was 41 %.

The bottom part of the casting was thin with the feeder on the top part of the casting allowing solidification pattern to start from the bottom to the top part of the casting. There is a direct correlation between these results and the filling results which showed bottom part of the casting with colder metal than the other part of the casting. During solidification, the ingates quickly solidifies blocking the supply of metal from the runner bar to the casting. The feeder was still full of metal which is good to compensate for any shrinkage inside the casting. The section thickness of thin-walled blades promoted quick solidification of metal which retard any possibility of metal feed from the feeder. Porosity at I-junction was caused by an increase in section thickness which happens at an intersection (I, L and T-junctions). The thicker the section, the higher will be the solidification time promoting possibility of misrun to form.

5.5.2 Chemical analysis and temperature reading of 2nd Trial (Austenitic stainless steel)

The chemical analysis obtained after melting was close to the targeted chemical analysis of the scrap charged. Though Mn was below the aim by 0.15, it was close to the Mn content of the scrap charged. The same was noted with the Si content of the melt which was 0.69 while the scrap Si content was 0.72. The major variation in chemistry was noted with the Cr content of

the melt which might be due to melting practice. Temperatures were all close to the targeted aim.

5.5.3 Casting results of 2nd Trial (Austenitic stainless steel)

The use of circular tapered runner system promoted the uniform filling of metal into the mould cavity. The use of 7X ingates positioned at the blades prove to promote filling ability of the mould especially thin-walled blades. The metal managed to fill up high volume of the thin-walled blades because of the multiple ingates from the mould design. The bottom part of the casting was filled but with some minor misrun which could have been caused by air entrapment and drop in temperature. The design had no venting system which also caused the air entrapment at the top surface of the casting. After solidification, these areas remain unfilled causing misrun defect. Approximately 80 % of the entire mould was filled with the remaining 20 % unfilled (misrun). A lot of entrapped air in the mould float up to the top surface of the casting hence the top part had high misrun defects than the bottom part. A drop in temperature of approximately 100 °C after 3.5 seconds which was noted in filling simulation results (illustrated in figure 4.47) also promoted quick solidification at the thin-walled sections. Therefore, the metal could not fill these isolated air entrapped spots thereby promoting misrun defects in these locations. Enough metal was melted and tapped reducing the chances of slag entrapment inside the casting. The casting showed no indication of slag or short cast.

5.5.4 Microstructural analysis of 2nd Trial (Austenitic stainless steel)

The presence of high Ni content (10 %) increases the austenite region and reduces the ferrite region promoting austenite matrix at room temperature (Rundman 2005). During solidification, liquid metal transforms to eutectic austenite and sigma ferrite as secondary phase. Precipitation of sigma ferrite was also promoted by the presence of Si in the melt. The presence of low C content (0.03 %) prevented the formation of carbides during solidification, the structure remained austenite with sigma ferrite precipitates (Askeland & Phule 2006).

5.5.5 Hardness of 2nd Trial (Austenitic stainless steel)

The hardness value at lower side were caused by austenitic matrix which is a soft phase. This was noted in position 1, 2 and 4. Position 3 and 5 had higher hardness value which was promoted by sigma ferrite which is hard and brittle.

5.6 Discussion of study 6 (2nd Trial): Optimization of filling and feeding of nodular cast iron pump impeller produced by sand casting

5.6.1 Simulation of 2nd Trial (Nodular cast iron)

The use of untampered 7x ingates improved the filling practice of nodular cast iron. The alignment of the ingates promoted the bottom part of the casting to fill first followed by middle part and lastly bottom part of the casting. Nodular cast iron showed better metal flow with less/no temperature variations since the metal enters the mould cavity at the same temperature as the pouring. Minor temperature variations which were noted after 70 % of mould filling ability was due to metal age inside the mould cavity.

Solidification pattern started in the thin section towards the thicker sections and lastly, the feeder. Good flowability of nodular cast iron promoted constant supply of metal from both the feeder and the runner system. Even with necking, the supply of metal was still possible but at the lower rate. The supply of the metal from the runner bar to the casting only stopped when the neck at the ingates cut off. Feeder was sufficient-enough to feed the casting and ensured that no hot islands are present inside the casting. The presence of minor shrinkage at the junctions was caused by an increase in the section thickness caused by intersection of two or more sections. The possibility of this porosity to form is too low that they might not even form during real casting process.

5.6.2 Chemical analysis and temperature reading of 2nd Trial (Nodular cast iron)

The high C which was noted was due to scrap received which could have been mixed up with grey cast iron. Though Si was also high, it might have been lost during melting by combining with Mn and form MnSi. Three different samples were taken with the last sample showing C drop from 3.4 to 3.77, Si drop from 2.14 to 2.11 and Mn drop from 0.28 to 0.22. No issues were noticed during measurements of tapping, ladle and pouring temperature.

5.6.3 Casting results of 2nd Trial (Nodular cast iron)

Tapered circular runner system promoted uniform filling across all 7X ingates. The molten metal entered the mould cavity through 7X ingates at the same time improving filling process. No indication of misrun and cold-shut were noted since solidification only started when the entire mould cavity was filled. The use of 7X ingates also reduced filling time which increases filling ability. Filling ability was also improved by the Si content which was close enough to the targeted aim. Molten metal nicely filled up the blades and bottom part of the casting. However, due to poor de-slagging practice the metal did not fill up the feeder. During solidification, the feeder was left with no metal affecting the top part of the casting. Slag was also noted at the middle part of the pouring basin. The charge prepared did not include slag allowance causing less metal to fill the mould cavity with no slag entrapment. Though enough weights were put on top of the mould, mould seal was not used to properly close the mould and prevent metal fin defect. The minor fin which was at the bottom opening of the casting was caused by assembly of the core. It was clear that the core did not seat tightly on the drag leaving minor spaces which promoted metal fin defect.

5.6.4 Microstructural results of 2nd Trial (Nodular cast iron)

Solidification of hypoeutectic steel started during eutectic solidification reaction. This reaction occurred at a temperature of approximately 1145 °C where pro-eutectic austenite and hypoeutectic graphite flakes formed. Since there was no metal treatment done (addition of MgFeSi), there was a delay in graphite nucleation and the graphite only precipitates as flakes than nodules (Rundman 2005). After nucleation of graphite flakes, solidification proceeds by diffusion of C through pro-eutectic austenite shell. When the temperature drops to approximately 720 °C, pro-eutectic austenite transformed to metastable ferrite and pearlite (ferrite and cementite). Since ferrite is a bcc structure which only take a maximum of 0.01 %C, the remaining C was diffused to the graphite flakes arms. This promoted the growth of the graphite flakes hence they are long (Rundman 2005).

5.6.5 Hardness results of 2nd Trial (Nodular cast iron)

The presence of the fine plates of iron carbide (present in pearlite matrix) which is hard and brittle could have promoted high hardness values which were noticed in position 2, 4 and 5 (197

HV_5, 222 HV_5 and 201 HV_5 respectively). However, the presence of graphite flakes which is a soft and weak material with low ductility could promote lower hardness noticed in position 1 and 3 (both 180HV_5).

CHAPTER 6

CONCLUSION

6.1 Conclusion of study 1: To optimise filling and feeding of thin-walled aluminium alloy component with complex geometry during sand casting.

The higher the backpressure, the lower will be the filling ability. Porosity dominant in the casting junctions promote cracking or tearing. As the pouring temperature increases, so does the filling ability. Misrun defect noted at test samples cast at the temperature lower than 761 $^{\circ}$C was caused by high viscosity. Simulation results showed complete mould filling at 800 $^{\circ}$C while casting results showed it at 761 $^{\circ}$C. Cracking was dominant when casting above 761 $^{\circ}$C, an optimal pouring temperature must therefore be 761 $^{\circ}$C. Metal fin which was only noted at the pouring temperature of 761 $^{\circ}$C was caused by poor mould assembly. MAGMAsoft® simulation tool proved to be an effective tool in predicting filling and feeding of thin-walled aluminum components during sand casting.

6.2 Conclusion of study 2: Evaluating effect of wall thickness on the filling and feeding of thin-walled aluminium alloy components during sand casting.

MAGMAsoft® simulation and 3D printing machine tools proved to be effective tools in predicting filling and feeding of thin-walled aluminum components during sand casting. As the wall thickness increases so did the filling ability. A complete filling ability was only noted when the wall thickness was increased to thicker section. There is a direct correlation between simulation and casting results since complete filling ability for both was at thicker wall thickness. Misrun defect noted in thin sections was due to quick solidification at thinner sections. Correlation for 2.5 mm was poor because of mould breakage. Microstructural result was in correlation with simulation results since an increase in wall thickness result in an increase in dendrite arms. Quick solidification which was observed in thin sections caused smaller dendrite arms and as the wall thickness increases, so did the dendrite arms. There was a decrease in hardness value as the dendrite arms increases.

6.3 Conclusion of study 3 (1st Trial): Optimization of filling and feeding of austenitic stainless-steel pump impeller produced by sand casting

High backpressure and quick solidification inside thin-walled blades (2 mm) prevented metal supply between the top and the bottom part of the casting. Small ingates, availability of junctions and insufficient material promote the formation of shrinkage porosity. The feeder

location plays a vital role in eliminating shrinkage porosity. The quality of the casting has an inverse relationship to casting yield. The feeder height showed less effect on the quality and yield of the casting produced. The feeder radius greatly reduces casting yield and shrinkage porosity. Increasing the number of feeders also reduces the casting yield and improve the quality of the casting produced. Simulation results showed complete filling ability of the austenitic stainless-steel pump impeller while casting results showed only 50 % filling ability. Presence of high Ni content reduce the flowability of the metal and caused misrun and cold lap defects. Lower pouring temperature greatly reduce filling ability. Thin-walled blades promote quick solidification which caused misrun and cold-shut defects. Overall, the poor results were due to pouring temperature difference, casting geometry, chemistry and poor runner system design. Simulation results were not in relation to casting results since a defective casting was produced yet simulation showed a defect free casting. It is therefore recommended to redesign the runner system to improve both filling and solidification of this product.

6.4 Conclusion of study 4 (1st Trial): Optimization of filling and feeding of nodular cast iron pump impeller produced by sand casting.

Feeder radius and number of feeders are inversely proportional to casting yield and directly proportional to the quality of the casting. The use of 3X feeders provide enough material to compensate for shrinkage defect with better casting yield (56 %). The fluidity of nodular cast iron which is highly improved by Si content, promotes mould filling ability and prevented any form of misrun defect.

The use of the higher pouring temperature also improves flowability level. Casting showed no indication of misrun or cold lap defects. The inconsistency of the hardness reading was due to presence of cementite (hard phase) and retained austenite (soft phase). Shrinkage defects which were present at the top surface of the pump impeller were caused by availability of junctions between thin-walled blades and the top part of the casting. Simulation tool was effective enough to predict filling and feeding of nodular cast iron pump impeller.

6.5 Conclusion of study 5 (2nd Trial): Optimization of filling and feeding of austenitic stainless-steel pump impeller produced by sand casting.

Additive manufacturing was used to print sand moulds with complex core using Voxeljet VX1000. Moulds were of high quality and were produced at a low period of time. Using tapered circular runner system enhance uniform filling of the mould cavity. Increasing the number of

ingates reduces filling time and promote filling ability of the mould cavity. Simulation results show completely-filled mould cavity while real casting showed only 80% filling ability with 20% unfilled (misrun). Poor venting system cause air entrapment in some locations of the casting and prevented metal to fill up those locations. The quick solidification of thin-walled blades which resulted in misrun defect was enhanced by temperature drop of approximately 100 $^{\circ}$C after just 3.5 seconds.

Austenitic matrix was caused by presence of high Ni content which prevent austenite to transform even at room temperature. The inconstancy in hardness value at different position was caused by different phases (austenitic matrix and sigma ferrite). Availability of enough metal melted reduces the chances of tapping with the slag thus prevent slag entrapment inside the mould cavity. The filling ability of the 2nd trial increased by 30% from the 1st trial (50%). The increase was caused by an increase in pouring temperature and change in runner design. The casting yield was also improved from 22% to 43%. Again, simulation was not in relation to the casting results but close enough as compared to the first design.

6.6 Conclusion of study 6 (2nd Trial): Optimization of filling and feeding of nodular cast iron pump impeller produced by sand casting

The filling process was greatly improved by using tapered circular runner system with 7X ingates. Feeder used was sufficient-enough to feed the casting and prevent any risk of porosity defect formation. The use of scrap with high C content affected the chemical composition of the charge. The presence of the Si content improved the fluidity which resulted in high filling ability of the casting. The presence of Si (graphite stabilizer) also promoted graphite precipitation. Poor charge calculation which did not include slag allowance caused less metal to fill up the entire mould cavity. Poor melting practice of not de-slagging enabled slag entrapment inside the casting and in the feeder. Poor assembly of the mould caused metal fin at the bottom of the casting and at the parting line. Unavailability of MgFeSi for metal treatment caused delay of graphite nucleation and result in grey cast iron formed than nodular cast iron. The presence of high C content favoured the extension of graphite flakes formed. Variation in hardness was caused by pearlitic matrix (hard phase) and graphite flakes (soft phase). Simulation results and real casting results were in correlation to each other with both showing 100% filling ability.

SUMMARY

The use of casting simulation software gives an insight on how the casting will come out. This was demonstrated several times in the dissertation from several designs where simulation results were correlating with the real casting process. Production of moulds with intricate shapes like pump impeller core can be challenging in sand casting industry. The use of additive manufacturing tool like Voxeljet VX1000 series does not only help with the production of intricate shapes but also reduce production time. One of the purest alloy (1060 Al) was chosen as a benchmark to evaluate how pouring temperature and wall thickness can affect the filling ability of the casting. Both pouring temperature and wall thickness showed a remarkable effect on how they affect the filling ability of the casting. As both increase, so did the filling ability.

Two papers were written on this topic and their titles are at the beginning of this dissertation. Casting results of the austenitic stainless-steel were very poor as compared to simulation results. Simulation results showed 100% filling ability while real casting showed only 50% filling ability and 50% unfilled (misrun). However, at the same time the casting results for nodular cast iron were in correlation with the simulation results. Due to poor results of the first trial, a second trial was conducted with the better runner system to improve filling ability of this casting. The second trial was also done for nodular cast iron. Again, poor casting results of austenitic stainless steel were obtained with 80% filling ability and only 20% unfilled (misrun). The new design proves to improve filling ability from 50% to 80% but it was not comparable to simulation results which showed 100% filling ability. At the same time, nodular cast iron again was in correlation with the simulation results. It was concluded that different factors contributed to the poor results obtained when casting austenitic stainless steel like wall thickness, junctions, pouring temperature, men, runner system design and chemistry. Of all these factors, the ones which showed a huge effect were chemistry, runner system and men. Numerical modelling and additive manufacturing did optimise filling and feeding of sand cast austenitic stainless-steel pump impeller. For future studies, the following concepts must be taken into consideration;

i) Change the type of the sand used to make core from silica to chromite sand. Chromite sand can withstand higher heat than silica sand which will increase solidification time and reduce quick solidification of thin-walled blades (Gorny 2007).

ii) The use of improved venting system can help reduce backpressure in the system and promote metal flow. Further optimization of this product with improved venting system can help reduce any formed defect.

iii) Proper melting practice must be followed to avoid any slag entrapment and use of the correct scrap. Unnecessary human error like use of the right temperature and proper handling of the moulds must be avoided for better results. Ensuring that every process is followed in a right way and in the same way as the simulation set-up could help improve the quality of the casting.

iv) Voxeljet VX 1000 must continuously be used in the production of moulds preferable with complex shapes. However, Voxeljet must consider the use of variety of sand type since some moulds require different sand type like chromite sand which currently cannot be used in Voxeljet VX1000 machine.

v) Simulation tool must be used only as a guide. It is very important for the operator to know the real foundry practice before using the tool.

Bibliography

Anglada, E., Melendez, A., Maestro, L. and Domiguez, I. 2013. Adjustment of numerical simulation model to the investment casting process. *The Manufacturing Engineering Society International Conference*, MESIC 2013. Industry and Transport Division. Spain, 63, pp. 75-83.

Ahmad, N., Brevick, J., Allen, T. and Castro, J. 2015. Riser feeding evaluation method for metal castings using numerical analysis. Graduate Software in Industrial and Systems

Arunkumar, P., Deshpande, A.S. and Gunjati, S. 2015. Analysis and optimization of investment castings to reduce defects and increase yield. *International Journal of Engineering Technology, Management and Applied Sciences.* KLS Gogte Institute of Technology, Karnataka, India. May 2015. 3, pp. 132-140.

Askeland, D.R. and Phule, P.P. 2006. The science and engineering of materials. International student edition. Canada. Bill Stenquist.

Beňo, J. and Špirutová, S. 2014. Computer support of casting and solidification process. Academic materials for the Metallurgy engineering study software at the Faculty of Metallurgy and Materials Engineering. Technical University of Ostrava. pp. 1-92.

Bhatt, H., Barot, R., Bhatt, K., Beravala, H. and Shah, J. 2014. Design optimization of feeding system and solidification simulation for cast iron. *2nd International Conference on Innovations in Automation and Mechatronics Engineering*, ICIAME 2014. Department of Production Engineering, BVM Engineering College, V.V. Nagar-388120, India. 14, pp. 357-364.

Bouska, O. 2008. The effect of different casting parameters on the relationship between flowability, mould filling capacity and cooling conditions of Al-Si alloys. *Association of Metallurgical Engineers of Serbia.* Journal of Metallurgy. 14, pp. 18-30.

Campbell, J. 1995. Review of fluidity Concepts in casting. Metallurgy and Materials, and Interdisciplinary Research Centre in Materials. School of Metallurgy and Materials, and The University of Birmingham. 7 (4), pp. 227-237.

Carlson, K.D., Hardin, R.A., Ou, S. and Beckermann, C., 2002. Development of new feeding-distance rules using casting simulation: Part I. Methodology. *Metallurgical and Materials transactions B*, *33*(5), pp.731-740.

Casting quality. 2009. *Pump impeller casting*. 25 July 2009. [Online]. Available at: *https://www.castingquality.com/casting-products/pump-fittings-casting-casting-products/pump-impeller-casting.html* [Accessed 26 July 2009].

Cellini, G.S. and Tomesani, L. 2008. Metal head-dependent HTC in sand casting simulation of aluminum alloys. *Journal of Achievements in Materials and Manufacturing Engineering*. Department of Mechanical Constructions Engineering, University of Bologna. Italy. 29 (1), pp. 47-52.

Choudhari, C.M., Narkhede, B.E. and Mahajan, S.K. 2014. Casting design and simulation of cover plate using AutoCAST-X software for defect minimization with experimental validation,

3rd International Conference on Materials Processing and Characterisation. ICMPC 2014. Department of Production Engineering. Jijabai Technological Institute. Mumbai, India. 6, pp. 786-797.

Chougale, S. and Bansode, S. 2016. Additive manufacturing of sand core by using CO_2 gas, *International Journal of Innovative Research in Science and Engineering*, Mechanical Engineering Department, KJ Somaiya College of Engineering, Mumbai (India), 2(3), pp. 697-700.

Ciobanu, I., Munteanu, S., Crisan, A., Bedo, T. and Monescu, V. 2014. Riser analysis using casting simulation technique during solidification. *International Journal of Metal casting.* Transilvania University of Brasov, Romania, 8 (4), pp. 63-75.

Cooper, G. 2013. Technology improving your meltshop performance. Transactions of 61st Indian foundry congress. pp. 1-10.

Di Sabatino, M., Arnberg, L., Rorvik, S. and Prestmo, A. 2005. The influence of oxide inclusions on the fluidity of Al7%Si. Norwegian University of Science and Technology. Department of Materials Technology. Norway. pp. 93-102.

Ding, M., Song, J. and Honghui, L. 2013. Effect of pouring temperature on typical structure of thin-walled ZL105A alloy casting. *Materials and Manufacturing Processes*. Harbin Engineering University. Harbin, China. 29 (7), pp. 853-863.

Fang, Y., Hu, J., Zhou, J. and Yu, Y. 2014. Numerical simulation of filling and solidification in exhaust manifold investment casting. *International Journal of Metal casting.* Changzhou University. Changzhou, China, 8 (4), pp. 39-45.

Ferguson, J.B., Meysam, T.-K., John, C.M., Pradeep, K.R., Cho, K. and Kim, C.S. 2014. Predicting the effect of pouring temperature on the crystallite density, remelting, and crystal growth kinetics in the solidification of aluminium alloys. *The Minerals, Metals and Materials Society & ASM International*. 45B, pp. 1407-1417.

Gajbhiye, A.K., Choudhari, C.M., Raut, D.N., Narkhede, B.E. and Bhandarkar, B.M. 2014. Minimization of shrinkage porosity in a sand casting process by simulation in AutoCAST-X software with experimental validation by destructive testing. *International Journal of Modern Engineering Research (IJMER).* Department of Production Engineering. Jijabai Technological Institute. Mumbai, India. 4 (5), pp. 18-27.

Glonia, J., Koshal, D., Skoczylas, R. and Sobula, S. 2013. Simulation of solidification conditions in high quality castings for mining industry. *Archives of Metallurgy and Materials.* AGH University of Science and Technology, Faculty of Foundry Engineering. Poland. 58 (3), pp. 791-794.

Górny, M. 2007. Structure of ductile iron in thin-walled castings, *Archives of Foundry Engineering*. AGH University of Science and Technology. Poland. 7 (4), pp. 73-78.

Gorny, M. 2012. Fluidity and temperature profile of ductile iron in thin sections. *International Journal of Iron and Steel Research*. Department of Cast Alloys and Composites Engineering. AGH University of Science and Technology. Poland. 19 (8), pp. 52-59.

Gorny, M. and Tyrala, E. 2013. Effect of cooling rate on microstructure and mechanical properties of thin-walled ductile iron castings. AGH University of Science and Technology, Poland. *Journal of Materials Engineering and Performance*. 22 (1), pp. 300-305.

Guofa, M., Xiangyu, L., Kuangfei, W. and Hengzhi, F. 2009. Numerical simulation of low pressure die-casting aluminium wheel. School of material science and engineering. Henan Polytechnic University. China. 6 (1). pp. 48-52.

Gwidz, A., Pysz, S. and Dworak, P. 2010. MAGMAsoft® simulation applied in verification of technology to produce new range of alloy steel casting. *Archives of Foundry Engineering.* Foundry research institute. Poland. 10 (3). pp. 67-72.

Hebsur, N. and Mangshetty, S. 2014. Casting simulation for sand casting of flywheel. *IOSR Journal of Mechanical and Civil Engineering.* Department of Mechanical Engineering. PDA College of Engineering. Karnataka, India. 11 (4/7), pp. 37-41.

Heidarzadeh, M., Keshmiri, H., Ebrahimi, G.R. and Arabshashi, H. 2011. Influence of mould and insulation design on soundness of tool steel ingot by numerical simulation. *International Journal of Science and Advanced Technology*. Esfarayen Industrial Complex. Esfarayen, Iran. 1(6), pp. 37-40.

Hu, L., Chen, S., Miao, Y. and Meng, Q. 2012. Die casting effect on surface characteristics of thin-walled AZ91D magnesium components. *Applied surface Science*. Department of Material Science and Engineering. 261, pp. 851-856.

Iqbal, H., Sheikh, A.K., Al-Yousef, A. and Younas, M. 2012. Mould design optimization for sand casting of complex geometries using advance simulation Tools. *Materials and Manufacturing Processes*. Department of Mechanical Engineering. King Fahd University of Petroleum and Minerals. Dhahran, Saudi Arabia, 27 (7), pp. 775-785.

Iratkar, G.G. and Gandigude, A. U. 2017. Structural Analysis, Material Optimization using FEA and Experimentation of Centrifugal Pump Impeller. *International Journal of Advance Research, Ideas and Innovations in Technology.* Pune, Maharashtra. 3 (4). pp. 97-105.

Iwata, Y., Dong, S., Sugiyama, Y. and Iwahori, H. 2014. Change in molten metal pressure and its effect on defects of aluminium alloy die casting. *Toyota Central R&D Labs, Material Transactions*. Japan Foundry Engineering Society. 55 (2), pp. 311-317.

Jadeja, M.G., Sheladiya, M.V and Gohil, M. 2016. A review on casting defect minimization through simulation. *International Journal for Scientific Research & Development*. Atmiya Institute of Technology and Science. Gujarat, India. 3 (11), pp. 380-385.

Joshi, D. and Ravi, B. 2010. Minimizing porosity in cast junctions, casting modelling helped to create general design guidelines to improve the manufacturability of junctions in metal castings. SGS Institute of Technology and Science. Indore, India. pp. 34-38.

Kamble, B.S. and Kadam, P.V. 2016. Optimized Design of risering system for casted component by using web based online simulation E-Tool. *International Research Journal of Engineering and Technology.* Department of Production Engineering. KIT's College of Engineering. Maharashta, India, 3 (3), pp. 1118-1122.

Khade, U. and Sawant, S. 2014. Riser design optimization based on feeding rules using 3D CAD modelling and casting simulation. *International Journal of Mechanical and Production Engineering*. Department of Mechanical Engineering. Maharashta, India. 2 (5), pp. 63-68.

Kumar, R. and Ravi, B. 2006. Casting design guidelines for junctions considering solidification. Department of Mechanical Engineering. Indian Institute of Technology, Bombay. pp. 1-22.

Kurz, W. and Fisher, D.J., 1986. *Fundamentals of solidification* (Vol. 1). Aedermannsdorf, Switzerland: trans tech publications.

Lei, T., Baoshan, Z., Shuliang, C., Hao, B., and Yuming, W. 2014. Influence of blade wrap angle on centrifugal pump performance by numerical and experimental study. *Chinese journal of Mechanical Engineering*. Tsinghua University, Beijing, China. 27 (1), pp. 171-177.

Li, F., Zhang, J., Bian, F., Fu, Y., Xue, Y., Yin, F., Xie, Y., Xu, Y. and Sun, B. 2015. Mechanism of filling and feeding of thin-walled structures during gravity casting. *Materials.* Shanghai Jiao Tong University, Shanghai, China, 8, pp. 3701-3713.

Mauchline, D.A., Van Tonder, P.J.M. and De Beer, D.J. 2017. Voxeljet – 3D printing solution for the foundry industry. pp. 1-34.

Mugeri, H., Matizamhuka, W.R. and Adebiyi, I.D. 2018. Optimisation of casting process of sand cast austenitic stainless-steel pump impeller using numerical modelling and additive manufacturing. Department of Metallurgical Engineering. Vaal University of Technology, South Africa. pp. 1-120.

Mugeri, H., Matizamhuka, W., Adebiyi, D.I. and Deppinnar, J.H., 2017. Effect of Wall Thickness on the Quality of 1060 Aluminum Produced by Sand Casting. *Procedia Manufacturing*, *7*, pp.402-412.

Nyembwe, K., Mashila, M., Van Tonder, P.J.M., De Beer, D.J. and Gonya, E., 2016. Physical properties of sand parts produced using a Voxeljet VX1000 three-dimensional printer. *South African Journal of Industrial Engineering*, *27*(3), pp.136-142.

Pedersen, KM., Hattel J.H. and Tiedje N. 2006. Numerical modelling of thin-walled hypereutectic ductile cast iron parts. *Acta Materialia*. Department of Manufacturing Engineering and Management, Technical University of Denmark, Denmark. 54, pp. 5103-5114.

Prajapati, T. and Sutaria, M. 2013. Geometry dependency of filling related defects. *International Journal of Engineering Trends and Technology*. Mechanical Engineering Department, Gujarat, India. 4 (5), pp. 1320-1324.

Radisa, R., Gulisija, Z. and Manasijevic, S. 2009. Optimization of casting process design. 49th Anniversary of the faculty of technical science, Movi Sad. pp. 111-114.

Raza, M. 2015. Process development for investment of thin-walled components: Manufacturing of light-weight components. School of Innovation, Design and Engineering. Malardalen University, Sweden pp. 85-120.
Rundman, K.B. 2005. Metal Casting (Reference Book for MY4130). *Dept. of Materials Science and Engineering, Michigan Tech. University*.

Saxena, P., Agrawal, P. and Jain, H. 2013. Casting simulation & optimization for T casting junctions using Response Surface Methodology. *International Journal of Engineering Research & Technology*. Department of Mechanical Engineering. Samrat Ashok Technological Institute Vidisha, India. 2 (5), pp. 2076-2081.

Sharma, P. 2014. Premature failure of ductile iron pump impeller in cooling tower system. *Journal of failure analysis and prevention*. Research and Development, Memphis, USA. 14 (3), pp. 303-306.

Shouzhu, O.U., Kent, D., Carlson, D., Richard, A., Hardin, D. and Beckermann, C. 2002. Development of new feeding-distance rules using casting simulation: Part II. The New Rules, Department of Mechanical and Industrial Engineering. The University of Iowa, Iowa City. 33B, pp. 731-755.
Singh, K., Reddy, P.K., Joshi, D., Subburaj, K. and Ravi, B. 2008. 3D junctions in castings: simulation-based DFM analysis and guidelines. *INAE International Conference on Advances in Manufacturing Technology*. Department of Mechanical Engineering. Indian Institute of Technology. Bombay, Mumbai. pp. 1-7.

Sleigh, A., and Noakes C.J. 2008. CIVE 1400: An introduction to fluid mechanics. Fluid Mechanics, School of Civil Engineering, University of Leeds. pp. 10-20.

Steel Founders' Society of America. 2001. Feeding and risering guidelines for steel casting. pp. 1-45.
Sulaiman, S. and Pio, L.Y. 2004. Validation of MAGMAsoft® simulation of the sand casting process. *Journal - The Institution of Engineers*. Department of Mechanical and Manufacturing Engineering. University of Malaysia, Malaysia. 65 (3/4), 55-64.

Sun, H.C. and Chao, L.S. 2009. An investigation into the effective heat transfer coefficient in the casting of aluminium in a green-Sand mould. *The Japan Institute of Metals, Materials Transactions.* Department of Engineering Science, National Cheng Kung University. Taiwan, China. 50 (6), pp. 1396-1403.

Traeger, C. 2016. 3D Printing as Source of Inspiration for Changes within the Foundry Industry, *AFI Conference 2016*, pp. 1-23.

Vaghasia, D. and Ravi, B. 2009. Gating system design optimization for sand casting. Manufacturing Engineering. Indian Institute of Technology, Bombay. pp. 2-19.

Voigt, R.C. 2002. Filling ability of thin-wall steel casting. Principal Investigator. Department of Energy. The Pennsylvania State University. pp. 7-60.

Whitley, B. 2013. Novel 3-dimensional modelling technology for advanced simulation, printing and casting of A356 impeller. *International Journal of Metal casting*. The University of Alabama, USA. pp. 57-59.

Zhang, L., Li, L. and Zhu, B. 2009. Simulation study on the LPDC process for thin-walled aluminium alloy casting Hunan University. Hunan, China, 24 (12), pp. 1349-1353.

Zhang, Y.F., Liu, W.K. and Wang, HP. 1995. Casting filling simulations of thin-walled cavities. Computer methods applications. Northwestern University, USA. pp. 199-230.

Ziolkowski, J. and Apelian, D. 2002. Modelling of an aerospace sand casting processes. Materials Science and Engineering. Worcester Polytechnic Institute. pp. 1-5.